Spatial distribution of stellar populations in nearby dwarf galaxies resolved in stars by Gaia

Maya K. Belcheva

Department of Astrophysics, Astronomy and Mechanics

Faculty of Physics

National and Kapodistrian University of Athens

A thesis submitted for the degree of

Doctor of Philosophy

Athens, 2012

Acknowledgements

I would like to acknowledge the financial support from EC FP6 Research Training Network "ELSA" (MRTN-CT-2006-033481).

A single sentence, yet it holds much more. Behind the name and the number of the contract stayed actual people, the people which made the network come to life. Among them I would like to mention three who I believe had the greatest impact during my participation in the "ELSA" network: Prof. Lennart Lindegren, the network coordinator, managed people and resources with such excellency and precision I have never encountered before; my supervisor at the University of Athens, Prof. Mary Kontizas - every time I thought I was at a scientific 'dead end' she knew exactly what to say and how to make me again believe in myself; I only spent about three months with Dr. Floor van Leeuwen at the Institute of Astronomy in Cambridge working on a topic not very related to my main work but in these three months I learned and grew and found myself.

Some of the 15 ELSA fellows I have known only for a short while, others were there from the beginning to the end. Thanks to all of them I was inspired and motivated after each meeting or school we attended together.

I would like to thank my supervisor comittee comprising Mary Kontiza, Ioannis Bellas Velidis and Panaiotis Niarchos for actually reading the whole text you are now holding and contributing on every level for improving the contents and style of the thesis.

I would also like to say a very special "Thank You!" to Antonios Karampelas who not only translated the Summary of the thesis into Greek but also helped me to understand and appreciate the Greek way of life.

Last but not least, I would like to thank all the people in the Greek administration who were willing to follow not the letter of the law but its spirit!

Contents

Περίληψη

Οι κυριότεροι στόχοι της παρούσας διατριβής είναι οι εξής:

1. Η διερεύνηση της χωρικής κατανομής των αστρικών πληθυσμών των γειτονικών γαλαξιών, και ειδικώτερα μέρος του αστρικού πληθυσμού ο οποίος αναμένεται να παρατηρηθεί από το δορυφόρο Gaia. Πιο συγκεκριμένα, μελετώνται το Μικρό και το Μεγάλο Νέφος του Μαγγελάνου, καθώς και έξι ακόμα νάνοι ανώμαλοι γαλαξίες του Τοπικού Σμήνους γαλαξιών: Ο NGC 6822, ο WLM, ο IC10, ο Phoenix, ο Sextans A και ο Sextans B. Οι κατανομές αυτών των αστέρων συμπεριλαμβάνονται στα εξωγαλαξιακά αντικείμενα τα οποία πρόκειται να προσομοιωθούν στα πλαίσια της προετοιμασίας του δορυφόρου Gaia. Στο πλαίσιο αυτής της έρευνας μελετάται η ακτινική κατανομή της πυκνότητας των ανωτέρω γαλαξιών με στόχο τη σύγκριση με τα επικρατέστερα θεωρητικά μοντέλα της γαλαξιακής δυναμικής.

2. Η εφαρμογή της παραπάνω διερεύνησης στο Μοντέλο του Σύμπαντος (Universe Model) αποτελεί μέρος της συμμετοχής της Ελληνικής ομάδας του ΕΚΠΑ στην προετοιμασία για την διαστημική αποστολή του δορυφόρου Gaia (από την Ευρωπαϊκή ομάδα DPAC, Data proceeding and Analysis Consortium). Στο πλαίσιο αυτής της συνεργασίας θα παραδοθούν προς προσομοίωση αστρικοί κατάλογοι των Νεφών του Μαγγελάνου. Οι κατάλογοι αυτοί θα περιέχουν μία σειρά παραμέτρων για κάθε αστέρα, όπως για παράδειγμα τα μεγέθη B, V, I και G, η ορθή αναφορά και η απόκλιση, το χρώμα $V-I$, η απόσταση, η ακτινική ταχύτητα, η ιδία κίνηση, η επιφανειακή βαρύτητα ($\log g$), η ενεργός θερμοκρασία (T_{eff}), η μεταλλικότητα ($[Fe/H]$), η επαύξηση σωματιδίων α (α ενηανσεμεντ - $[\alpha/Fe]$) και η εξάλειψη του φωτός (extinction - A_V).

Τοπικό Σμήνος γαλαξιών

Το Τοπικό Σμήνος γαλαξιών, η άμεση γειτονιά μας, είναι η ομάδα των γαλαξιών στην οποία σχηματίστηκε και εξελίσσεται ο Γαλαξίας μας. Ο Γαλαξίας μας και η Ανδρομέδα (M31) είναι οι δύο κυρίαρχοι σπειροειδείς γαλαξίες στο Τοπικό Σμήνος, και κάθε ένας από αυτούς περιβάλλεται από δορυφόρους γαλαξίες μικρότερης μάζας.

Το Τοπικό Σμήνος μοιάζει με ένα συνηθισμένο σύστημα νάνων γαλαξιών που κυριαρχείται από τους δύο γιγαντιαίους σπειροειδείς γαλαξίες, τον Γαλαξία μας και τον M31. Παρόλα αυτά έχει ιδιαίτερη σημασία για τους αστρονόμους στη Γη. Η εγγύτητα του Τοπικού Σμήνους γαλαξιών καθιστά τα μέλη του ιδανικά σημεία αναφοράς για τη μελέτη της δημιουργίας και της εξέλιξης των γαλαξιών, επειδή είναι τα μόνα συστήματα όπου η ακρίβεια και ο πλούτος των παρατηρησιακών δεδομένων μας επιτρέπει να τα κατανοήσουμε με έναν επαρκώς αξιόπιστο τρόπο (Tosi 2003). Τα 25 τελευταία χρόνια έχει υπάρξει ένα πλήθος δημοσιεύσεων που ασχολούνται με τη

χημική εξέλιξη των νάνων γαλαξιών. Ενώ οι περισσότεροι συγγραφείς συμφωνούν πως η αρχική συνάρτηση μάζας στους γαλαξίες αυτούς είναι αρκετά παρόμοια με τη συνάρτηση Salpeter, τόσο στα συστήματα αστρογέννεσης όσο και στην ύπαρξη γαλαξιακών ανέμων, διαφορετικές ερευνητικές ομάδες έχουν καταλήξει σε διαφορετικά συμπεράσματα. Οι διαφοροποιήσεις αυτές οφείλονται στην ανεπάρκεια παρατηρησιακών δεδομένων.

Μεταξύ των νάνων γαλαξιών του Τοπικού σμήνους, τα Νέφη του Μαγγελάνου είναι οι πλησιέστεροι στον Γαλαξία μας. Αν και η σημασία τους είναι πολλαπλή, Επιπλέον, μπορούμε να τους χρησιμοποιήσουμε για να κατανοήσουμε άλλους γαλαξίες, οι οποίοι είναι πολύ μακρινοί για οποιοδήποτε είδος αναλυτικής μελέτης. Τα Νέφη του Μαγγελάνου είναι θεμελιώδους σημασίας για τη βαθμονόμηση των εξωγαλαξιακών αποστάσεων. Αποτελούν μία από τις λίγες ευκαιρίες που έχουμε για να συγκρίνουμε σπάνια αντικείμενα, όπως οι λαμπρότεροι μπλε υπεργίγαντες αστέρες, οι μεταβλητοί αστέρες, τα αστρικά σμήνη και οι περιοχές ιονισμένου υδρογόνου, με κοινά αστέρια παρόμοια με τον Ήλιο, και όλα στην ίδια απόσταση και σχετικά ανεπηρέαστα από τη μεσοαστρική σκόνη. Στη συνέχεια, και με ακριβείς βαθμονομήσεις ανά χείρας, μπορούμε με αξιοπιστία να προχωρήσουμε στη μελέτη πιο απομακρυσμένων συστημάτων, στους οποίους μπορούμε να έχουμε πρόσβαση μόνο στα πολύ λαμπρά αντικείμενα.

Η αποστολή Γαια

Το 2013 η επιστημονική κοινότητα αναμένει την εκτόξευση του δορυφόρου Gaia. Πρόκειται για έναν αστρομετρικό δορυφόρο, η έγκριση του οποίου πραγματοποιήθηκε το 2000 από την επιτροπή επιστημονικών προγραμμάτων του Ευρωπαϊκού Οργανισμού Διαστήματος (ESA). Σε αντίθεση με τις αποστολές HST και SIM, όπου οι παρατηρήσεις γίνονται με βάση μία λίστα προεπιλεγμένων αντικειμένων, ο δορυφόρος Gaia θα σαρώσει συστηματικά και επανειλημμένως τον ουρανό, πραγματοποιώντας κατ'αυτόν τον τρόπο μία ευρύτερη αστροφυσική έρευνα.

Η φωτομετρία του δορυφόρου HST, καθώς και η φασματοσκοπία των τηλεσκοπίων της τάξης των 10 μέτρων, επέτρεψαν τη μοντελοποίηση της χημικής εξέλιξης των νάνων γαλαξιών του Τοπικού Σμήνους, και μάλιστα ασφαλέστερα από την αντίστοιχη στη γειτονιά του Ήλιου. Μπορεί λοιπόν η αποστολή Gaia να μην είναι σε θέση να συναγωνιστεί τα συγκεκριμένα όργανα, αλλά θα παράσχει (*i*) τη δυνατότητα να πραγματοποιήσει μία αστρομετρική έρευνα όλου του ουρανού, (*ii*) το μοναδικό συνδυασμό σε ένα διαστημικό σκάφος τριών οργάνων, του αστρομετρικού πεδίου AF, των φασματογράφων χαμηλής ανάλυσης BP/RP, και του φασματογράφου υψηλής ανάλυσης RVS, και (*iii*) τον τεράστιο αριθμό αντικειμένων και παρατηρήσεων που επιτρέπουν να επιτευχθεί η ακρίβεια της θέσης τεράστιου πλήθους ουρανίων σωμάτων, αποφέροντας στατιστική σημαντικότητα.

Παρόλο που το άμεσο προϊόν της αποστολής Gaia θα είναι μία αστρομετρική και φωτομετρική έρευνα υψηλής ακρίβειας μέχρι το μέγεθος $V = 20mag$, οι επιστημονικοί στόχοι είναι πολύ ευρύτεροι και υποστηρίζονται από μία τεράστια επιστημονική κοινότητα. Η ποικιλία των επιστημονικών στόχων του δορυφόρου Gaia απαιτεί μία ιδιαιτέρως περίπλοκη προετοιμασία τόσο της διαστημικής αποστολής, όσο και της αναγωγής των δεδομένων. Για να αντιμετωπιστεί η πρόκληση αυτή, η επιστημονική κοινότητα και η ESA ξεκίνησαν μία κοινή προσπάθεια για να δημιουργήσει την ομάδα επεξεργασίας δεδομένων, (DPAC, Data Processing and Analysis Consortium) η οποία και θα παραδώσει τα ενδιάμεσα και τα τελικά επιστημονικά προϊόντα. Η ανάπτυξη ενός συστήματος λογισμικού κατάλληλου να καλύψει τις ανάγκες προσομοίωσης του DPAC, δεν απαιτεί μόνο την επάρκεια στην τεχνολογία λογισμικού, αλλά και μία ισχυρή επιστημονική συνιστώσα που θα διασφαλίσει ότι το σύστημα λογισμικού θα ικανοποιήσει τους επιστημονικούς στόχους.

Το Μοντέλο του Σύμπαντος (Universe model) που έχει ήδη αναπτυχθεί για τις ανάγκες των προσομοιώσεων της αποστολής, αποτελείται από ένα σύνολο αλγορίθμων για τον υπολογισμό της θέσης ανά πάσα στιγμή, καθώς και των ιδιοτήτων, κάθε αντικειμένου που πρόκειται να παρατηρηθεί από τα όργανα του δορυφόρου Gaia. Οι κατανομές των αντικειμένων αυτών και η στατιστική των παρατηρούμενων παραμέτρων πρέπει να είναι όσο το δυνατόν περισσότερο ρεαλιστικές, ώστε οι προσομοιώσεις να είναι χρήσιμες στην εκτίμηση της τηλεμετρίας, στις δοκιμές των λογισμικών, την προσομοίωση εικόνων κλπ. Πρόκειται να προσομοιωθούν αντικείμενα του Ηλιακού συστήματος (πλανήτες, δορυφόροι, αστεροειδείς, κομήτες), γαλαξιακά αντικείμενα (αστέρες, νεφελώματα, αστρικά σμήνη, διάχυτο φως) και εξωγαλαξιακά αντικείμενα (άστρα γειτονικών γαλαξιών, γαλαξίες και quasars, AGN, εξωγαλαξιακοί υπερκαινοφανείς). Για τα προσομοιωμένα αντικείμενα απαιτείται η τρισδιάστατη χωρική τους κατανομή, τα φασματικά τους χαρακτηριστικά (για τον υπολογισμό της φωτομετρίας και της φασματοσκοπίας, τόσο χρονικά σταθερά όσο και μεταβαλλόμενα), και οι κινήσεις τους (για αστρομετρικούς υπολογισμούς και φασματικές διορθώσεις). Θα προσομοιωθεί επίσης το φαινόμενο των βαρυτικών φακών για αστέρες και για γαλαξίες.

Συμπεράσματα

Τα αποτελέσματα της παρούσας διατριβής μπορούν να διαχωριστούν σε δύο κατηγορίες, οι οποίες αντιστοιχούν στους δύο προαναφερθέντες κύριους στόχους, και είναι τα εξής:

1. Μελετήθηκε η χωρική κατανομή των αστρικών πληθυσμών του Μικρού και του Μεγάλου Νέφους του Μαγγελάνου, καθώς και έξι ακόμα νάνων ανώμαλων γαλαξιών του Τοπικού Σμήνους γαλαξιών: Του NGC 6822, του WLM, του IC10, του Phoenix, του Sextans A και του Sextans B.

- Δημιουργήθηκαν χάρτες ισοπληθών καμπυλών και διαγράμματα ακτινικής επιφανειακής πυκνότητας των παραπάνω γαλαξιών, βασισμένα σε δεδομένα από τη βιβλιογραφία.
- Υπολογίστηκαν παράμετροι δομής των παραπάνω γαλαξιών από την προσαρμογή θεωρητικών μοντέλων στα διαγράμματα ακτινικής επιφανειακής πυκνότητας.
- Διαπιστώθηκε πως παρόλο που τα νέφη του Μαγγελάνου θεωρούνται ως ανώμαλοι γαλαξίες, χωρίς κάποια προφανή ακτινική συμμετρία, οι γηραιότεροι πληθυσμοί συμπεριφέρονται ως ελλειπτικοί γαλαξίες με συμμετρική δομή
- Επιβεβαιώθηκε το γεγονός πως η τιμή της κλίμακας μήκους (scale length) του εκθετικού δίσκου του Μεγάλου Νέφους του Μαγγελάνου είναι περίπου διπλάσια της αντίστοιχης τιμής του Μικρού Νέφους του Μαγγελάνου.
- Διαπιστώθηκε πως υπάρχει ένα σύστημα νεαρών αντικειμένων τα οποία είναι περισσότερο συγκεντρωμένα στην κεντρική περιοχή του Μεγάλου Νέφους του Μαγγελάνου, κατανεμημένα σχεδόν κάθετα στο ελλειπτικό σύστημα του γηραιού πληθυσμού, όπως παρατηρείται στους χάρτες ισοπληθών καμπυλών από το 2MASS και τον κατάλογο των αστέρων άνθρακα.
- Καταδείχθηκε πως υπάρχουν δύο συστήματα αστέρων άνθρακα στο Μεγάλο Νέφος του Μαγγελάνου, με ακτίνα πυρήνα (core radius) ίση με $3.3 \pm 0.1 deg$ και $0.9 \pm 0.1 deg$ για τους αμυδρούς και τους λαμπρούς αστέρες άνθρακα, αντίστοιχα. Ένας τέτοιος διαχωρισμός προέκυψε επίσης και στις κλίμακες ύψους (scale height) με βάση ένα εκθετικό μοντέλο, με τιμές $1.69 \pm 0.07 deg$ και $0.98 \pm 0.05 deg$, αντίστοιχα, αποκαλύπτοντας ένα κεντρικό σύστημα όπου ευρίσκονται οι αστέρες άνθρακα μεγάλης μάζας.

2. Τα αποτελέσματα της παραπάνω μελέτης για την περίπτωση των Νεφών του Μαγγελάνου βρήκαν εφαρμογή στο Universe model του δορυφόρου Gaia, στα πλαίσια της προετοιμασίας της συγκεκριμένης αποστολής.

   - Έγινε εμπεριστατωμένη διερεύνηση όλων των υπαρχόντων δεδομένων σε αστρικούς κατάλογους των Νεφών του Μαγγελάνου από τη βιβλιογραφία, ώστε να ευρεθεί ο καλύτερος κατάλογος που θα χρησιμοποιηθεί στις προσομοιώσεις για τους γειτονικούς γαλαξίες, άστρα των οποίων πρόκειται να παρατηρηθούν από τον δορυφόρο Gaia. Οι προσομοιώσεις αυτές αποτελούν τμήμα των προσομοιώσεων των εξωγαλαξιακών αντικειμένων, στα πλαίσια της προετοιμασίας του δορυφόρου Gaia.

- Στα πλαίσια του πιο πάνω βασικού στόχου της διατριβής, παραδόθηκε το απαιτούμενο προς προσομοίωση υλικό των Νεφών του Μαγγελάνου στην κατάλληλη μορφή, στο πλαίσιο των υποχρεώσεων μας για το Universe model του δορυφόρου Gaia.

Δομή διατριβής

Η παρούσα διατριβή αποτελείται από τέσσερα κύρια μέρη. Η δομή της περιγράφεται περαιτέρω στα παρακάτω: Το εισαγωγικό πρώτο μέρος παρέχει μία επισκόπηση (1ο Κεφάλαιο) των γαλαξιών του Τοπικού Σμήνους που επελέγησαν για τη διερεύνησή μας και παρουσιάζει τα θεωρητικά μοντέλα που περιγράφουν τη χωρική κατανομή των διαφόρων αστρικών συνιστωσών των γαλαξιών (2ο Κεφάλαιο). Μία περισσότερο αναλυτική επισκόπηση της αποστολής Gaia δίνεται στο 3ο Κεφάλαιο.

Στο δεύτερο μέρος παρουσιάζουμε τα αποτελέσματα από τη μοντελοποίηση της χωρικής κατανομής αστρικών πληθυσμών των Νεφών του Μαγγελάνου. Το 4ο Κεφάλαιο περιλαμβάνει μία επισκόπηση του συστήματος των Νεφών του Μαγγελάνου. Στο 5ο Κεφάλαιο γίνεται περιγραφή των δεδομένων σχετικά με τα Νέφη του Μαγγελάνου, τα οποία ήταν αρχικώς διαθέσιμα. Παρουσιάζονται επίσης οι πηγές των δεδομένων τα οποία επελέγησαν βάσει των απαιτήσεών μας. Στο 6ο Κεφάλαιο παρουσιάζονται τα αποτελέσματα της μοντελοποίησης αρκετών αστρικών ομάδων διαφόρων ηλικιών των Νεφών του Μαγγελάνου. Σε αυτά συμπεριλαμβάνονται και διαγράμματα μεγέθους-χρώματος, χάρτες ισοπληθών καμπυλών και διαγράμματα ακτινικής επιφανειακής πυκνότητας.

Το τρίτο μέρος περιέχει δύο Κεφάλαια. Στο 7ο Κεφάλαιο δίνεται μία σύντομη περιγραφή της μονάδας συντονισμού (coordination unit) της Κοινοπραξίας Ανάλυσης και Επεξεργασίας Δεδομένων του δορυφόρου Gaia (Gaia Data Processing and Analysis Consortium), η οποία είναι υπεύθυνη για τις προσομοιώσεις των δεδομένων. Παρέχεται επίσης και μία περιγραφή του Μοντέλου του Σύμπαντος του δορυφόρου Gaia. Στο 8ο Κεφάλαιο παρουσιάζεται η συνεισφορά μας στο Μοντέλο του Σύμπαντος του δορυφόρου Gaia, η οποία συνίσταται στην εφαρμογή των δεδομένων των Νεφών του Μαγγελάνου.

Το τέταρτο μέρος παρουσιάζεται η μελέτη της χωρικής κατανομής των αστέρων σε έξι νάνους ανώμαλους γαλαξίες του Τοπικού Σμήνους γαλαξιών με τη μεθοδολογία που αναπτύχθηκε στο κεφάλαιο 2 για τα Νέφη του Μαγγελάνου. Στο 9ο Κεφάλαιο δίνεται μία εισαγωγή για τους γαλαξίες αυτούς, συμπεριλαμβανομένων των ιδιοτήτων τους και των αποτελεσμάτων από προηγούμενες έρευνες στη βιβλιογραφία. Το 10ο Κεφάλαιο περιγράφει την έρευνα (LGGS) η οποία παρέχει τα φωτομετρικά δεδομένα των γαλαξιών του δείγματός μας. Στο 11ο Κεφάλαιο παρουσιάζονται τα αποτελέσματα της μοντελοποίησης της αστρικής κατανομής στους έξι

παραπάνω νάνους ανώμαλους γαλαξίες. Σε αυτά συμπεριλαμβάνονται και διαγράμματα μεγέθους-χρώματος, χάρτες ισοπληθών καμπυλών και διαγράμματα ακτινικής επιφανειακής πυκνότητας.

Στο τελευταίο μέρος της διατριβής περιέχονται γενικά σχόλια, ιδέες για περαιτέρω διερεύνηση στο ίδιο αντικείμενο, καθώς και κατάλογοι όλων των εικόνων και των πινάκων της διατριβής και οι αναφορές.

Summary

Local Group of galaxies

The Local Group, our immediate neighbourhood, is the group of galaxies in which our Galaxy, the Milky Way, formed and is evolving. The Milky Way and the Andromeda galaxy (M31) are the two dominant spiral galaxies in the LG, and each is surrounded by an entourage of lower mass companions.

It looks like an ordinary collection of dwarf galaxies dominated by two giant spirals. However for astronomers on Earth it is special. The proximity of Local Group galaxies makes them the ideal benchmarks to study galaxy formation and evolution, because they are the only systems where the accuracy and the wealth of observational data allows us to understand them in a sufficiently reliable way (Tosi 2003). In the last 25 years there has been a wealth of papers dealing with the chemical evolution of dwarfs: a rather frustrating challenge, if one considers how inconsistent with each other the results of these papers have been. While most authors agreed that the initial mass function in these galaxies is fairly similar to Salpeter's, both on the star formation regimes and on the existence of galactic winds, different groups have reached very different conclusions. These inconsistencies are due to the lack of adequate observational data.

Among the Local Group dwarf galaxies the Magellanic Clouds are the nearest to our Galaxy. Their importance is many-fold but two aspects especially stand out. First, they act as a guide to our own Milky Way galaxy as to how it would appear if we could view it from a vantage point high above its dusty disk. Second, we can make use of them to understand other galaxies far too remote for any sort of detailed study. The Magellanic Clouds are fundamentally important for the calibration of the extragalactic distance scale. They represent one of the few opportunities we have to compare rare objects like the most luminous blue supergiant stars, variable stars, star clusters, and HII regions directly with common stars similar to the Sun, all at the same distance and all comparatively unobscured by interstellar dust. With firm calibrations in hand, we can then confidently proceed to more distant systems where only the very brightest objects may be accessed.

The Gaia mission

In 2013 the scientific community expects the launch of Gaia. It is an astrometric satellite, which was approved by ESA's Science Programme Committee in 2000. Unlike HST and SIM, which are pointing instruments observing a preselected list of objects, Gaia is a scanning satellite that will repeatedly survey in a systematic way the whole sky, making possible broader astrophysical investigations.

HST photometry and 10 m class telescope spectroscopy allowed modelling

the chemical evolution of dwarf galaxies in the Local Group even more safely than that of the solar neighbourhood. The Gaia mission might not be able to compete with these instruments, but what it will provide beyond sheer measurement accuracy is (i) its capability to perform an all-sky and sensitivity limited absolute astrometric survey, (ii) the unique combination into a single spacecraft of the three instruments, AF astrometric field, BP/RP low-resolution spectrophotometres and RVS radial-velocity spectrometre, (iii) the huge number of objects and observations which allow the accuracy on single objects to be achieved on very large samples, thus yielding statistical significance.

Whereas the direct product of the Gaia mission will be a highly accurate astrometric and photometric survey to $V = 20$ mag, the science goals are much broader and account for the support of a large scientific community. The diversity of the science goals for Gaia requires a very complex mission and data reduction preparation. To cope with the challenge, the scientific community, together with ESA, started a joint effort to set up a data processing ground segment comprising a single processing pipeline which will deliver the intermediate and final mission science products. The development of a software system capable of covering the simulation needs of the Gaia Data Processing and Analysis Consortium (DPAC) requires not only software engineering competence alone; a strong scientific component is also needed to ensure that the system fulfills the scientific goals.

A Universe Model is developed for the simulation needs of the mission. It is a set of algorithms for computing the positions at any time, and observational properties of any objects expected to be observed by the Gaia instruments. The distributions of these objects and the statistics of observables should be as realistic as possible for simulations to be usable for estimating telemetry, testing software, simulating images, etc. Solar system objects (planets, satellites, asteroids, comets), Galactic objects (stars, nebulae, stellar clusters, diffuse light) and extra-galactic objects (neighbour galaxies resolved in stars, unresolved but extended remote galaxies and quasars, AGN, extra-galactic supernovae) will be simulated. For each of these simulated objects one needs to have their three-dimensional spatial distribution together with their spectral characteristics (for computing photometry and spectroscopy, stable or variable in time), and their motions (for astrometric computations and for spectral corrections). Gravitational lensing for stars and galaxies are also to be simulated.

Main goals

The goals of the current study are:

1. the investigation of the spatial distribution of stellar populations in nearby galaxies, expected to be resolved in stars by Gaia. These are part of the

extra-galactic objects to be simulated in the framework of the Gaia mission preparation. The main targets are the Large and Small Magellanic Clouds, along with six dwarf irregular galaxies in the Local Group - NGC 6822, WLM, IC10, Phoenix, Sextans A and Sextans B.

2. the implementation of results from this investigation in the Gaia Universe Model. Catalogues of stars known to be part of both the Large and Small Magellanic Clouds and their characteristics (B, V, and I magnitudes) are to be provided to be used for simulations, including parameters such as Right Ascension, Declination, V magnitude, $V-I$ colour, G magnitude, distance, radial velocities, proper motions, surface gravity $\log g$, effective tempearture T_{eff}, metallicity $[Fe/H]$, α enhancement $[\alpha/Fe]$, and extinction A_V.

Main results

The results of the current study can be divided in two categories, according to the main goals presented above:

1. The spatial distribution of stellar populations in nearby galaxies was studied. The main targets were the Large and Small Magellanic Clouds and additionally six dwarf irregular galaxies in the Local Group - NGC 6822, WLM, IC10, Phoenix, Sextans A and Sextans B.

    - Isopleth contour maps and radial surface density profiles of several dwarf irregular galaxies in the Local Group have been produced, based on data from the literature;
    - Structural parameters have been obtained for these galaxies by fitting theoretical models to the stellar radial surface density distribution;
    - Although the Magellanic Clouds are assumed to be irregular galaxies, our results suggest that the older populations appear to behave as tidally truncated systems, even if they do not show obvious radial symmetry;
    - It is confirmed that the exponential disk scale length of the LMC is about twice the SMC value;
    - It was shown that there is a system of young objects more concentrated in the central region of the LMC with a position angle nearly perpendicular to the other system - this is observed in the isopleth maps from both 2MASS and the carbon stars catalogue;

- From the carbon stars in the LMC, it was shown that two different systems exist with a core radius of 3.3 ± 0.1 deg for the faint and 0.9 ± 0.1 deg for the bright carbon stars. An exponential model also shows such a difference in the scale height, 1.69±0.07 deg and 0.98±0.05 deg, respectively, revealing a smaller central system of more massive carbon stars.

2. The results of this study were used to implement Magellanic Clouds data in the Gaia Universe Model in the framework of the Gaia mission preparation.

   - Catalogues of stars known to be members of both Magellanic Clouds have been obtained from the literature and their characteristics have been provided for the simulation of nearby galaxies, resolved in stars by Gaia. These are part of the extra-galactic objects to be simulated in the framework of the Gaia mission preparation;
   - Within the second goal of the project, we provided the requested material in appropriate format that were adopted for the simulations of the Magellanic Clouds in the framework of the Gaia Universe Model.

Structure

The Thesis is divided in four main parts. The structure is further described below.

The introductory Part I provides an overview (Chapter 1) of the Local Group galaxies census in connection with our investigation and presents the theoretical models describing the spatial distribution of various stellar components in the galaxies (Chapter 2). A more detailed overview of the Gaia mission is given in Chapter 3.

In Part II we present the results from modelling the spatial distribution of some stellar populations in the Magellanic Clouds. Chapter 4 includes an overview of the Magellanic System. Chapter 5 describes the data available at the start of the project for the Magellanic Clouds. The data sources are presented which were selected based on our requirements. In Chapter 6 are shown the results from modelling several age groups in the Large and Small Magellanic Clouds, including colour-magnitude diagrams, isopleth contour maps and radial surface density profiles.

Part III contains two chapters. Chapter 7 gives a short description of the coordination unit of the Gaia Data Processing and Analysis Consortium responsible for data simulations and a description of the Gaia Universe Model itself. Chapter 8 presents our contribution to the Gaia Universe Model consisting in the implementation of Magellanic Clouds data.

In some aspects Part IV is analogous to Part II. It presents the study of the stellar spatial distribution in six dwarf irregular galaxies of the Local Group. Chapter 9 gives an introduction of the galaxies, including their properties and results from previous investigations from the literature. Chapter 10 describes the survey (LGGS) which provides the photometric data for the galaxies in our sample. Chapter 11 shows the results from modelling the stellar distribution in these six dwarf irregular galaxies, including colour-magnitude diagrams, isopleth contour maps and radial surface density profiles.

The final part of the Thesis contains the concluding remarks, some ideas for future work on the subject, as well as lists of all the figures and tables in the Thesis and the References.

SUMMARY

Part I

Introduction

Part I is devoted to the overview of this thesis, which has three aspects - i) the astronomical objects which are the subjects of the current investigation, ii) the methods used in the process, and iii) the tool which is going to be used to observe these objects and is going to be improved due to input from the current investigation.

A short description of our Local Group of galaxies is given in Chapter 1. The content, structure and general properties are presented, as well as common features of dwarf galaxies in the Local Group. The galaxies in our sample are the Large Magellanic Cloud, the Small Magellanic Cloud, NGC 6822, WLM, IC10, Phoenix, Sextans A, and Sextans B.

In Chapter 2 the theoretical models are presented which were used to describe the spatial distribution of stars in the Local Group galaxies under investigation. Both the exponential-disk and King law are found to describe to some degree the distribution of the various stellar populations. In some cases one is better at fitting the stellar distribution than the other and vice versa.

The Gaia satellite is described in Chapter 3. Gaia is an ESA satellite, expected to be launched in 2013. The science case is very broad and is covering topics, such as Milky Way mapping and kinematics, Galaxy formation and evolution, stellar physics, Solar system science, extra-solar planet detection, distance scales, reference frames, etc.

Chapter 1

The Local Group

1.1 General Information

The Local Group (LG), our immediate neighbourhood, is the group of galaxies in which our Milky Way galaxy formed and is evolving. It looks like an ordinary collection of dwarf galaxies dominated by two giant spirals (see Figure 1.1). The Milky Way and M31 are the two dominant spiral galaxies in the LG, and each is surrounded by an entourage of lower mass companions. Apart from the late-type spiral M33, more than 50 galaxies forming the LG are either dwarf elliptical (dE), dwarf spheroidal (dSph) or dwarf irregular (dIrr) galaxies.

Grebel (2001b) characterized galaxies as dwarf galaxies if their total B- or V-band magnitude is fainter than −18 mag. While the primary distinguishing feature between dIrr and dSph galaxies is whether they have or do not have neutral hydrogen (HI), there are other distinguishing features. Galaxies of the dIrr type typically have central surface brightnesses of $\mu_{V,0} \leq 23$ mag arcsec^{-2} and total HI masses of $M_{HI} \leq 10^9 M_\odot$. As their name suggests, their optical appearance is irregular, which tends to be caused by scattered HII regions for the more massive dIrr galaxies. They are mainly found at larger distances from massive galaxies. Dwarf elliptical galaxies are spherical or elliptical in appearance, typically with $M_V \geq -17$ mag, and have $\mu_{V,0} \leq 21$ mag arcsec^{-2} and $M_{HI} \leq 10^8 M_\odot$. Along with the dSph galaxies, they are usually found in the vicinity of massive galaxies. Dwarf spheroidal galaxies tend to have $M_V \geq$ -14 mag, $\mu_{V,0} \geq 22$ mag arcsec^{-2} and $M_{HI} \leq 10^5 M_\odot$.

A comprehensive study of the nearby Local Group galaxies requires instrumentation with high sensitivity and large field of view (FOV), as most of them occupy large areas on the sky. The demand for high sensitivity will imply the use of the largest telescopes available; however, their FOVs are prohibitively small compared to the spatial extent of Local Group galaxies, especially the nearby ones. Thus current studies of Local Group dwarfs are mostly limited to small

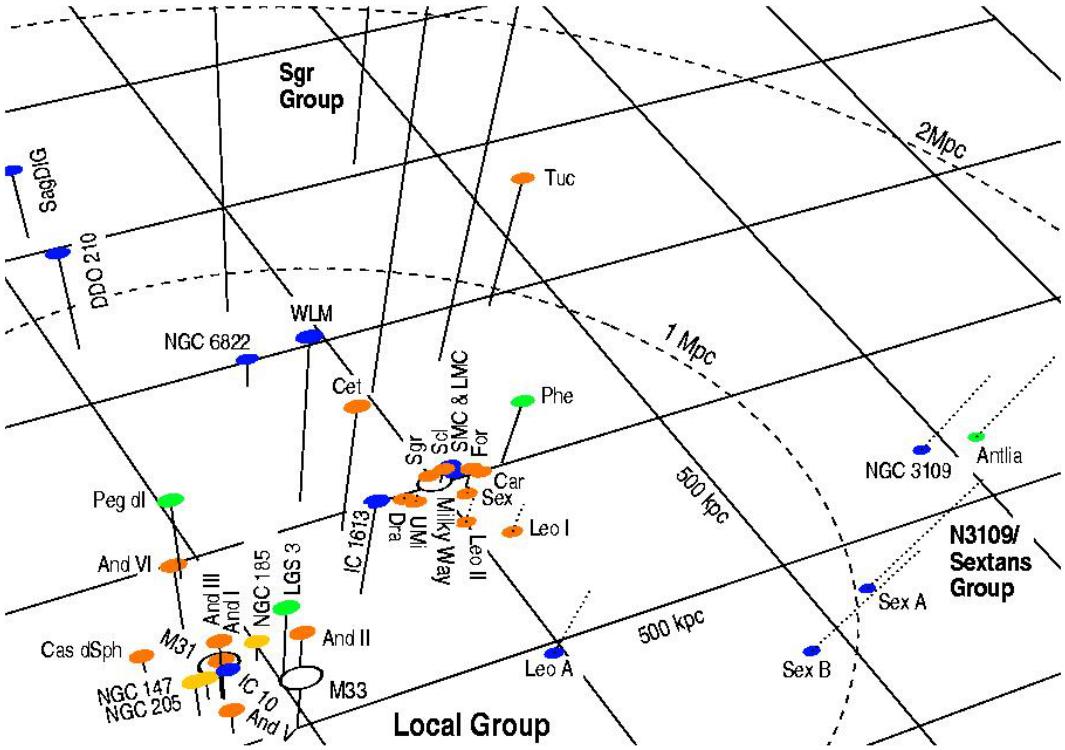

Figure 1.1: A scaled 3-D representation of the Local Group by Grebel (2001a). The dashed ellipsoid marks a radius of 1 Mpc around the LG barycentre (assumed to be at 462 kpc toward l = 121.7 and b = −21.3. Distances of galaxies from the the arbitrarily chosen plane through the Milky Way are indicated by solid lines (above the plane) and dotted lines (below).

areas in individual galaxies (typically their central parts).

The all-sky survey Gaia mission will provide precise information both on kinematical and astrophysical properties of individual stars, obtained with a single, stable and well-calibrated instrument. Moreover, the data will be acquired in the same instrumental system as for the millions of stars in the Milky Way. This will deliver an unique and homogeneous data set, which will allow to perform a comprehensive and in-depth analysis of the formation and evolution of the Local Group galaxies.

1.2 Dwarf galaxies in the Local Group

The dwarfs of the Local Group provide a unique sample of low-luminosity galaxies. Dwarf galaxies represent the dominant population, by number, of the present-day

universe (Marzke and da Costa 1997). If low-luminosity galaxies are universally dominated by dark matter to the extent LG dwarfs may be, they could account for a large fraction of the mass of galaxy clusters, and perhaps of the entire Universe. Photometric investigations of the stellar populations in LG dwarf galaxies provide firm constraints on cosmological parameters and the unique opportunity to investigate galaxy formation models. Although the number of dwarf galaxies known in the Local Group is rapidly growing in the last few years, current statistics indicate that the dIrrs are at least one quarter of LG galaxies (McConnachie et al. 2008; Sanna et al. 2009).

There are two types of dwarf galaxies: gas-poor dwarf spheroidals/ellipticals (dSph/dE), and gas-rich irregulars (dIrr). Most emphasis has been laid on the role of dwarf spheroidals in galaxy merging. However, dwarf spheroidals are found primarily in the cores of dense clusters, indicating they have already undergone significant evolution through interaction (Binggeli et al. 1987). Also, it is clear that gas-rich spiral galaxies such as the Milky Way could not have formed by merging of only dSph galaxies. In contrast, the dIrr galaxies are rather unevolved, as indicated by their abundance in low-density regions. The significance of dIrr galaxies as possible elements contributing to build larger galaxies like our own has to some extent been overlooked: it is likely that they are in fact the major surviving representatives of the original building blocks.

Recently, Weisz et al. (2011) uniformly analyzed star formation histories (SFH) of 60 dwarf galaxies in the nearby universe based on observations and data processing done as part of the ANGST program. While the SFHs of individual galaxies are quite diverse, it has been found that the mean star formation histories of the different morphological types are generally indistinguishable outside the most recent ~ 1 Gyr. On average, the typical dwarf galaxy formed ~ 50% of its stellar mass by z ~ 2 and 60% by z ~ 1.

The dwarf galaxies in the ANGST sample show a strong morphology-density relationship. This suggests that internal mechanisms, e.g., stellar feedback, cannot solely account for gas-loss in dwarf galaxies, as the corresponding models are unable to produce this observed relationship. Weisz et al. (2011) also identify 12 transitional dwarfs (dTrans) in their sample, based on the literature definition of present day gas fraction and star formation as measured by Hα. Within this sample of dwarf transitional galaxies, they find that galaxies with high gas fractions are associated with more isolated galaxies, while those with lower gas fractions are less isolated. This suggests that there are two mechanisms that can produce the observed dTrans characteristics: the isolated gas-rich galaxies are simply between episodes of SF due to the stochastic nature of star formation in low mass galaxies, while the less isolated galaxies could be in the process of interacting with a more massive companion.

Because they are so numerous, the LG dwarfs can be used effectively as tracers

of substructure. To first approximation, the Local Group is a binary system with massive clumps of galaxies centered on M31 and on the Galaxy. Within each of the two main Local Group subclusters there are additional subclumps such as M31 + M32 + NGC 205 triplet, the NGC 147 + NGC 185 binary, and the LMC + SMC binary (van den Bergh 2006). For the entire Local Group one finds, at the 99% confidence level, that low luminosity early-type dSph galaxies are more concentrated in subclumps than late-type dIrr galaxies. In other words, most dIrr galaxies appear to be free-floating members of the Local Group, whereas the majority (but not all) of the dSph galaxies seem to be directly associated with either M31 or the Galaxy. It seems quite possible (Skillman et al. 2003) that the faint dIrr and dSph galaxies have similar progenitors, and the observed differences between them are due to environmental factors favouring gas loss from those dwarfs that occupied dense environments, i.e., near giant galaxies.

No diffuse X-ray emission has been detected in the LG dwarf irregulars (Fabbiano 1989; Gizis et al. 1993; Markert and Donahue 1985). This is not surprising: if hot gas was produced during periods of active star formation in any LG dwarf, it would have been rapidly expelled from the galaxy and faded to invisibility. However, Jeltema and Profumo (2008) present the first systematic study of X-ray observations of local dwarf spheroidal galaxies aimed at the search for WIMP dark matter. Their results indicate that X-ray observations of dwarf galaxies currently constrain dark matter models at the same level as or even more strongly than gamma-ray observations of the same systems.

1.3 Age indicators

Mateo (1998) provides a nice summary of specific evolutionary phases that have been proven especially useful as age tracers in the dwarf galaxies in the Local Group. Figure 1.2 shows where these age groups are located on the Hertzsprung-Russell diagram. Below is given a short description of these evolutionary phases.

Wolf-Rayet stars These high mass stars signal vigorous star formation during the past 10 Myr. The frequency of Wolf-Rayet stars depends on mass-loss rates, metallicity, the star-formation rate for high-mass stars, and the high-mass end of the initial mass function. Among LG dwarfs, only IC 1613, NGC 6822 and IC 10 are known to contain Wolf-Rayet stars.

Blue-loop stars Stars of intermediate mass evolve through prolonged 'blue loops' after they ignite He in their cores. The luminosity at which the loops occur depend principally on the mass of the star, though the color and extent of

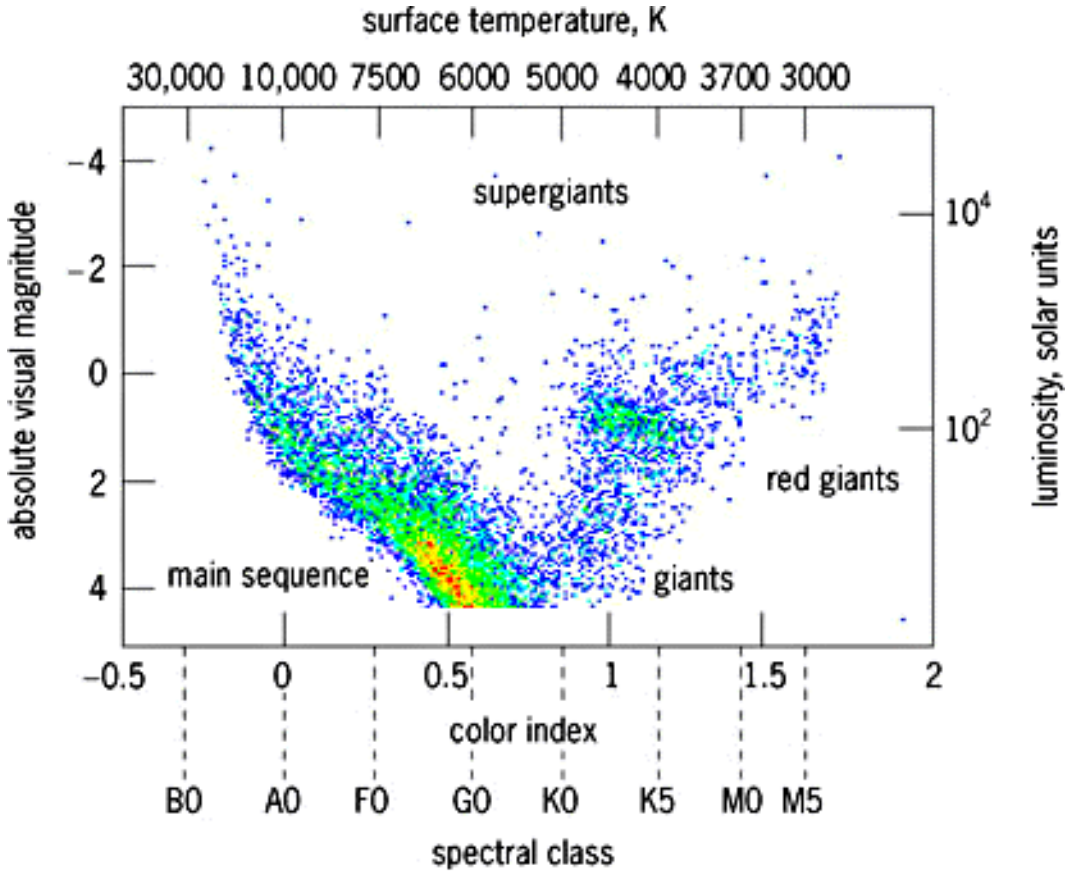

Figure 1.2: Hertzsprung-Russell diagram, showing the main evolutionary phases accessible for LG galaxies.

the loop is critically sensitive to metallicity. For stars ranging in age from 100-500 Myr, the loop luminosities fade monotonically with age.

Red supergiants Red supergiants also fade monotonically with age for populations ranging from about 10-500 Myr in age. However, these stars exhibit a moderate spread in luminosity at a given age. For a composite system such as a dwarf galaxy - the red-supergiant luminosity function will contain stars exhibiting a range of ages at a given luminosity. Both the blue-loop and red supergiant phases are short-lived, and therefore subject to added uncertainties from the stochastic nature of star formation, particularly in dwarfs.

Asymptotic giant branch (AGB) stars The AGB are referred as the 'red tail' extending redward from the red giant branch. Although ages for AGB stars probably cannot be determined to better than a factor of 2-3, they often provide

our only constraint on stellar populations older than ≈ 1 Gyr in many distant galaxies within and beyond the Local Group. Long-period variables are often found among luminous AGB stars.

Red giant branch (RGB) stars The RGB plays an important role in understanding the chemical enrichment histories of dwarf galaxies, largely because its properties are relatively insensitive to age. Unfortunately, for a given metallicity, stars spanning a large age range are funneled into a very narrow corridor within optical color-magnitude diagrams. The RGB serves only as a relatively crude age indicator for populations older than 1 Gyr. Long-period variable stars are found near the upper tip of the RGB.

Red-clump (RC) and horizontal branch (HB) stars The He core burning phase occurs in a 'red clump' located at the base of the RGB for populations with ages in the range 1-10 Gyr. The clump evolution in luminosity ($\lesssim$ 1 mag) and color ($\lesssim$ 0.5 mag) is small even for large age differences. Horizontal branch (HB) stars signal the presence of ancient populations ($\gtrsim$ 10 Gyr). RR Lyr stars are an easily identified example of HB stars; blue HB stars are also distinctive but are known to exist in only two LG dwarfs (Carina and Ursa Minor). The red HB is also indicative of an old population, but distinguishing it from the red clump in an intermediate-age population can be difficult.

Subgiant branch stars Stars with main-sequence lifetimes longer than about 2-4 Gyr evolve slowly towards the RGB after they exhaust hydrogen in their cores resulting in a well-populated sub-giant branch below the luminosity of the HB/red-clump stars. At a given metallicity, the minimum luminosity of subgiant branch stars fades monotonically with increasing age.

Main-sequence stars The main sequence (MS) is the only evolutionary phase present in populations of all ages. Unlike the SGB, the maximum luminosity of the MS (the main-sequence turnoff) fades with increasing age. When an age spread is present, older populations can be hidden by the unevolved main-sequence stars of younger populations. However, used in conjunction with the SGB, the MS provides the only method of determining ages for populations older than 1-2 Gyr with ≈ 1 Gyr resolution. The main sequence has one particularly useful feature: the maximum luminosity on the main sequence can always be related to the age of the youngest population at the precision of sampling uncertainties.

It has to be noted, however, that not all of the above age indicators are observed in all of the galaxies in this study. The MS is the only evolutionary phase present in populations of all ages. At the distances of the galaxies in

the LG only the upper part of the MS is accessible. Other evolutionary phases observed in LG dwarf galaxies include red clump and horizontal branch stars, red supergiant and asymptotic giant branch stars, as well as red supergiant stars.

Chapter 2

Methodology and Theoretical Models

2.1 Methodology

To determine approximately the shape and the stellar density distribution of the galaxies we used two approaches. First, star counts were performed in a rectangular grid and isodensity contour maps were obtained. They show the overall shape of the galaxies and offer an initial insight into their spatial distribution. After that radial surface density profiles (RDPs) were used to obtain the radial distribution of the stars in the galaxies. The RDPs were then compared to existing theoretical models. A more detailed description of each of these steps is provided below.

2.1.1 Isopleth Maps

The star counts were performed in a rectangular grid. The data coordinate range was divided using a grid in Right Ascension and Declination. The size of the grid cell was different for the various stellar populations. It was chosen in such a way as to include a sufficient number of stars and also to provide enough detail for the isopleth contour maps. Then the number of stars in each cell was counted and a contour map was created which describes the surface density of the stars. The contours in these maps trace areas with equal stellar density.

The contour maps were created using the CONTOUR procedure in IDL[1] programming language for data analysis. The galaxies inclination were not taken into account and no corrections were applied for projection effects. Figure 2.1

[1]Interactive Data Language, `http://www.ittvis.com/`

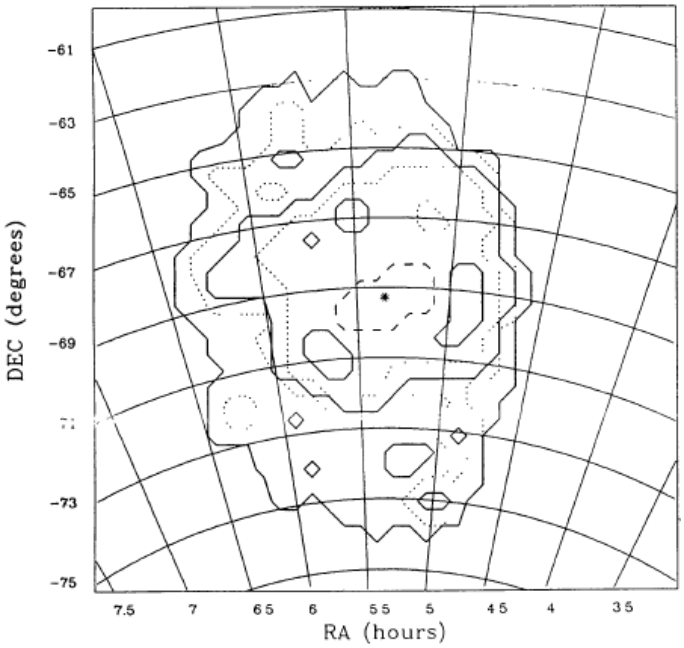

Figure 2.1: An example for an isopleth map. Number surface density contours of the LMC clusters from Kontizas et al. (1990). The asterisk marks the LMC optical centre.

is an example of an isopleth map, it shows the number surface density of star clusters in the LMC obtained by Kontizas et al. (1990).

For estimating the foreground contamination by Galactic stars we used the Besançon Galaxy Model (Robin et al. 2003). Areas were selected around the specific galaxy and the stellar density was compared with the stellar density given by the Besançon Model. The lowest contour levels are selected to have a value higher than the stellar density given by the Besançon model.

2.1.2 Radial Density Profiles

Radial density profiles (RDPs) were used to obtain the projected stellar density distribution of the galaxies. The RDPs correspond to the projected radial number density (i.e. the surface density) of objects contained in concentric rings around the galaxy centroids. The underlying assumption for this kind of analysis is that the structures should present an important degree of radial symmetry. For the Magellanic Clouds this is not always the case, but RDPs can still be used as probes of the radial distribution of the various objects averaged over all azimuthal directions, hence of the large-scale structure.

The area around each galaxy was divided in concentric annuli of increasing radii outwards and the number of stars within each annulus was determined. The number of stars per unit area in each annulus gives the stellar density, corresponding to the mean distance from the centre of the galaxy. The so derived density profiles for each age and/or object group are compared with existing theoretical models. This allows us to obtain some representative structural parameters, which describe the spatial distribution of the specific age and/or object group. The theoretical models used are further described below.

Sérsic Law

The $R^{1/4}$-law was introduced by de Vaucouleurs (1948) to describe the projected luminosity density (or surface brightness) $I(R)$ of elliptical galaxies. It has no free parameters and depends on two well defined physical scales: a characteristic linear scale, R_e, and a luminosity density factor, I_0. The surface brightness of elliptical galaxies is well fitted by the $R^{1/4}$-law. de Vaucouleurs and Capaccioli (1979) have shown that the surface brightness of NGC 3379 (an E1 galaxy) is fitted over 10 magnitudes and more than two decades in radius by such a law. New fits made by Capaccioli et al. (1990) based on fresh data are in excellent agreement with the previously cited results. However, Makino et al. (1990) stated that in the range of radii usually investigated in the observations, $R^{1/n}$-law models are practically undistinguishable from the de Vacouleurs law, for $3 \leq n \leq 10$, and then that the universality of the $R^{1/4}$-law is only apparent.

The $R^{1/n}$-law models can be defined as a one-parameter family of stationary, spherical stellar systems, with surface brightness profile generalizing the de Vaucouleurs law in the following way (Sérsic 1963):

$$\ln I(R) = \ln I_0 - b\eta^{1/n}. \tag{2.1}$$

I_0 is the central surface brightness and $\eta = R/R_e$, where R_e is the *effective radius* (i.e. the projected radius inside which the projected luminosity, equals half of the total luminosity). The curvature controlling parameter n is a positive real number, while b is a dimensionless parameter whose value is determined by the definition of R_e.

Ciotti (1991) investigates the dynamical properties of $R^{1/n}$-law models focusing on the following questions: i) is the property of an exponential differential energy distribution a characteristic of stellar systems following the de Vaucouleurs law or is it a more common feature of the sufficiently concentrated stellar systems, as $R^{1/n}$-law models with $n > 1$ and ii) if this is the case, is there a significant physical property that characterizes the de Vaucouleurs law among the $R^{1/n}$-law models?

The results of Ciotti (1991) suggest that the distribution function is nowhere negative in the phase space for spherical, isotropic $R^{1/n}$ stellar systems with $2 \leq n \leq 10$, i.e. these systems are physically admissible. Moreover, they are also stable to both radial and nonradial perturbations. The exponential behaviour of the differential energy distribution is a common property of all the $R^{1/n}$-law models. Thus, it is really an efect of the central concentration. The special property shown by the $R^{1/4}$-law is that the mass fraction corresponding to the Boltzmannian zone is maximized. Models with lower concentration than the de Vaucouleurs law are depressed in the external part of the normalized differential energy distribution with respect to a pure Boltzmann law. Models with higher concentrations have too high a differential energy distribution. Generally in a stellar system, most of the mass is bound at higher energies, i.e. near the tidal radius.

Márquez et al. (2000) have shown that the observational data for galaxies belonging to clusters confirm the hypothesis that their specific entropy is, to first order, unique. As a consequence, the galaxies tend to stay in a thin plane (the Entropic Plane) in the space of the Sérsic light profile parameters. They have also shown that, besides the Entropic Plane, another relation must exist between the Sérsic profile parameters of galaxies. The intersection of this relationship with the Entropic Plane defines a curve in the 3D Sérsic parameter space which appears very well defined in their data. After further investigation Márquez et al. (2001) confirm the fact that elliptical galaxies lie on a line in the three dimensional space of the Sérsic parameters. This fact, they believe, implies that elliptical galaxies are indeed a one-parameter family.

The left panel of Figure 2.2 shows the Sérsic profiles with index $n = 1$ to 10, plotted as magnitudes $(\mu - \mu_e)$ and log radius $(\log R/R_e)$. In the current study we use the exponential-disk model to fit the stellar density profiles of stellar populations in nearby dwarf galaxies and to determine their structural parameters. This exponential law is a case of Sérsic law with n=1 and b=1.67.

King Law

King (1962) re-examines the density distribution in globular clusters and finds an empirical formula that represents the density from centre to edge in globular clusters of all degrees of central concentration. Galactic clusters and Sculptor-type dwarf galaxies also appear to follow the same density law.

In his Figure 1 he presents the star counts in M15, both scales are logarithmic. On such a plot any simple power law would be a stright line. Far from straghtening out, however, these points plunge more and more steeply with increasing r, suggesting that the surface density f actually drops to zero at some finite value

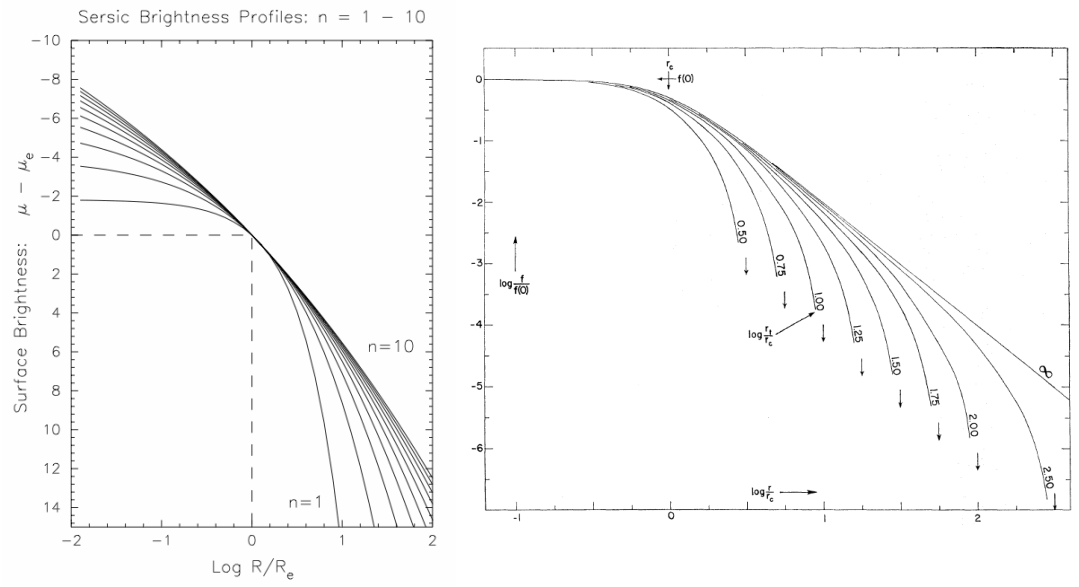

Figure 2.2: Left: Sérsic profiles with index n = 1 to 10, plotted as magnitudes ($\mu - \mu_e$) and log radius ($\log R/R_e$) from `http://www.astro.virginia.edu`; Right: Standard curves calculated from Equation 2.4. Here r_c is the core radius and r_t is the limiting radius, r is the distance from the centre. Diagram is taken from King (1962).

of r. After some experimentation the following form was obtained

$$f = f_1 \left(1/r - 1/r_t\right)^2, \tag{2.2}$$

where f_1 is a constant and r_t is the value of r at which f reaches zero.

For the central regions of a globular cluster, however, Eq. 2.2 is completely inadequate. The surface density in the inner parts of a concentrated cluster can be represented by the formula

$$f = \frac{f_0}{1 + \left(r/r_c\right)^2}, \tag{2.3}$$

where f_0 is the central surface density and r_c is a scale factor that may be called the core radius.

The single formula that embodies the characteristics of both Eq. 2.2 and Eq. 2.3 is

$$f = k\left[\frac{1}{\sqrt{1 + \left(r/r_c\right)^2}} - \frac{1}{\sqrt{1 + \left(r_t/r_c\right)^2}}\right]^2. \tag{2.4}$$

The density law has three parameters: a number factor k, a core radius r_c, and a limiting radius r_t. The core radius is determined by the internal energy of the system, while the limiting radius is set by external tidal forces. The right panel of Figure 2.2 shows the standard curves calculated from this law for various values of the concentration parameter $c_p = \log(\frac{r_t}{r_c})$.

The observed density law suggests that all these systems have been subjected to some relaxation process. It is suggested that all have been relaxed by initial mixing and that stellar encounters thereafter produce a slow change in the density parameters without changing the basic model. It does not seem likely that cluster expansion through stellar mass loss is a major factor in the relaxation.

The data considered by King (1962) do not include any young galactic clusters; nor do they establish whether equipartition exists in a system whose age is less than its time of relaxation. Relative to the other systems considered, giant elliptical galaxies have an excess of brightness near the centre. It is suggested that this results from equipartition in a system dominated by dwarf stars.

2.2 Profile Fitting

A conventional first approach to describe the spatial distribution of various stellar populations in the Magellanic Clouds from the RDPs is to use an exponential-disk profile

$$f(r) = f_{0D} \times exp\left(-\frac{r}{h_D}\right), \tag{2.5}$$

where h_D and f_{0D} are the scale length and the central density of objects respectively and r is the distance from the centre.

As a second approach we use a King-like profile based on the King law (King 1962),

$$f(r) = f_{0K}\left(\frac{1}{\sqrt{1+\frac{r^2}{{r_c}^2}}} - \frac{1}{\sqrt{1+\frac{{r_t}^2}{{r_c}^2}}}\right)^2 \tag{2.6}$$

where r_t and r_c are the core and tidal radii respectively, f_{0K} is the central projected density of objects and r is the distance from the centre.

The empirical density law is derived for globular clusters but in the same article King (1962) also tested it in the cases of galactic, or open, clusters (M67, NGC 188, NGC 7789) and dwarf elliptical galaxies. The law only fails in the case of the more luminous elliptical galaxies such as M32. Hodge (1961a,b, 1962) show that the observed limiting radii for the Fornax, Sculptor, and Leo II dwarf galaxies are in agreement with those to be expected as a result of the tidal force

of the Milky Way. The law also applies to dwarf spheroidal galaxies - systems in dynamical equilibrium tidally truncated by the external gravitational field of the host galaxy.

The best fitting profiles are found by performing a Levenberg-Marquardt least-squares fit to the considered functions. This fit was performed with IDL, with the use of the MPFIT program (Markwardt 2009). MPFIT is a translation into IDL of the non-linear least squares fitting program MINPACK-1. The resulting fitting engine provides all of the original MINPACK-1 capability and is optimized for speed within IDL with the added functionality within the semantics of IDL.

Chapter 3

The Gaia Satellite Mission

By the second half of the 18th century those in the forefront of celestial research were considering methods for measuring the distances to the stars. The most direct way of measuring the distance of an object that can't be reached is through triangulation: using a known-length baseline and measuring the difference in direction when the object is observed at either end of this baseline. This difference is called the parallax of the object; the smaller the parallax, the greater the distance. The largest baseline astronomers have readily available is the diameter of the orbit of the Earth around the Sun.

Measurement accuracies at the end of the 18th century were around several arcseconds with which it was not possible to detect stellar parallaxes. However, this did allow the discovery detection of aberration and nutation, and the confirmation of the finite speed of light. What had also been detected were the so-called proper motions of stars: although the positions of the stars on the sky appear fixed over an individual lifetime, they were actually observed to be moving, though very slowly. It was one of the stars which showed a relatively large proper motion, 61 Cyg, which led to the detection of the first parallax in the middle of the 19th century by Bessel. Bessel had correctly argued that stars showing large proper motions were more likely to be among the closest to the Sun. Bessel used a special telescope: a Heliometer built by Fraunhofer, an instrument designed for very accurate position measurements. In some ways this instrument prefigures the technique used 140 years later on the Hipparcos satellite: cut the objective or main mirror in two, and allow each half to project a different part of the sky on the same detector. By measuring differential rather than absolute positions, very precise relative measurements could be obtained.

In the Heliometer used by Bessel the relative positions of two stars were measured through shifting one half of the objective with respect to the other half such that images of the two stars would coincide. The shift applied to the lens was a measure of the distance on the sky between the two stars. Assuming one

star to be relatively nearby, and the other relatively far away, this difference will primarily show the displacements of the nearby star. Those displacements are the proper motion linear as a function of time and a motion induced by the Earth's motion around the Sun, which describes a small ellipse over a year. Bessel concluded that the parallax of 61 Cyg A was 314 ± 20 mas (compared to the current best estimate of 287.18 ± 1.51 mas).

An important development that led to significant improvements of measurement precision was the introduction of photographic plates and subsequently of measuring machines to extract the positional information from those plates. Two main driving forces led to the subsequent development of space astrometry: the need to be able to observe the entire sky with one instrument, and the need to measure absolute rather than differential parallaxes. With the introduction of novel observing techniques, which had been pioneered on transit instruments by Erik Høg in the 1960s, a mission emerged that would be capable of measuring around 100 000 stars over a 30 months period: the Hipparcos astrometric mission was born. Hipparcos was designed as a survey satellite, scanning each part of the sky in at least two directions every six months.

The Hipparcos Catalogue was not yet published when the scientists involved in finishing the data processing were already thinking of a new, much more ambitious space mission combining a high-accuracy astrometric and photometric survey of faint stars. Without invoking too much change from the Hipparcos concept it was clear that CCD detectors had reached a level of maturity to allow a change from the old technology of photomultipliers used in Hipparcos into the more efficient and space qualified electronic detectors available in 1995. Gaia was approved by ESA's Science Programme Committee in 2000, and redesigned in 2002.

Unlike HST and SIM, which are pointing instruments observing a preselected list of objects, Gaia is a scanning satellite that will repeatedly survey in a systematic way the whole sky, tying together without regional errors widely separated sources. Beyond sheer measurement accuracy, a major strength of Gaia follows from (i) its capability to perform an all-sky and sensitivity limited absolute astrometric survey, (ii) the unique combination into a single spacecraft of the three major electronic detectors carrying out nearly contemporaneous observations, (iii) the huge number of objects and observations which allow the accuracy on single objects to be achieved on very large samples, thus yielding statistical significance. This last feature is immensely valuable for astrophysics.

3.1 The Payload

The Gaia payload consists of three distinct instruments mounted on a single optical bench (see Figure 3.1). Gaia has two telescopes with two associated

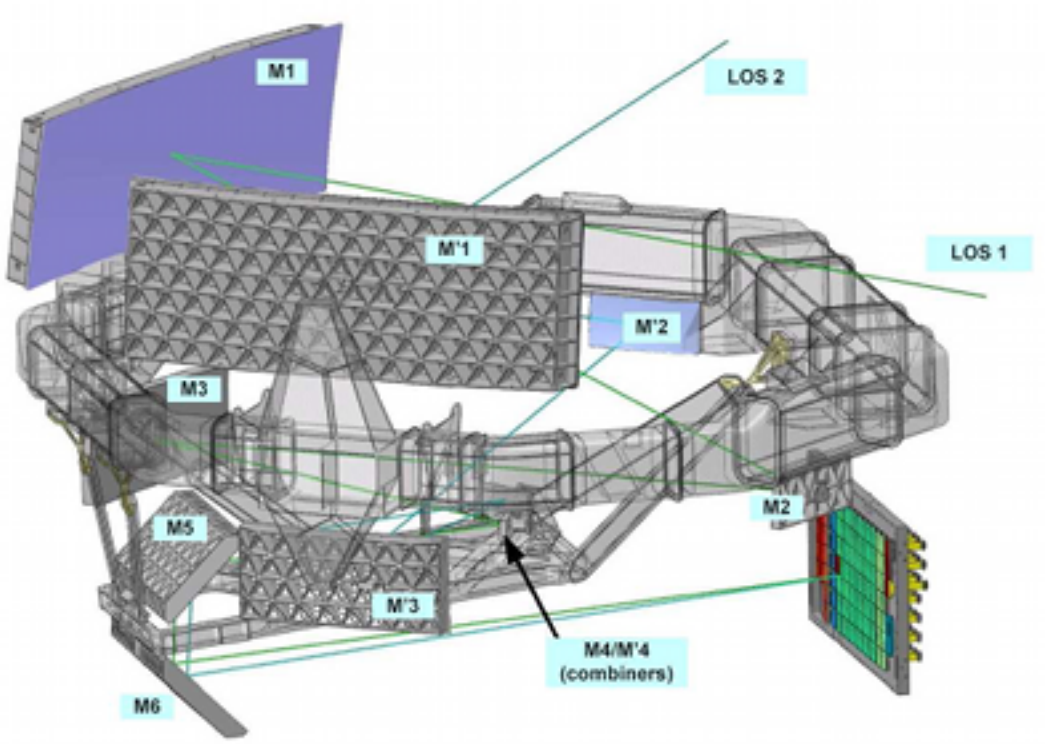

Figure 3.1: Gaia's optical bench. The 3-metre diameter, quasi-octagonal torus, which will support the two Gaia telescopes and the focal plane assembly, is composed of 17 individual custom-built Silicon Carbide segments. M1 through M6 are the mirrors, LOS1 and LOS2 are the two lines-of-sight. Image courtesy of EADS Astrium.

viewing directions of size 0.7° × 0.7° each. The two viewing angles are separated by a highly-stable 'basic angle' of 106.5°. The two field of views are combined into a single focal plane covered with CCD detectors (DPAC 2007).

The spacecraft operates in a continuously scanning motion, such that a constant stream of relative angular measurements is built up as the fields of view sweep across the sky. High angular resolution (and hence high positional precision) in the scanning direction is provided by the primary mirror of each telescope, of dimension 1.45 × 0.5 m^2 (along scan × across scan). Figure 3.2 shows the focal plane array. Each coloured rectangle indicates one CCD of approximately 4 × 6 cm size. The direction of star image motion is indicated at the bottom. It takes a star image about 4.4 sec to cross one of the CCDs and this defines the effective exposure time for the individual scientific observations.

The astrometric field (AF) in the focal plane is sampled by an array of 62 CCDs, each read out in TDI (time-delayed integration) mode, synchronised to

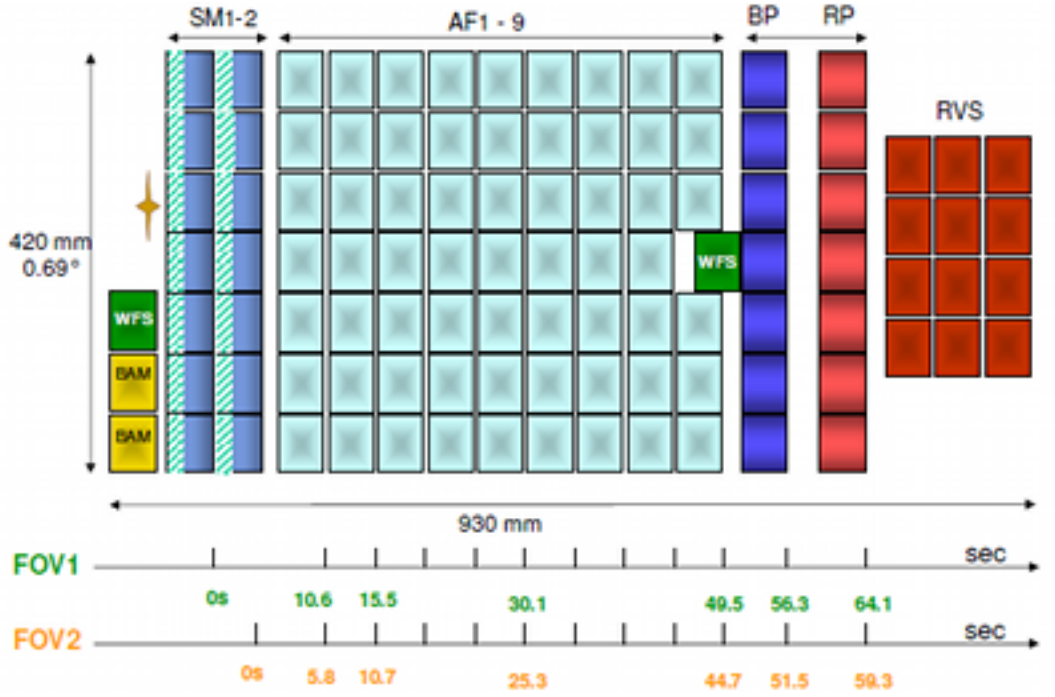

Figure 3.2: The Gaia Focal Plane Array. Each coloured rectangle indicates one CCD of approximately 4 × 6 cm size. The various acronyms denoting the scientific instruments of Gaia are explained in more detail in the text. In addition, there are detectors for auxiliary instruments: the basic angle monitoring (BAM) system and the wavefront sensors (WFS). The two bottom lines give the time to reach the different parts of the field from SM1 or SM2 (DPAC 2007).

the scanning motion of the satellite. In practice, stars entering the combined field of view first pass across dedicated CCDs which act as a 'sky mapper' - each object is detected on board and information on its position and brightness is processed in real-time to define the windowed region read out by the following CCDs. Gaia's limiting magnitude is about 20th magnitude and all objects brighter than this limit at the epoch of observation will be measured.

Before stars leave the field of view, spectra are measured in three further sets of dedicated CCDs. The BP and RP CCDs - BP for Blue Photometre and RP for Red Photometre - record low-resolution prism spectra covering the wavelength intervals 330–680 and 640–1000 nm, respectively. These simultaneous semi-photometric measurements of the spectral energy distribution yield key astrophysical information, such as temperatures, gravities, metallicities and reddenings for each of the vast number of objects observed. In addition to the low-resolution photometric instrument, Gaia features a high-resolution integral-

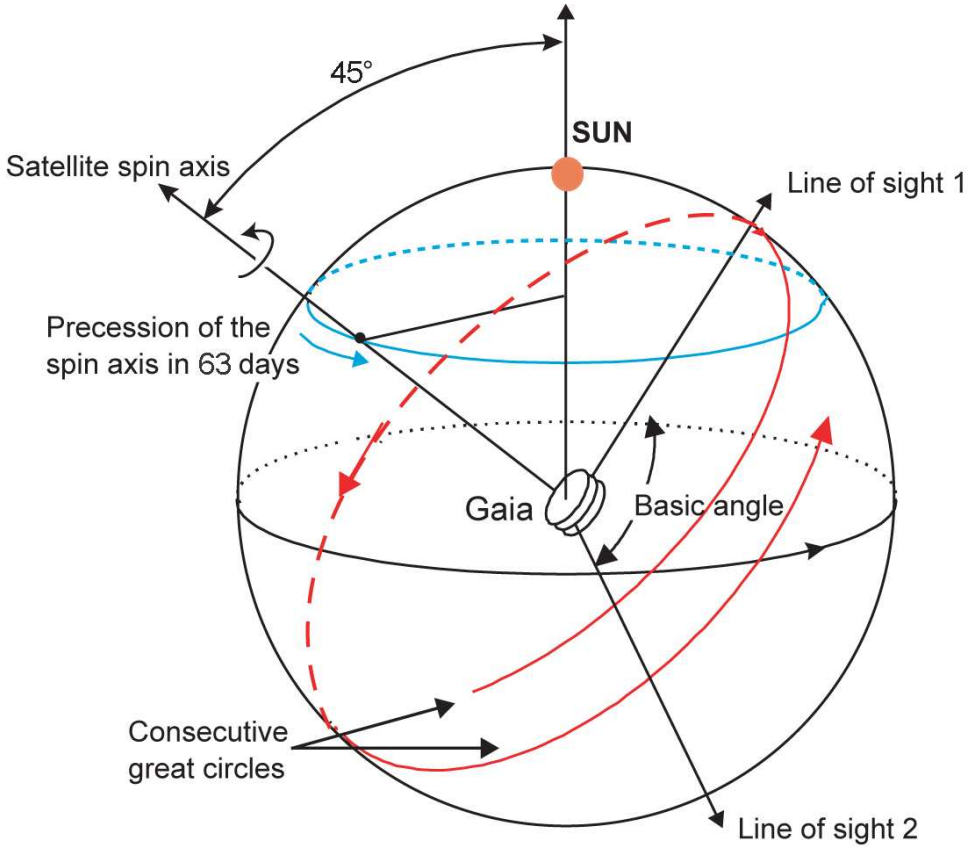

Figure 3.3: Gaia's two fields-of-view scan the sky according to a carefully prescribed 'revolving scanning law'. The constant spin rate of 60 arcsec s^{-1} corresponds to 6-hour great-circle scans. The angle between the slowly precessing spin axis and the Sun is maintained at 45°. The basic angle is 106.5°. Schematic courtesy of J. de Bruijne (ESA/ESTEC).

field spectrograph, the so-called Radial Velocity Spectrometre (RVS) instrument. The RVS provides the third component of the space velocity of each star down to about 17th magnitude.

The whole sky is systematically scanned so that observations extending over several years yield some 50-100 sets of relative measurements for each star. Figure 3.3 shows the way Gaia's two fields-of-view scan the sky. A 5-year mission permits the determination of additional parameters, for example those relevant to orbital binaries, extra-solar planets and solar-system objects.

3.2 The Science Case

The immediate objectives of space astrometry are, in principle, the same as those of ground based astrometry: to determine the apparent positions of celestial bodies over time and derive from them astrophysically important parameters such as distances, proper motions and motions within double and multiple star systems. However, the current generation of CCD-based astrometric instruments can also be used as stable photometres to acquire photometric measurements. Such an approach has appeared in every proposal of a scanning mission having astrometry as a first goal. Whereas the direct product of the Gaia mission will be a highly accurate astrometric and photometric survey down to V = 20 mag, the science goals are much broader and account for the support of a large scientific community and include mapping the Galaxy in three dimensions (parallaxes, positions, extinction), galactic kinematics (proper motions and radial velocities), formation and evolution of the Milky Way, stellar physics (classification, M, L, $\log g$, T_{eff}, $[Fe/H]$), distance scale (geometric distances to Cepheids and RR Lyrae stars, HR diagram), age of the Universe (cluster diagrams, distances, luminosities), dark matter (stars as tracers of gravitational potential), reference frame (quasars, absolute astrometry), extrasolar planet detection ($\sim M_J$, astrometry and photometric transits), fundamental physics (relativistic parameters $\gamma \sim 5 \times 10^7, \beta \sim 5 \times 10^{-4}$), and solar system science (taxonomy, masses, orbits for 5×10^5 bodies).

Gaia will create the largest and most precise three-dimensional map of our Galaxy by providing unprecedented positional and radial velocity measurements for about one billion stars in our Galaxy and throughout the Local Group (Perryman et al. 2001). The detection of stars is expected to be complete to V = 20 mag (astrometry + photometry), but the radial velocities will not be measured for stars fainter than V = 17.5 mag. The astrometric precision should be 25 μas at V = 15 mag and the distances will be known with a precision better than 10% for hundreds of millions of stars.

Stellar Physics

Gaia will provide accurate distances to massive numbers of stars, which combined with photometric and other data give luminosities, surface temperatures, abundances, masses and ages for very many stars. The availability of high-precision fundamental data for large stellar samples, including rare objects (such as extremely metal-poor stars and rapid evolutionary phases), will greatly advance the theoretical modelling of stellar interiors. Multi-epoch, multi-colour photometry of all stars brighter than 20 mag plus multi-epoch spectral information for the 20 million brightest stars, will provide a description of stellar stability and variability across the HR diagram.

Gaia will be able to resolve binaries with an apparent separation of less than 20 mas. The Radial Velocity Spectrometre (RVS) will observe about 10^6 spectroscopic binaries and about 10^5 eclipsing binaries. Of these 10^5 eclipsing binaries, 25% will be double-lined spectroscopic binaries (SB2) for which it will be possible to derive the masses of the two components (Söderhjelm 2005).

Galactic structure and evolution

The Galaxy could be considered as the primary science target of the Gaia mission. For the brightest stars our kinematic knowledge will be complete, and these include important tracers: the radial velocities of K giants as far as ~ 20 kpc will be measured with a precision better than ~ 10 km s^{-1}; the kinematics of stars at the tip of the red giant branch together with asymptotic giant branch stars and CH-type carbon stars will be observable to ~ 50 – 75 kpc in the outer halo; the brightest and youngest stars in the spiral arms will have radial velocity precisions better than ~ 5 km s^{-1} up to ~ 2.5 kpc (for a B5V star).

Extrasolar planets

Currently more than 200 planets have been detected around nearby stars, almost all of them from the radial-velocity variations induced in their parent stars. The spectroscopic method is, however, limited by the number and types of stars that can be surveyed and its bias to short orbital period companions. In contrast, Gaia will survey hundreds of thousands of nearby stars for planetary companions using the astrometric variation of stellar position (Lattanzi et al. 2000). The astrometric method is applicable to all spectral types, allows unambiguous determination of orbital inclinations and planetary masses, and is more sensitive to longer orbital periods (up to 510 years).

General Relativity

At an accuracy of a few μas, relativistic effects can no longer be considered as small corrections to a Newtonian model and General Relativity becomes a fundamental part of the mathematical framework for the data processing (Klioner 2003). Gaia appears capable of measuring departures from the General Relativity value ($\gamma = 1$) of the PPN parameter γ of the order of a few parts in 10^{-7} (Vecchiato et al. 2003). These accuracies compare quite favourably with recent findings of scalar-tensor cosmological models, which predict for γ a present-time deviation from the General Relativity value between 10^{-5} and 10^{-7}. Combining millions of measurements will map these effects to unprecedented accuracy.

Solar System

Solar System objects appear in the Gaia proposal at a high level in the science program achievable within the current design, with a relevance to virtually all categories of minor planets. Solar System studies will receive a massive impetus through the repeated observations of several hundred thousands of minor planets of every type (main belt, Trojans, near-Earth and trans-Neptunian objects). Gaia will observe a given asteroid about 15 times per year with an accuracy better than 1 mas (per observation), 500 times better than that of most present large surveys.

3.3 Impact of Gaia on the Local Group

Due to the spatial resolution of Gaia nearby galaxies will be resolved in stars. Kučinskas et al. (2003) believe that of the many methods available for dating stellar populations in nearby galaxies only a few are directly applicable to Gaia. Although the traditional approach of tracing star formation histories with turn-off stars will be limited in terms of distance and/or reddening (~3 kpc), it is possible that stars on the RGB/AGB will provide an alternative for extending these limits.

An important contribution of Gaia will be proper motions (precise parallaxes of late type giants, $\sigma(\pi)/\pi \leq 0.1$, will not be available beyond ~10 kpc). Proper motions of individual giants and supergiants in Local Group galaxies will allow to discriminate between the member and field stars (Kucinskas et al. 2005). However, the accuracy may not be sufficient for detailed kinematical studies of individual galaxies which will require the precision in proper motions of 1-2 km s^{-1} see, e.g. Wilkinson et al. (2002). Proper motions of individual stars in Local Group galaxies will be also feasible with future wide-field instrumentation (e.g., with PanSTARSS), with the time spans between the measurement epochs of $\sim 5-10$ years possible already in 2010-2015 (though the accuracies will be lower than those obtained with Gaia).

Radial velocities will be considerably more difficult with Gaia, as sufficient precision may be achieved only for stars brighter than $V \sim 17$, or up to the distances of ~ 40 kpc (~ 80 kpc with AGB stars, M_V = -2.5). Indeed, bright supergiants may be accessible at considerably larger distances, however, they will be available only in a few galaxies, as stellar populations in the majority of nearby Local Group galaxies are old, showing no signs for recent star formation (Aparicio 2002). Moreover, their numbers will be too scarce to perform a detailed kinematical analysis.

With their high sensitivity and large FOVs, other instruments will be serious competitors for Gaia, especially if backed-up with the capability for multi-colour

medium-band photometry and multi-object spectroscopy. However, the superiority of Gaia will be in the high accuracy and homogeneity of its data. Gaia will provide precise information both on kinematical and astrophysical properties of individual stars, obtained with a single, stable and well-calibrated instrument. Moreover, the data will be acquired in the same instrumental system as for the millions of stars in the Milky Way. This will deliver an unique and homogeneous data set, which will allow to perform a comprehensive and in-depth analysis of the formation and evolution of the Local Group galaxies.

Different explanations for the dynamical behaviour of the LMC/SMC, in particular whether these systems are gravitationally bound to our own Galaxy, implies systematic proper motions of below $\sim$ 1 mas yr^{-1}, which was very much at the limit of the Hipparcos capabilities. Large numbers of stars measured in the LMC/SMC at the level of 50 μas or better, would clarify their dynamical relationship with our own Galaxy (Perryman et al. 1997).

3.4 Data Processing and Analysis Consortium

Following Gaia's launch data will be transmitted by the spacecraft from its vantage point around L2 at a few Mbps for at least five years, delivering to the ground station an uncompressed raw data set of approximately 100 TB. Scientifically valuable information will be encased in this continuous data stream resulting from the collection of photons in the approximately 100 on-board CCDs in the astrometric, photometric and spectroscopic fields of Gaia. However in its original telemetry format the data is totally unintelligible to scientists, not only because it is squeezed into packets by the numerical coding but, more significantly, because of the way Gaia scans the sky, picking up fragments of the astrometric parameters at each transit of the one billion plus observable sources in the sky. Therefore a large and complex data analysis must follow this raw harvest in order to decipher Gaia's signal and translate it into positional and physical parameters useful to scientists to probe the very nature of astronomical objects.

To cope with this challenge the scientific community, together with ESA, started a joint effort to set up a data processing ground segment comprising a single processing pipeline which will deliver the intermediate and final mission science products. The Data Processing and Analysis Consortium (DPAC) is a European collaboration including the ESA Gaia Science Operations Centre (SOC) and a broad, international science community of over 320 individuals, distributed in more than 15 countries, and including six large Data Processing Centres (DPCs). It was proposed in response to ESA's Announcement of Opportunity for the ground-segment data processing of the Gaia data (DPAC 2007).

The Consortium is structured around a set of eight Coordination Units (CUs)

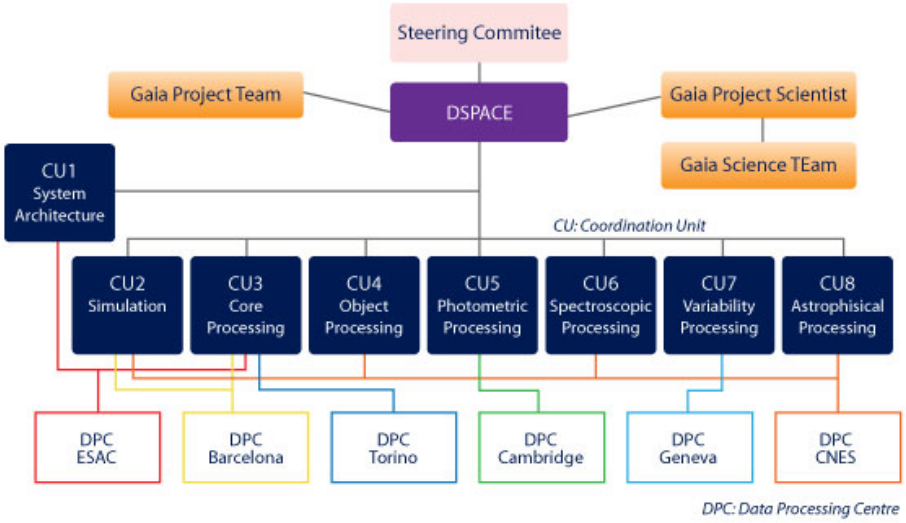

Figure 3.4: DPAC Coordination Units (CU) and Data Processing Centres (DPC). Schematic from `http://www.altecspace.it/?page_id=650`.

each in charge of a specific aspect of the data processing (see Figure 3.4). The CUs are the building blocks of the Gaia DPAC. They are reasonably small in number, with clearly-defined responsibilities and interfaces, and their boundaries match naturally with the main relationships between tasks and the associated data flow. Responsibilities of the coordination units include: (i) defining data processing tasks and assigning responsibilities; (ii) establishing development priorities; (iii) optimizing, testing and implementing algorithms; (iv) verifying the quality of the science products. Each coordination unit is headed by a scientific manager assisted by one or two deputies and, where appropriate, a technical manager. The management team of each CU is responsible for acquiring and managing the resources needed for their activities. While the CUs are primarily structured for software development, all of them are closely associated with at least one DPC where the algorithms will be implemented for the data processing in the operational phases.

The catalogue production for Gaia was understood to be covered by an Announcement of Opportunity to be issued at some later point in time. Thus, the DPAC was concentrated on the data processing to produce the science products, not wishing to divert effort to considerations of how the catalogue will be presented. Currently a Gaia Archive Preparation Unit is foreseen which will be responsible for the catalogue access and the scientific exploitation.

Part II

The Magellanic Clouds

In Part II are presented the results from modelling the stellar populations of the Magellanic Clouds, expected to be resolved in stars by ESA's satellite Gaia.

The Magellanic System is descibed in details in Chapter 4. It consists of two dwarf irregular galaxies, the Large Magellanic Cloud and the Small Magellanic Cloud, as well as two structures related to the Clouds - the Bridge connecting both Magellanic Clouds, and the Magellanic Stream - a narrow band of neutral hydrogen gas which extends about 100 degrees from the inter-Cloud region.

The data used for the investigation of the spatial distribution of the Clouds' stellar populations is presented in Chapter 5. Observational data in the optical and near-infrared part of the spectrum are used. The sources include all-sky surveys, wide area surveys, as well as catalogues of specific types of objects, in this case carbon stars.

The spatial distribution of the stellar content of the Magellanic Clouds is studied using isopleth (isodensity) maps and radial surface density profiles. In Chapter 6 are presented these isopleth maps of the Large and Small Magellanic Clouds, their radial density profiles obtained from the data sources presented in Chapter 5. Moreover, the spatial distribution of both Clouds is discussed and compared to results from previous studies.

Chapter 4

The Magellanic Clouds System

Although the Magellanic Clouds were observed for centuries by the people of the southern hemisphere, it was not until the 13th century that they came to the attention of the northern hemisphere inhabitants. By the 19th century serious astronomical studies of the Clouds were being done. However, progress in Magellanic Clouds research in the first half of the 20th century was slow.

By the 1950's and 1960's developments in stellar and galactic astronomy helped to precipitate a strong new interest in the Magellanic Clouds. Stellar evolution and the meaning of stellar populations was finally becoming understandable and the Clouds offered a myriad of objects, all at the same distance, which could be compared to the new theoretical models. At the same time large telescopes were probing nearby galaxies and the distant cosmos, making the Clouds important as the foundation of the extragalactic distance scale. In the end of the 20th and the beginning of the 21st century Magellanic Cloud research benefited greatly from the new ground-based and space observatories.

The extent of the Magellanic System on the night-sky is enormous (Mathewson and Ford 1984). It includes the Large Magellanic Cloud, the Small Magellanic Cloud, the Bridge and the Magellanic Stream. The structure can be analyzed nowadays on the basis of radio, infrared, optical, UV, and X-ray observations. In spite of all the available data (or due to them) the structure of the LMC is a controversial topic and that for the SMC is probably worse.

The Parkes Galactic All-Sky Survey (GASS) is a survey of Galactic HI emission in the Southern sky covering declinations $\delta \leq 1^{\circ}$ using the Parkes Radio Telescope. McClure-Griffiths et al. (2009) outline the survey goals, describe the observations and data analysis, and present the first-stage data release. Figure 4.1 shows the Large and the Small Magellanic Cloud together with the Magellanic Stream - the entire GASS dataset is shown in a Zenithal Equal-Area projection (ZEA) centered on the south celestial pole with 0 h right ascension at the top and with R.A. increasing counter-clockwise. The colors correspond to integra-

Table 4.1: Basic properties of the Large and Small Magellanic Clouds

Parameter	LMC	SMC
Type	IrrIII-IV	Irr IV-V
l	280.5	302.8
b	-32.9	-44.3
Distance moduli	18.58[a]	18.97[b]
Distance, kpc	49	58

[a] - Szewczyk et al. (2008)
[b] - Szewczyk et al. (2009)

tions over velocity chunks of ~40 km s^{-1} as indicated by the bar on the right of the image. The intensity of each colour corresponds to the brightness temperature integrated over the ~ 40 km s^{-1} velocity chunk, and is scaled logarithmically as shown by the horizontal extent of the colour bar.

The two Clouds are about 23° apart in the sky, but radio observations prove that they have a common envelope of neutral hydrogen (Bok 1969). This indicates that they have been bound to each other for a long time. It is generally assumed, though not definitely proven, that the Clouds have also been bound to the Galaxy for at least the last 7 Gyr. Most models assume that the Clouds lead the Magellanic Stream. The Magellanic System moves in the gravitational potential of our Galaxy and in the plane of the Local Group. It is also exposed to ram pressure through its movement in the Galactic halo. The influence of our Galaxy ought to be noticeable in the present structure and kinematics of the System.

Kallivayalil et al. (2006a,b) presented a measurement of the systemic proper motion of the Large and Small Magellanic Clouds from astrometry with the High Resolution Camera (HRC) of the Advanced Camera for Surveys (ACS) on the Hubble Space Telescope (HST). Their PM determination (μ_W) appears to be on the high end of what was found in previous studies (Anderson and King 2004; Freire et al. 2003; Irwin et al. 1996; Kroupa and Bastian 1997; van Leeuwen and Evans 1998). Further investigations of the past orbital motions of the Clouds in a simple model for the dark halo of the Milky Way imply that the Clouds could be unbound from each other. However, their data are also consistent with orbits in which the Clouds have been bound to each other for approximately a Hubble time.

The proper motions by Kallivayalil et al. (2006a,b) lead to spatial velocities of both Clouds which are unexpectedly higher than previous values resulting from agreement between the available theoretical models of the Magellanic System and the observations of HI associated with the LMC and SMC. Such proper

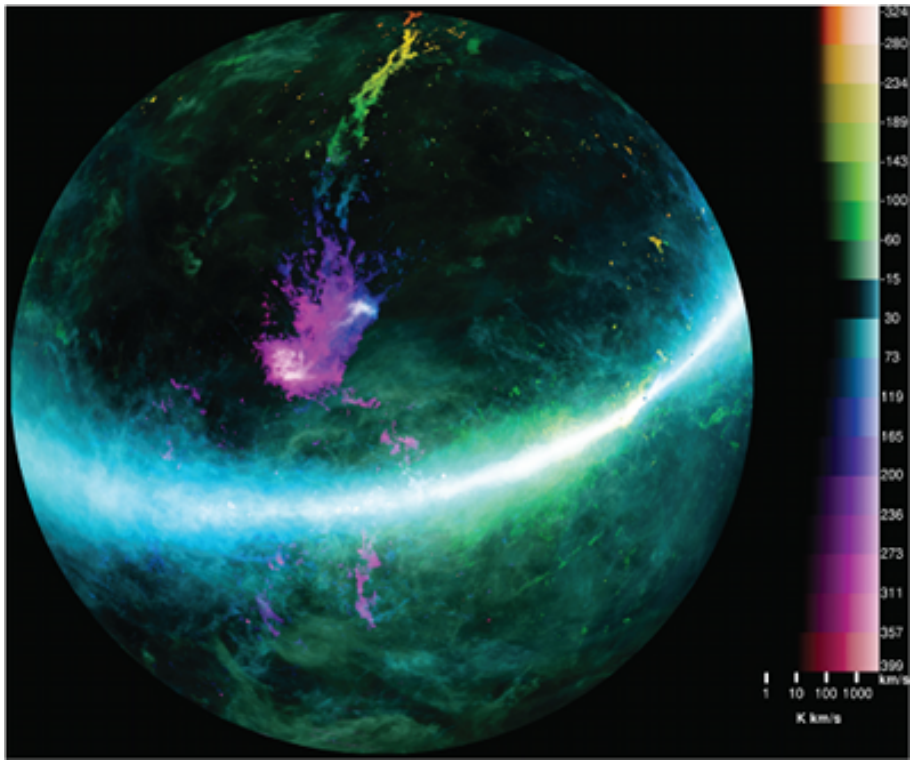

Figure 4.1: McClure-Griffiths et al. (2009) present the entire GASS dataset shown in a ZEA projection centered on the south celestial pole with 0 h right ascension at the top and with R.A. increasing counter-clockwise. The colors correspond to integrations over velocity chunks of ~40 km s^{-1} as indicated by the bar on the right of the image.

motion estimates are likely to be at odds with the scenarios for creation of the large-scale structures in the Magellanic System suggested so far. Ružička et al. (2009) investigated this hypothesis for the pure tidal models, as they were the first ones devised to explain the evolution of the Magellanic System, and the tidal stripping is intrinsically involved in every model assuming the gravitational interaction. However, assuming the tidal interaction, no satisfactory reproduction of the HI data available for the Magellanic Clouds was achieved with the new proper motions. Therefore, for the proper motion data by Kallivayalil et al. (2006a,b), within their 1-σ errors, the dynamical evolution of the Magellanic System with the currently accepted total mass of the Milky Way cannot be explained in the framework of pure tidal models.

Generally speaking, the proposed formation mechanisms are not efficient enough unless the Clouds orbit around the Galaxy. Several perigalactic approaches of the Clouds are expected by the tidal models (Connors et al. 2006; Gardiner et al.

1994). Shorter timescales for the interaction may be sufficient within the ram pressure scenario (Heller and Rohlfs 1994; Mastropietro et al. 2005). However, the proper motions by Kallivayalil et al. (2006a,b) lead to timescales further dramatically reduced, as the Clouds should be approaching the Galaxy for the first time (Besla et al. 2007). The research of the dynamical evolution of the Magellanic System is at the point where our understanding of the MW-LMC-SMC interaction is at odds with some crucial observational constraints. The results of Ružička et al. (2009), together with the conclusions by Besla et al. (2007), do not allow for more than little doubts, that despite the high spatial velocities of the Clouds, the models of the interaction may succeed if sufficiently efficient physical mechanisms are introduced (Mastropietro et al. 2005; Nidever et al. 2008).

At the LMC and SMC distance of roughly 50 kpc, individual bright stars, with $I = 12-16$ mag, will have transverse velocities determined to approximately $1-2$ km s^{-1} (~20 μas yr^{-1}). Gaia will allow kinematic mapping and membership analyses of young star-forming regions in the LMC and SMC with comparable precision to that presently available in the Milky Way. In other words, it will be possible to compare directly the kinematics and structure of star-forming regions in a large spiral disk with those in a mid-sized irregular galaxy.

4.1 The Large Magellanic Cloud

The de Vaucouleurs (1954) model of the Large Magellanic Cloud (LMC, Figure 4.2) as a flattened disk tilted to the plane of the sky with an inclination angle of $30-40°$ still remains the best overall description. Kontizas et al. (1993) separated LMC clusters into two groups on the basis of age, an inner system containing young clusters dynamically at very early stages, and an outer system of intermediate in age and old clusters dynamically advanced and small open-like clusters (see their Figure 1). The inclination of the inner system, considered to be a flattened disk, is 30°, while the similar outer system has an inclination of 42.3° (Kontizas et al. 1990).

This is confirmed by van der Marel and Cioni (2001) who determined the viewing angles of the LMC. The observed spatial brightness variation of tracers (AGB and RGB stars) as function of position angle along a circle are well fit by a geometric model of an inclined plane with an inclination angle of $i = 34.7° \pm 6.2°$. The average line-of-nodes position angle $\Theta = 122.5° \pm 8.3°$. They also suggest that there is a tentative evidence for variations in the viewing angles with distance from the LMC centre. This may indicate that the LMC disk plane is warped. It is now well established that the east side of the LMC is closer than the west.

A basic feature of the LMC structure is the Bar, covering an area on the sky of ~ 3° × 1°, with its major axis at PA=120°. The pattern of rich OB associations

Figure 4.2: The LMC is classified as a dwarf irregular galaxy because of its normally chaotic appearance. In this deep and wide exposure by Yuri Beletsky (from `http://apod.nasa.gov/apod/ap080409.html`) the full extent of the LMC becomes visible. Surprisingly, during longer exposures, the LMC begins to resemble a barred spiral galaxy. North is up, east is to the left.

and large HII regions has been interpreted as a spiral structure (Russell 1890); a faint outer loop, which has been looked upon as an extension of the main spiral arm, is devoid of bright supergiants and emission regions and rather weak in HI. The feature can be traced by carbon stars to the east of the main body of the LMC, from −68° to −73° at 06^h15^m, and by carbon stars and old clusters to the south, near −75° from 04^h50^m to 06^h10^m. The 30 Doradus complex does not fit into most structural interpretations except in those where it is considered as the centre of the spiral structure of the LMC.

The radio centre (at 05^h20^m −68.8°) of the LMC is displaced from the optical center (at 05^h24^m −69.8°); from the centroid of the projected HI distribution, at 05^h35^m, −68.5°; and from all other centroids. All the centroids of Extreme population I objects lie to the north of those of the older ones, e.g. the PN, the novae, the outlying clusters. One possible explanation is that the interaction between the two Clouds during the last close encounter 0.2 Gyr ago pulled much of the gas northwards in the LMC.

The simplest explanation of the present structure of the youngest population in the LMC is the simultaneous bursts of star formation at several locations all over the gas-containing area, followed by stochastic self-propagating star forma-

Figure 4.3: The Small Magellanic Cloud is pictured above by Stéphane Guisard (from `http://apod.nasa.gov/apod/ap071001.html`). This view includes two foreground globular star clusters NGC 362 (bottom right) and 47 Tucanae. Spectacular 47 Tuc is a mere 13 000 light-years away and seen here to the left of the Small Magellanic Cloud. North is down, east is to the right.

tion processes (Westerlund 1991).

4.2 The Small Magellanic Cloud

The early efforts to define the Small Magellanic Cloud (SMC, Figure 4.3) as a rotating galaxy with a spiral structure have been replaced by intense efforts to understand its extension in depth and its possible fragmentation. The double peaks in the SMC HI profiles separated by $30 - 40$ km s^{-1}, as well as the separation in the radial velocities of stars, HII regions and planetary nebulae, lead Mathewson and Ford (1984) to believe that the SMC has been badly torn during its near collision with the LMC 0.2 Gyr ago, and a large fragment, the Mini-Magellanic Cloud (MMC), is now separting from the remnant of the SMC (SMCR) at about 30 km s^{-1}.

The SMC (Figure 4.4) is comprised of three main components: the Bar, Wing, and high-density portion of the Magellanic Bridge. Boyer et al. (2011) determine that the RSG, AGB, and RGB stars contribute near equal amounts of flux to the global (extended + point-source) 3.6 μm flux within the Bar and Wing area.

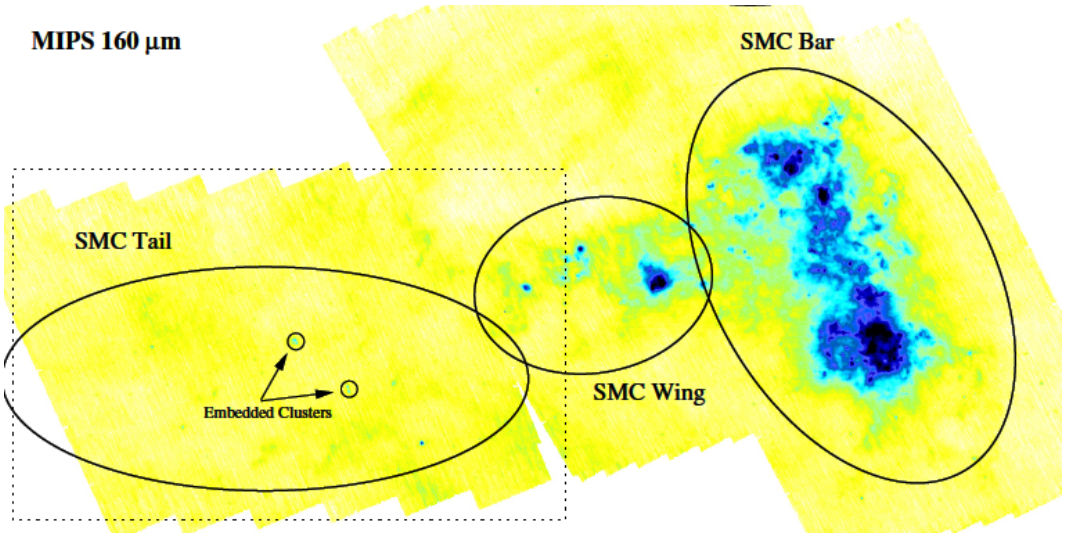

Figure 4.4: Full SMC at 160 μm is shown and various regions are labeled. Figure is from Gordon et al. (2009).

However, the RSG stars show a stronger contribution in the Wing. Perhaps this is indicating an aging stellar population in the outskirts of the SMC.

Determinations of i and Θ exist but have little relevance if the extension of the SMC is mainly in depth with the Wing and the northeastern part closer to us than the southern part. Caldwell and Coulson (1986) found the SMC Cepheids system to be an elongated structure seen nearly edge on, which stretches 15 to 20 kpc in the line of sight. Martin et al. (1989) conclude that most young objects lie within a depth of less than 10 kpc. There is a tendency for the older populations (novae, PN) to be displaced towards the west.

The SMC contains the same age groups as those seen in the LMC. Major differences are: the intermediate-age clusters in the SMC appear older than those in the LMC (Olszewski 1988); the HI distribution is not as clumpy as in the LMC (the clumps surround HII regions and stellar associations); the Bar contains proportionally more blue stars and gas than the LMC Bar; and the Wing exists.

Hatzidimitriou et al. (1989) undertook a detailed two-colour (B and R) study of the stellar content of the SMC outer regions, using 1.2-m UK-Schmidt Telescope photographic plates. In their next paper (Hatzidimitriou and Hawkins 1989) they present the three-dimensional distribution of the old disk and halo populations in the SMC outlying north-eastern and south-western regions (with projected distances from the optical centre larger than 2 kpc). They find a significant line-of-sight depth of 17 kpc in the mean, reaching a maximum value of 23 kpc, in the north-eastern regions; these regions are ~10 kpc deeper along the line-of sight than the south-western regions. In the southern and western regions

of the SMC there is a depth of less than 10 kpc along the line-of-sight; this value is comparable with the SMC 'tidal radius' of ~5 kpc (Welch et al. 1987).

Moreover, the asymmetrical structure of the SMC halo has been confirmed by Gardiner and Hawkins (1991) from surface counts of red horizontal branch/clump stars. They assume that the large radial extent of the 'halo' in the northern direction which appears to extend beyond 6 kpc from the SMC optical centre is probably due to the influence of the tidal field of the Galaxy. In the northern areas of the SMC away from the areas of large depth, the underlying (assumed spherically symmetric) space-density distribution of halo clump stars is best represented by an exponentially decaying relation. This is a relation which also offers an explanation for the observed small but well-defined increase in depth with distance from the SMC centre for these regions. Gardiner and Hatzidimitriou (1992) show that the bulk of the field populations in the outer parts of the SMC possess a median age of 10–12 Gyr. The observed existence of a red horizontal branch suggests the existence of a very old 15–16 Gyr population. The projected distribution of populations younger than about 2 Gyr has been shown to be biased towards the eastern side of the SMC.

4.3 The Bridge and Inter-Cloud region

The Large and Small Magellanic clouds represent the nearest examples of tidally interacting galaxies and the Magellanic Bridge is a clear manifestation of a close encounter of these two galaxies some 200 Myr ago (Zaritsky and Harris 2004). The Magellanic Bridge (Figure 4.5) is a lament of neutral hydrogen, which joins the SMC and LMC over some 15 kpc (McGee and Newton 1986; Staveley-Smith et al. 1998). Gordon et al. (2009) detected the diffuse IR emission from dust in the SMC Tail portion of the Magellanic Bridge. They define the SMC Tail as the portion of the Magellanic Bridge that is adjacent to the SMC Wing and has a higher density and metallicity than the rest of the Magellanic Bridge. The gas-to-dust ratio in the SMC Tail region was measured to be 1200±350, (12±3.5) times MW value.

Neutral hydrogen was detected in the LMC and SMC in 1954 (Kerr et al. 1954) and nine years later in the region between the two Clouds (Hindman et al. 1963a,b). No stellar member were detected between the SMC Wing and the LMC until 1980, when Kunkel identified a group of young stars at 2^h30^m, $-74°$. The extensive young stellar population found afterwards forms an optical counterpart to the HI Bridge (Irwin et al. 1985). The SMC Wing is the brightest part in this link and contains even younger objects. The main-sequence stars in the inter-Cloud region have an age of 0.1 Gyr, whereas the youngest objects in the Wing are about 5 Myr (Meaburn 1986).

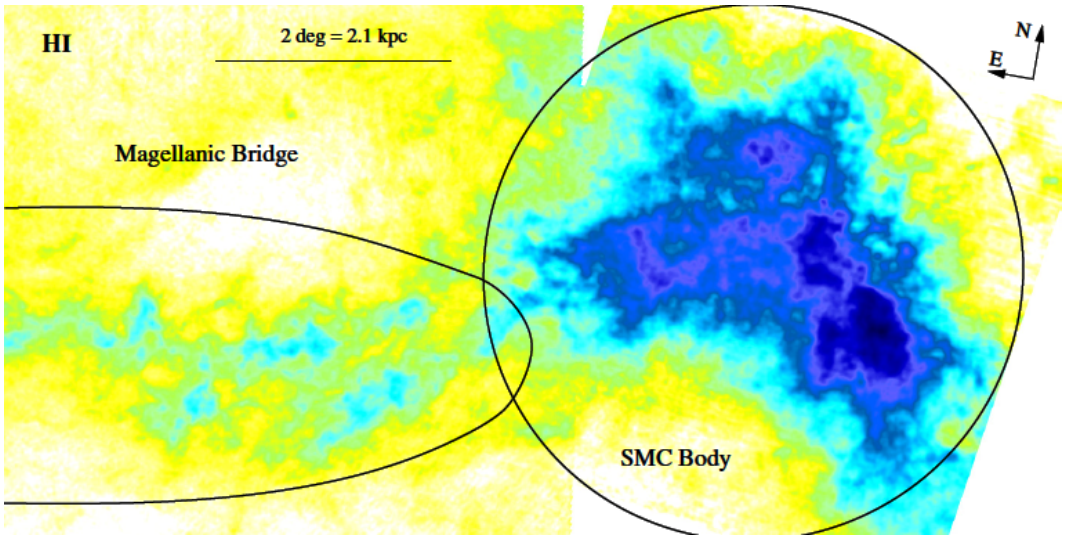

Figure 4.5: Full SMC in HI is shown and various regions are labeled. Figure is from Gordon et al. (2009).

The long spurs extending northwards from the bridge towards the Magellanic Stream (see Figure 4.6) are a noticeable feature of the inter-Cloud region. Mathewson and Ford (1984) believe that these spurs must be the result of tidal forces between the LMC and SMC and are the start of the Magellanic Stream. Mathewson et al. (1987) suggested that the inter-Cloud gas and the Stream were produced in a close encounter between the LMC and the SMC about 0.4 Gyr ago. The Clouds in the Stream formed in collisions between the inter-Cloud gas and the high-velocity clouds in the Galactic halo.

4.4 The Magellanic Stream

The Magellanic Stream is a narrow band of neutral hydrogen gas along a small circle 7° from, and parallel to, a great circle that passes through the south galactic pole and cuts the galactic plane at $l = 280°$, ending with the HI clouds detected by Wannier et al. (1972) If the reasonable assumption is made that the Stream forms part of a great circle when viewed from the galactic centre, then this parallax places the Stream at about the distance of the Magellanic Clouds (Mathewson et al. 1977). It extends about 100° from the inter-Cloud region and as an essentially continuous filament. It is bifurcated for most of its length into horseshoe-shaped structures. There are six main concenrations, MS I - MS VI (see Figure 4.6). The surface density is greatest at MS I and weakest at MS VI, with each successive cloud having a lower density than the previous one (Mathewson et al.

1987).

The velocity gradient along the Stream is striking, although much of it is a reflex motion due to solar motion around the Galactic Centre. Putman et al. (2003) show that the Stream begins near the Clouds at $V_{LSR} \approx 250$ km s^{-1} and extends to -450 km s^{-1} at its tail, an overall range of 700 km s^{-1}. In terms of a Galactic reference frame, it begins at $V_{GSR} \approx 100$ km s^{-1} and extends to -290 km s^{-1}. This is still substantial and indicates that there are non-circular motions present.

Mastropietro et al. (2005) carried out high-resolution gravitational/hydrodynamical simulations of the interaction between the LMC and the Milky Way covering the previous 4 Gyr of the orbit of the LMC. As the LMC spirals inwards towards the Galaxy, it suffers ever-increasing gravitational tidal forces and hydrodynamical stripping. It was found that the combined effects of gravity and ram-pressure stripping can account for the majority of the LMC's kinematical and morphological features and the morphology of the Magellanic Stream. Moreover, the complexity of the HI geometry in the region surrounding the Magellanic Clouds suggests that a close encounter between the Clouds and gas stripped from the SMC contributed not negligibly to the formation of the MS.

The gas stripped from the LMC disk formed a great circle, or a polar ring, around the Galaxy, consistent with the discovered extension of the MS into the Northern Hemisphere by Braun and Thilker (2004). Less material was stripped during the pericentric passage 4 Gyr ago since dynamical friction has moved the Clouds closer today. Very few stars are tidally removed from the LMC, but its disk becomes severely warped dur to the tidal interaction.

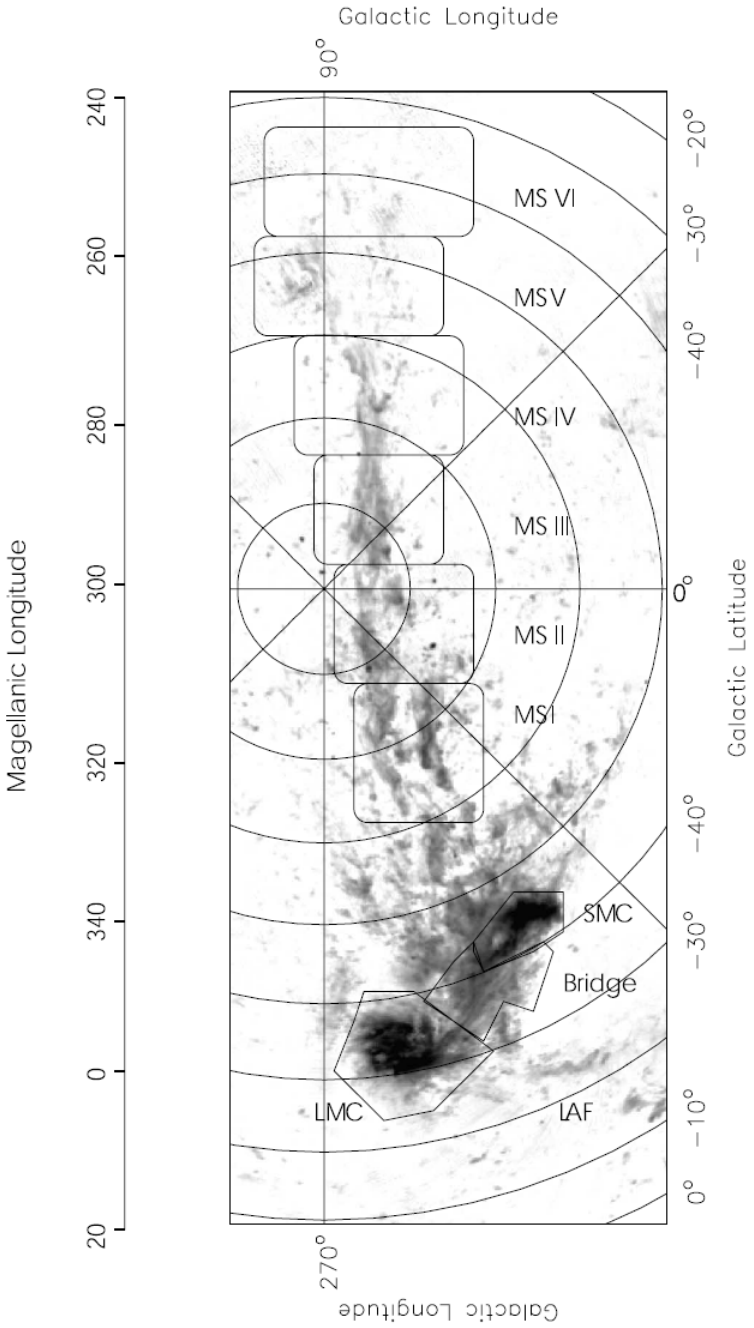

Figure 4.6: Annotated HI column density image of the Magellanic Clouds, Bridge, Stream, and the beginning of the Leading Arm feature by Putman et al. (2003). Velocities from −450 to 400 km s^{-1} are included, excluding ± 20 km s^{-1} due to confusion with Galactic emission. Magellanic longitudes for positions along the Stream are also labeled. The intensity values are on a logarithmic scale with black corresponding to $N_{HI} > 6 \times 10^{20}$ cm^{-2}, and the faintest levels corresponding to $\sim 2 \times 10^{18}$ cm^{-2}. Galactic longitude increases in a counterclockwise direction.

Chapter 5

Observational Data

5.1 Requirements

In order to obtain the spatial distribution of various stellar populations in the Magellanic Clouds archive data were used - both all-sky surveys and dedicated catalogues. The requirements were chosen with respect to the performance expected from the Gaia mission - an all-sky survey with a limiting magnitude $V \sim 20$ mag. These requirements are listed below:

- to cover the whole galaxy
- to be homogeneous
- to be complete, preferably to $V = 20$ mag
- to be deep enough

The Magellanic Clouds are the nearest neighbours of our Milky Way galaxy and among the most studied galaxies in the Local Group. This makes them the ideal target in a range of scientific topics - variable (Cepheids, RR Lyr) stars for determining the distance to the MCs and perfecting the period-luminosity relation, MCs spatial velocities (proper motions, radial velocities) for understanding their movement in the Local Group and their interaction with other members of the group, chemical evolution, stellar and galactic evolution.

Vast amounts of observational material for this area of the southern sky has been acquired for the last hundred years in every wavelength range available. Therefore, one would expect that finding archive data will pose no difficulties. However, their proximity results in a large angular dimensions on the sky. This means that when searching for observational material on the Magellanic Clouds it is very difficult to find data sources which have the appropriate data coverage needed for this project.

At the beginning of this project several possible data sources were available. Some of them met the above criteria, and others did not. All of catalogues will be presented and their advantages and disadvantages will be further discussed below.

5.2 Catalogues

5.2.1 SuperCOSMOS

The SuperCOSMOS Sky Survey (SSS) provides digitized sky survey plates taken with the UK Schmidt telescope (UKST), the ESO Schmidt, and the Palomar Schmidt. The survey covers a very large area, although, not as large as the 2MASS. However, it has one disadvantage: stars in the centres of both LMC and SMC are selectively missed, probably due to crowding (which at this spatial resolution becomes crucial in dense regions), or maintaining low error on determination of positions, proper motions and colours. Access to the data is provided through `http://surveys.roe.ac.uk/ssa/`.

It can still be possible to use SuperCOSMOS data to investigate the outer parts of the Clouds, but the overall combination from insufficient completeness, coverage and homogeneity makes this unnecessary with the more recent and comparable as quality surveys, such as 2MASS and MCPS.

5.2.2 The Magellanic Catalogue of Stars (MACS)

Tucholke et al. (1995) provide a catalogue of positions for 243561 stars, based on scans of ESO Schmidt plates (see Figure 5.1). The positional accuracy is better than 0.5 arcsec for 99% of the stars and the limiting magnitude is $B < 16.5$ mag. Only those stars are included which are undisturbed by close neighbours as verified by visual screening in order to obtain a clean astrometric reference.

Therefore, this catalogue does not seem to satisfy any of the requirements listed above.

5.2.3 The Magellanic Clouds Photometric Survey (MCPS)

The Magellanic Clouds Photometric Survey (Zaritsky et al. 2002, 2004) offers very rich and complete catalogues of the Magelanic Clouds but the area they cover is somewhat limited. Using the Las Campanas Swope telescope (1 m) and the Great Circle Camera with a 2K CCD they obtained drift-scan images for both Magellanic Clouds in the Johnson U, B, and V and the Gunn I filters. The effective exposure time is between 4 and 5 minutes for SMC scans and 3.8 and

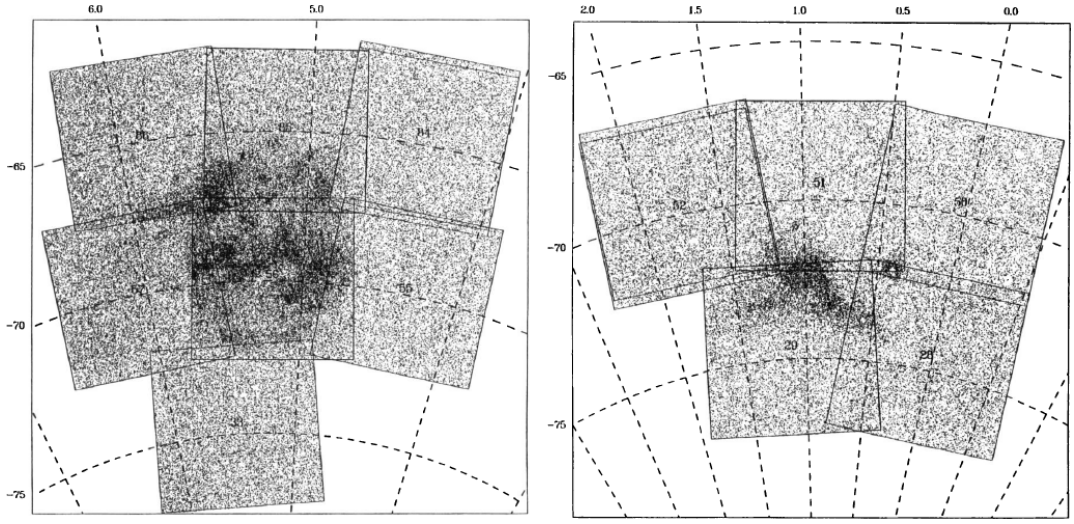

Figure 5.1: Sky distribution of 175779 catalogue stars towards the LMC (left) and 67782 in the direction of the SMC. Also given are numbers identifying the ESO/SERC atlas fields, the outlines of the plates used, and a J2000.0 coordinate grid. Figures from Tucholke et al. (1996).

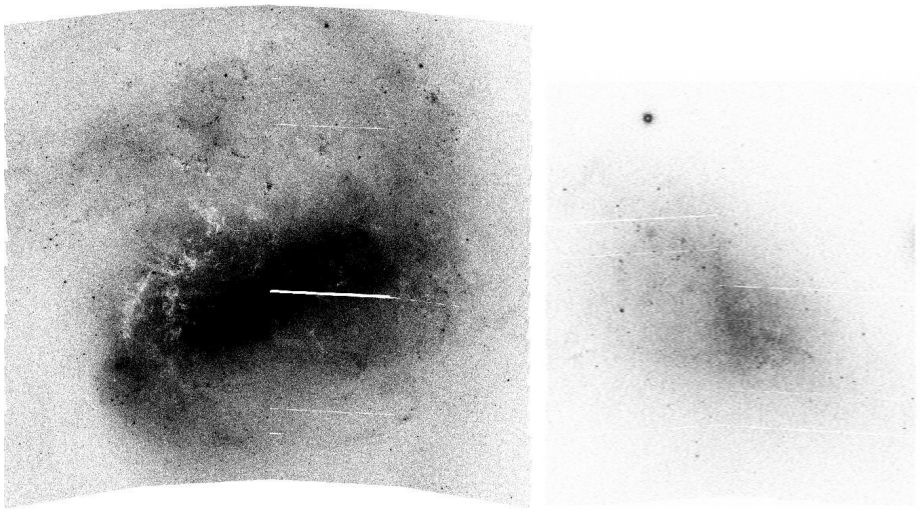

Figure 5.2: Grey-scale representation of the LMC (left) and SMC (right) - stellar density maps of stars with $V \leq 20$. Figures from Zaritsky et al. (2002, 2004). The images show the entire survey region ($\sim 8.5^\circ \times 7.5^\circ$ for the LMC and $\sim 4.5^\circ \times 4^\circ$ for the SMC).

5.2 minutes for LMC scans. The pixel scale was 0.7 arcsec pixel^{-1}. Typical seeing is ~1.5 arcsec, and scans with seeing worse than ~2.5 arcsec were not accepted.

The catalogues of the SMC and LMC cover the central 18 deg^2 and 64 deg^2 area respectively. The incompleteness becomes significant at magnitude fainter than $V > 20$. A grey-scale representation of the LMC and SMC is presented in Figure 5.2. The data are combined with 2MASS (J, H, and Ks) and Deep Near-Infrared Southern Sky Survey (I, J, and Ks) catalogues to provide, when available, U through Ks data for the stars. The survey description as well as the various data products can be found at `http://ngala.as.arizona.edu/dennis/mcsurvey.html`.

Thus, MCPS provides deep homogeneous data complete down to $V = 20$. This is convenient since stars fainter than 20th magnitude will not be detected by Gaia because of its observational limit. However, only the central parts of the Clouds have been surveyed.

5.2.4 Master Catalogue of stars towards the MCs (MC2)

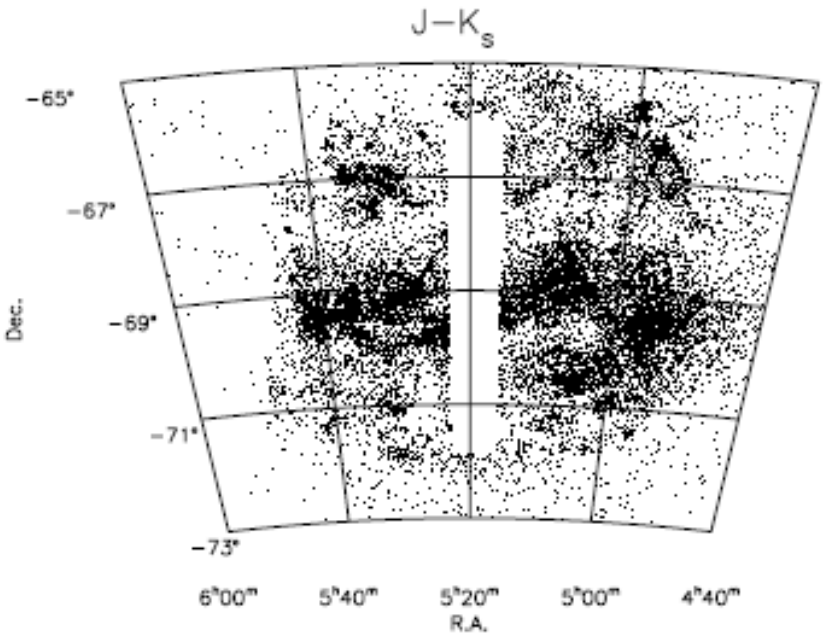

Figure 5.3: The spatial distribution of the blue stars selected with $(V - Ks) \leq 1$ in the $(I, V - Ks)$ diagram. There are 19 646 sources. The I band is from DENIS and the J, H and Ks are from 2MASS.

Delmotte et al. (2002) provide a multi-wavelength reference catalogue. They started with a massive cross-identification of two near-infrared surveys: the DENIS Catalogue towards the Magellanic Clouds (DCMC) with more than 1.3 million sources identified in at least two of the three DENIS filters (I, J, Ks) and

the 2nd Incremental Release of the 2MASS point source catalogue (J, H, Ks) covering the same region of the sky. Both point source catalogues provide an unprecedented wealth of data on the stellar populations of the Magellanic Clouds (MCs). The cross-matching procedure has been extended to optical wavelength ranges, including the UCAC1 (USNO) and GSC2.2 catalogues.

However, as can be seen in Figure 5.3 the case of LMC, for example, areas in the central parts of the Magellanic Clouds are missing in the 2MASS release used for this catalogue. Another problem which arises from the cross-matching and combination of several sources is that the stellar density is not homogeneous across the two galaxies. Therefore, we decided not to use the MC2 in our study.

5.2.5 2MASS

The Two-Micron All Sky Survey (2MASS) has uniformly scanned the entire sky in three near-infrared bands to detect and characterize point sources brighter than about 1 mJy in each band, with signal-to-noise ratio greater than 10. The limiting magnitude of 2MASS is somewhat bright with $J < 15.8$, $H < 15.1$ and $Ks < 14.3$ mag (Skrutskie et al. 2006). 2MASS used two highly-automated 1.3-m telescopes, one at Mt. Hopkins, AZ, and one at CTIO, Chile. Each telescope was equipped with a three-channel camera, each channel consisting of a 256 × 256 array of HgCdTe detectors, capable of observing the sky simultaneously at J (1.25 μm), H (1.65 μm), and Ks (2.17μm).

The 2MASS arrays imaged the sky while the telescopes scan smoothly in declination at a rate of $1'$ per second. The 2MASS data "tiles" are 6° long in the declination direction and one camera frame ($8.5'$) wide. While the entire telescope scanned in the declination direction, the telescope's secondary mirror tilted opposite the scan direction to momentarily freeze the focal plane image. At the end of a 1.3 s exposure the secondary flew back to its start position and froze a new piece slightly displaced from the previous frame. The dead time between frames used for secondary flyback and array reset was less than 0.1 s. The camera field-of-view shifted by ~1/6 of a frame in declination from frame-to-frame. The camera images each consisted of six pointings on the sky for a total integration time of 7.8 s, with sub-pixel "dithering", which improves the ultimate spatial resolution of the final Atlas Images. When accounting for dead time and the time to point the telescope and initiate a scan, the 2MASS observing system integrated on the sky approximately 84% of each night.

Although 2MASS is an all-sky survey and one is able to select as large an area around their target as is necessary, the survey is not as deep as needed for Gaia. Still, it can be useful for studying the overall distribution of stellar populations in the Magellanic Clouds over a larger area than it is possible with the MCPS for example. It gives us the distribution of the massive and intermedi-

ate mass stellar component and is very useful due to its homogeneity and its unique coverage. Access to the various data products of 2MASS is provided at IRSA (`http://irsa.ipac.caltech.edu/applications/Gator/`). IRSA is chartered to curate the calibrated science products from NASA's infrared and sub-millimeter missions, including major large-area/all-sky surveys.

5.2.6 UBVR CCD survey of the Magellanic Clouds

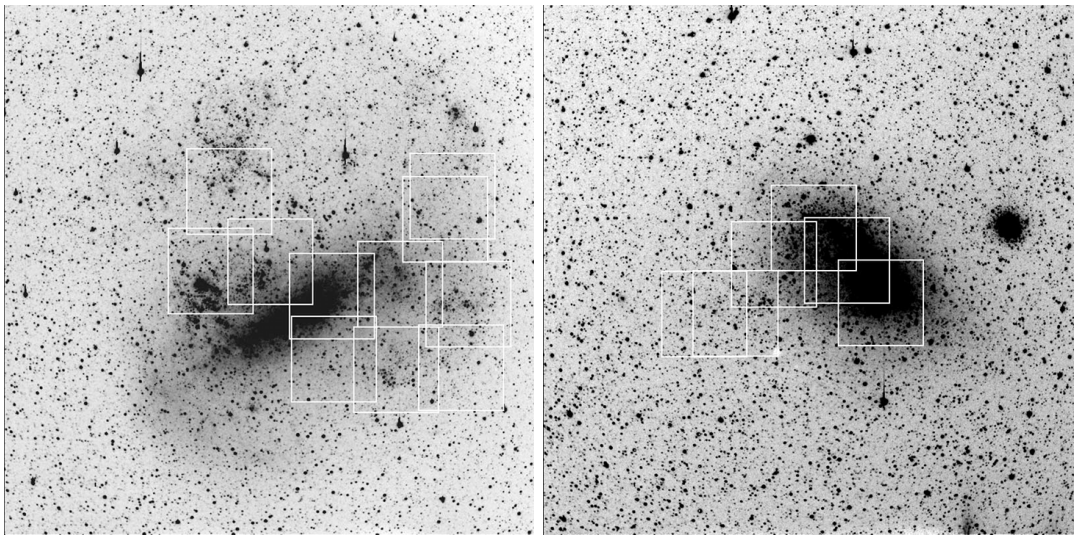

Figure 5.4: Outlines of the eleven 1.2° × 1.2° Schmidt fields in the LMC (left) and of the six fields in the SMC (right). North is to the top and east is to the left. Figures from Massey (2002a).

The MCs survey of Massey (2002b) covers 14.5 deg^2 and 7.2 deg^2 of the LMC and SMC respectively. The catalogue contains 179655 LMC and 84995 SMC stars brighter than $V \approx 18$, and is photometrically complete to $U \sim B \sim V \sim 15.7$ and $R \sim 15.2$, although stars in crowded regions were selectively missed. As can be seen in Figure 5.4 (Massey 2002a) the mosaic of the Schmidt plates does not cover the entire galaxies.

Thus, neither does this catalogue cover both galaxies, nor is it deep or complete enough for the purposes of this project.

5.2.7 Carbon stars catalogues

The carbon stars data we use comes from three separate sources - one catalogue for the LMC, one for the inner parts of the SMC, and another one for the outer

parts of the SMC. (Kontizas et al. 2001) provide a catalogue of 7760 carbon stars in the LMC. The stars were identified during a systematic survey of objective-prism plates taken with the UK 1.2m Schmidt Telescope.

Rebeirot et al. (1993) provide accurate positions and charts for 1707 carbon stars in the Small Magellanic Cloud identified on GRISM plates. The catalogue provides data on magnitudes, colours, and carbon-abundance measurements. Morgan and Hatzidimitriou (1995) completed the survey of carbon stars in the outer parts of the Small Magellanic Cloud. The candidate objects were identified by inspecting UK Schmidt Telescope objective-prism plates which cover a total area of ~220 deg^2 on the sky, including the inter-Cloud region. Coordinates are given for 1185 newly identified carbon stars.

The above catalogues cover not only the Magellanic Clouds themselves but also the inter-Cloud region. There are no obvious inhomogeneities or incompleteness. This makes the carbon stars data the most complete in terms of both coverage, depth and numbers.

5.3 Summary

In the beginning of this project a list of requirements was created in order to account for the specific needs of the Gaia Universe Model, used for simulations of the Gaia mission. Various catalogues were considered. The advantages and disadvantages of these catalogues were descussed in the previous Section 5.2. Table 5.1 lists all the catalogues that were considered and shows if this source was fulfilling the various requirements.

Table 5.1: Catalogues available at the beginning of the project. It is shown if they fulfill the requirements and if they were used in this work.

Catalogue	coverage	homogeneity	completeness	depth
MCPS	~	yes	yes	yes
2MASS	yes	yes	~	no
Carbon stars	yes	yes	yes	~
UBVR CCD survey	no	~	no	no
SuperCOSMOS	~	no	no	no
MC2	yes	no	no	~
MACS	~	no	no	no

Many of the catalogues considered did not satisfy most of our requirements, like SuperCOSMOS, MC2, and the UBVR CCD survey. In fact, some of them actually did not satisfy any of the requirements, like the MACS. On the other hand, there were also catalogues, which were an acceptable compromise and in

the end they were approved to be used for this study. The MCPS, 2MASS, and the three carbon stars catalogues were selected:

- 2MASS, because of the full coverage, although it is not as deep as would be desirable. The data used here are from the 2MASS All-Sky Point Source Catalog,
- the Magellanic Clouds Photometric Survey, because of the completeness, even though barely covering the central parts of the galaxies, and
- carbon stars catalogues - they are complete both in terms of numbers and spatial distribution.

Chapter 6

Data Analysis

In this chapter we study the spatial distribution of the stellar content of the Magellanic Clouds using isopleth (isodensity) maps and radial surface density profiles. The isopleth maps of the Large and Small Magellanic Clouds are presented, as well as the radial surface density profiles obtained from the various data sources. Moreover, the spatial distribution of both Clouds is discussed and compared to results from previous studies.

6.1 Colour-Magnitude Diagrams

In order to investigate the distribution of the various stellar populations in terms of evolutionary age one needs the colour-magnitude diagrams (CMD). For very large data sets the colour-magnitude diagrams are more useful in the form of Hess diagrams. A Hess diagram shows the relative density of occurrence of stars at different colour-magnitude positions in the colour-magnitude diagram.

Such diagrams were produced from both catalogues of the Magellanic Clouds: the Magellanic Clouds Photometric Survey (MCPS) and the 2 Micron All-Sky Survey (2MASS). The colour-magnitude range from the MCPS and 2MASS data sets was divided in a grid with different numbers of cells for each data set. The size of the cells was chosen in such a way as to provide a fine grid and at the same time contain enough stars for the statistics. The diagrams from the MCPS and 2MASS are shown in Figure 6.1 and Figure 6.2, respectively. Isochrones for 10 Myr, 100 Myr, 300 Myr, and 1 Gyr are displayed on top of the contours in the Hess diagrams. The density levels are logarithmic.

The stellar content of both Magellanic Clouds was divided into several age groups, matching features of the CMD with isochrones obtained from `http://stev.oapd.inaf.it/cmd` based on Marigo et al. (2008) and Bertelli et al. (1994). The selection criteria we use are summarized in Table 6.1. It contains the colours

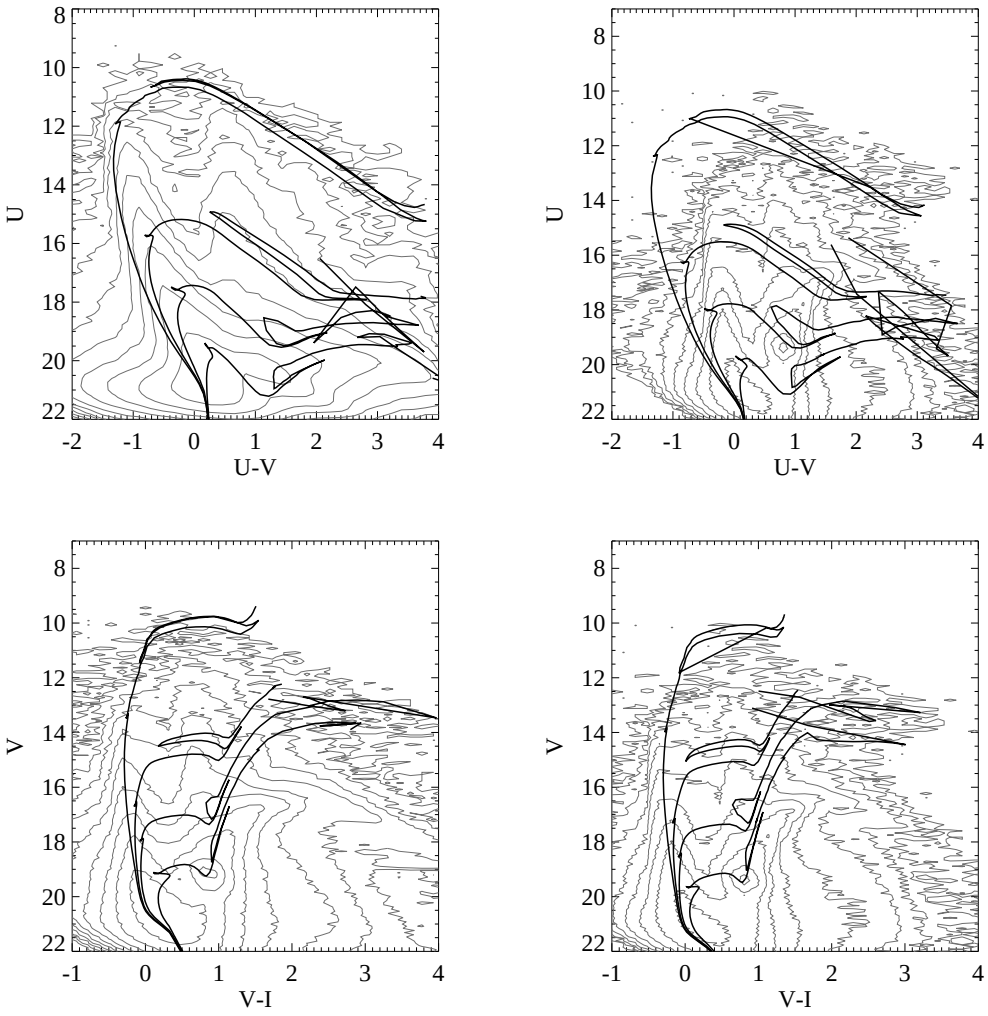

Figure 6.1: Hess diagrams of the LMC (left) and SMC (right) from the Magellanic Clouds Photometric Survey. The density levels are logarithmic. Isochrones are obtained from `http://stev.oapd.inaf.it/cmd` based on Marigo et al. (2008) and Bertelli et al. (1994). Isochrones for 10 Myr, 100 Myr, 300 Myr, and 1 Gyr are displayed on top of the contours in the Hess diagrams.

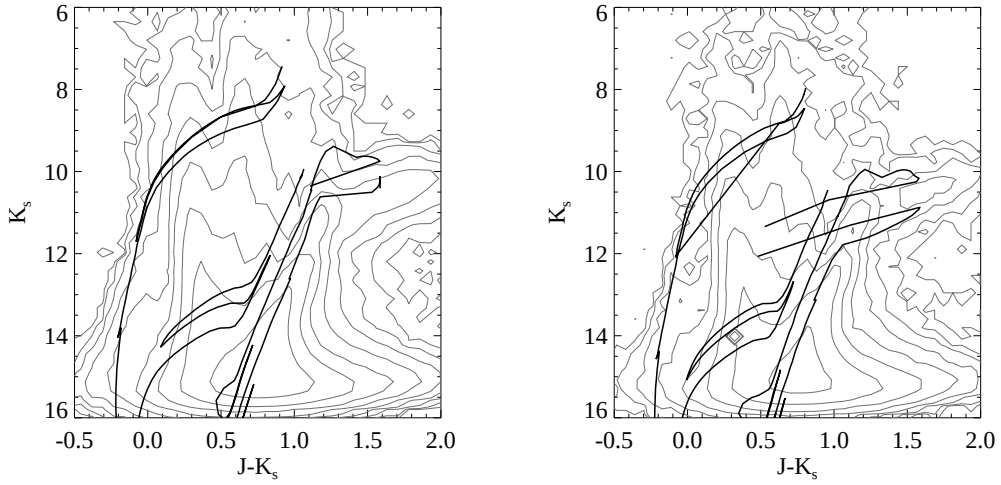

Figure 6.2: Hess diagrams of the LMC (left) and SMC (right) from the 2 Micron All-Sky Survey. The density levels are logarithmic. Isochrones are obtained from `http://stev.oapd.inaf.it/cmd` based on Marigo et al. (2008) and Bertelli et al. (1994). Isochrones for 10 Myr, 100 Myr, 300 Myr, and 1 Gyr are displayed on top of the contours in the Hess diagrams.

and magnitude criteria and ages for the various age groups. The oldest group contains Red Clump stars with ages > 1 Gyr. The younger stars are divided in one age group younger than 1 Gyr (for 2MASS) and three age groups with ages < 0.1 Gyr, between 0.1 and 0.3 Gyr, and between 0.3 and 0.9 Gyr (for MCPS). There are two separate sets of criteria - one for the MCPS data and another one for the 2MASS data. This was necessary because the MCPS allows more detailed age grouping than the 2MASS.

Table 6.1: Age groups of Magellanic Clouds stellar content. There are two separate sets of criteria - one for the MCPS and another one for the 2MASS data.

	age	magnitude	colour	source catalogue
A	< 0.1 Gyr	11 < U < 16	-1.5 < U-V < -0.6	MCPS, MS 1
B	0.1 - 0.3 Gyr	16 < U < 18	-1.3 < U-V < 0.2	MCPS, MS 2
C	0.3 - 0.9 Gyr	18 < U < 21	-0.8 < U-V < 1.2	MCPS, MS 3
D	> 1 Gyr	17 < V < 20	0.4 < V-I < 1.8	MCPS, Red Clump
E	< 0.1 Gyr	K < 15	-0.5 < J-K < 0.2	2MASS, MS
F	> 1 Gyr	13.5 < K < 15.5	0.2 < J-K < 1.2	2MASS, Red Clump

6.2 Isopleth Maps

The isopleth maps of the Large and Small Magellanic Clouds were produced using data from the MCPS, 2MASS, and three carbon stars catalogues (one covering the LMC, and two - the SMC). These data sources were described in more detail in Chapter 5.

The isodensity contour maps obtained from the MCPS for both the Large and Small Magellanic Clouds are shown in Figures 6.3 and 6.4, respectively. The age in the four panels grows from age group A to age group D from below 100 Myr to above 1 Gyr. The contour maps from 2MASS for the main sequence and red clump stars are presented in Figure 6.5. Again, stars younger than 1 Gyr are located in the upper panel, and the Red Clump stars are in the lower panel. Figure 6.6 contains the isodensity contour maps obtained from the combined carbon star catalogues.

The contour levels in all figures are logarithmic. The lowest levels for the isopleth maps from the MCPS are chosen somewhat arbitrarily, and mostly for clarity, because the data cover only the central parts of the Magellanic Clouds and the foreground stars are found at much lower densities. The colour bar shows the stellar surface density in terms of $\deg^{-2}$.

The spatial distribution of the various age groups is as expected. The older stars have a more regular and smoother appearance, while younger stars form fragmented and less symmetric structures (Belcheva et al. 2011; Cioni et al. 2000; Gonidakis et al. 2009; Maragoudaki et al. 1998, 2001; Zaritsky et al. 2000). This progression is clearly seen in Figure 6.3, as well as in Figure 6.4 from oldest group D to the youngest in age group A.

In Figure 6.3 panel A contains the youngest stars in the LMC and their distribution is extremely fragmented. Almost no sign of any structure is present. Then, in panels B and C one can clearly discern not only the LMC bar but also possibly a spiral arm to the SW. In panel D the distribution of stars older than $\sim$ 1 Gyr becomes smoother and less remarkable.

The same effect is observed in the SMC too. The youngest stars with ages $<$ 100 Myr in Figure 6.4 present the most disturbed contours. The Bar of the SMC and an extension towards the Wing are dominating the appearance of the galaxy. As age increases these features become again less pronounced, until they almost completely smooth out in the last panel D.

Figure 6.5 shows that the distribution of the younger and older stars in the LMC and SMC from NIR data follows the same trend as is observed from the MCPS. The age group E shows a more fragmented distribution in both galaxies. In the LMC younger stars are clumped in the central parts and in the SMC they trace the Bar and Wing region extending towards the Bridge. The older, intermediate age stars' distribution as seen in Figures 6.5 and 6.6 is smooth and

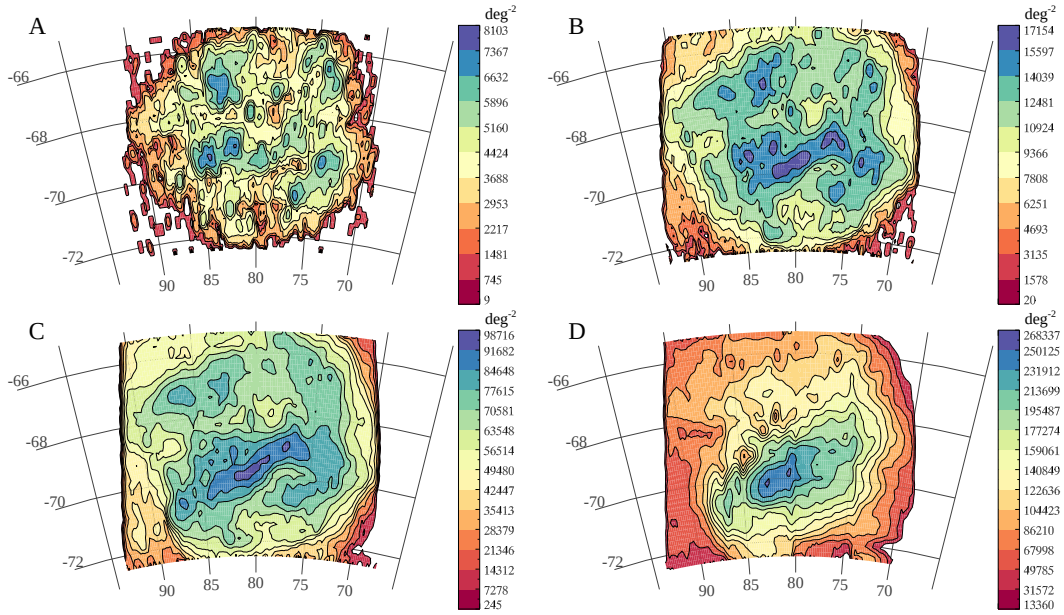

Figure 6.3: Isopleth contour maps of the LMC stars from the MCPS with various ages. The age in the panels grows from A to D from less than 100 Myr to above 1 Gyr.

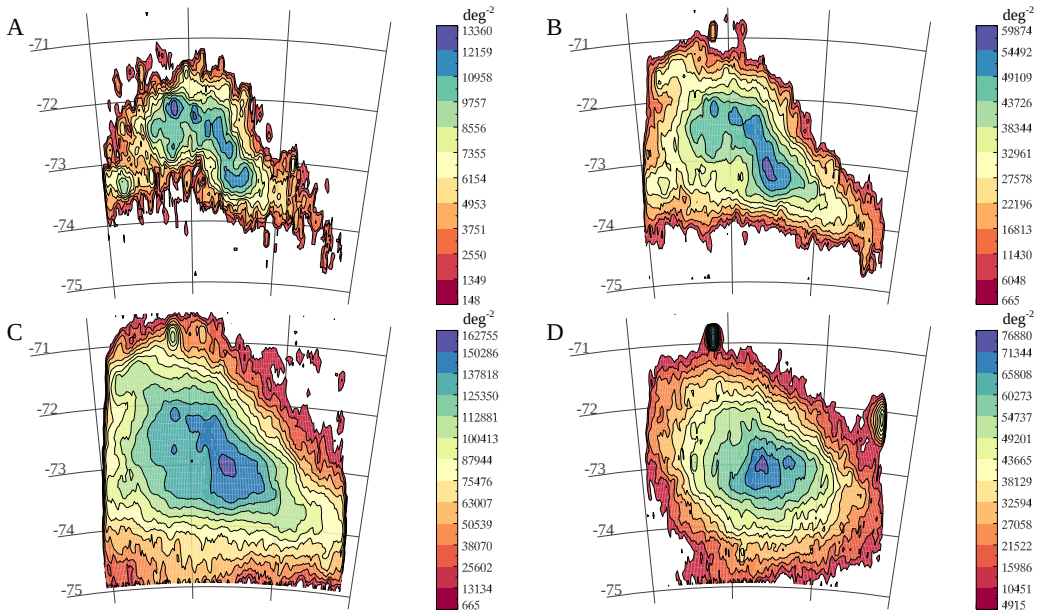

Figure 6.4: Isopleth contour maps of the SMC stars from the MCPS with various ages. The age in the panels grows from A to D from less than 100 Myr to above 1 Gyr.

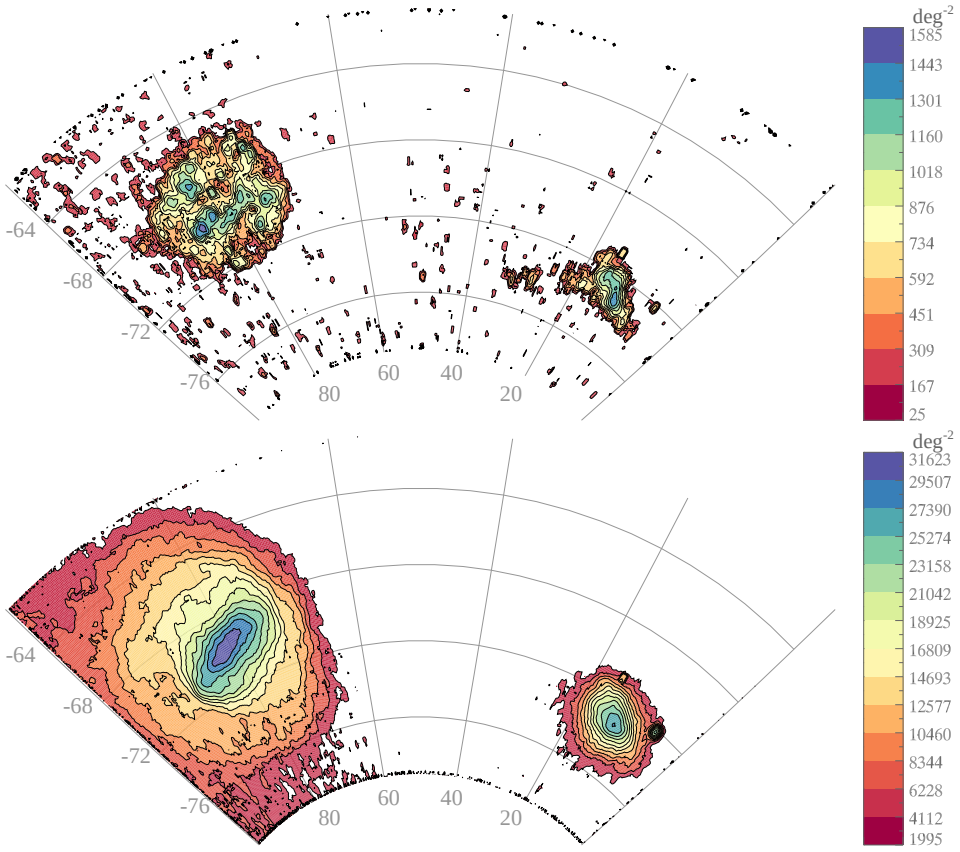

Figure 6.5: Isopleth contour maps of the Magellanic Clouds from 2MASS. Top - age group E, bottom - age group F. Left - LMC, right - SMC.

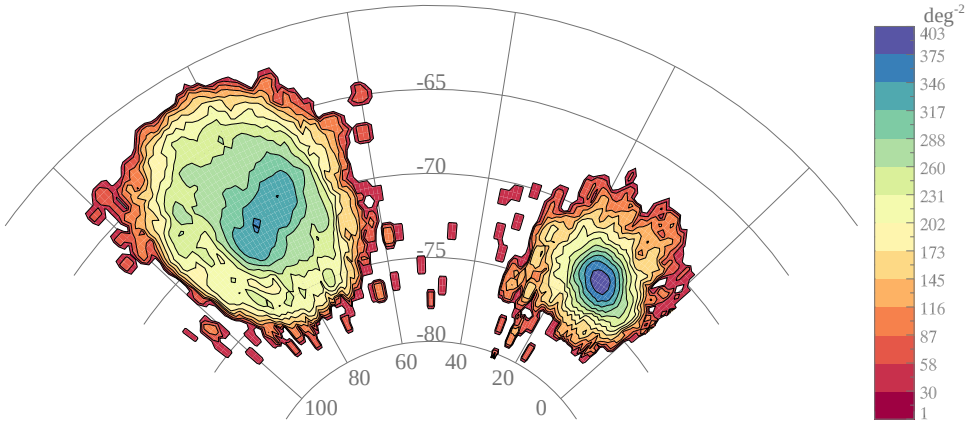

Figure 6.6: Isopleth contour maps of the Magellanic Clouds carbon stars. Left - LMC, right - SMC.

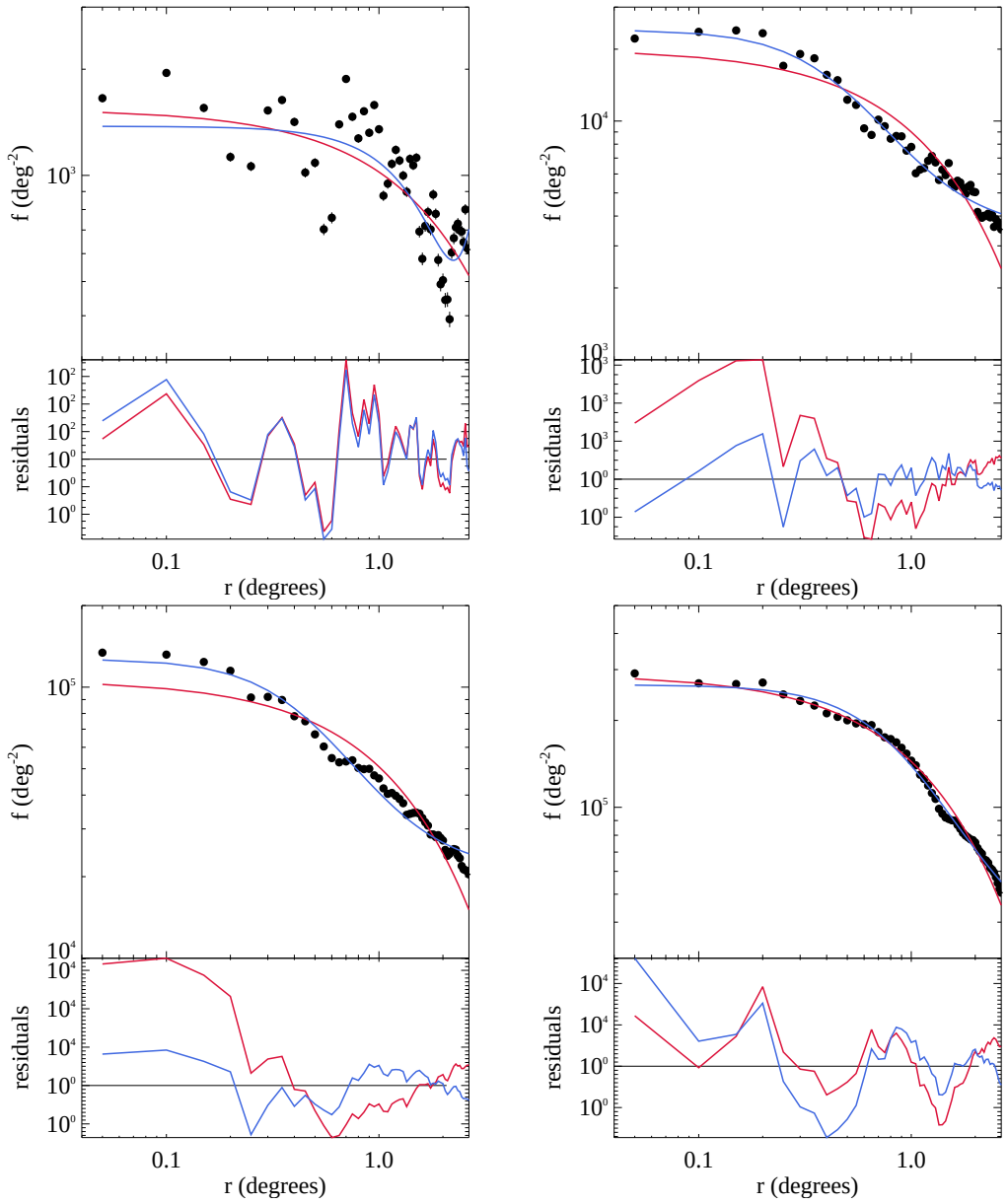

Figure 6.7: RDPs for the subsets of LMC stars from the MCPS, fitted with exponential-disk (red line) and King profiles (blue line). Top row - age groups A and B; bottom row - age groups C and D. Error bars are not shown, because the Poisson errors are comparable in size to or smaller than the symbols. Below each profile are the residuals from the fit.

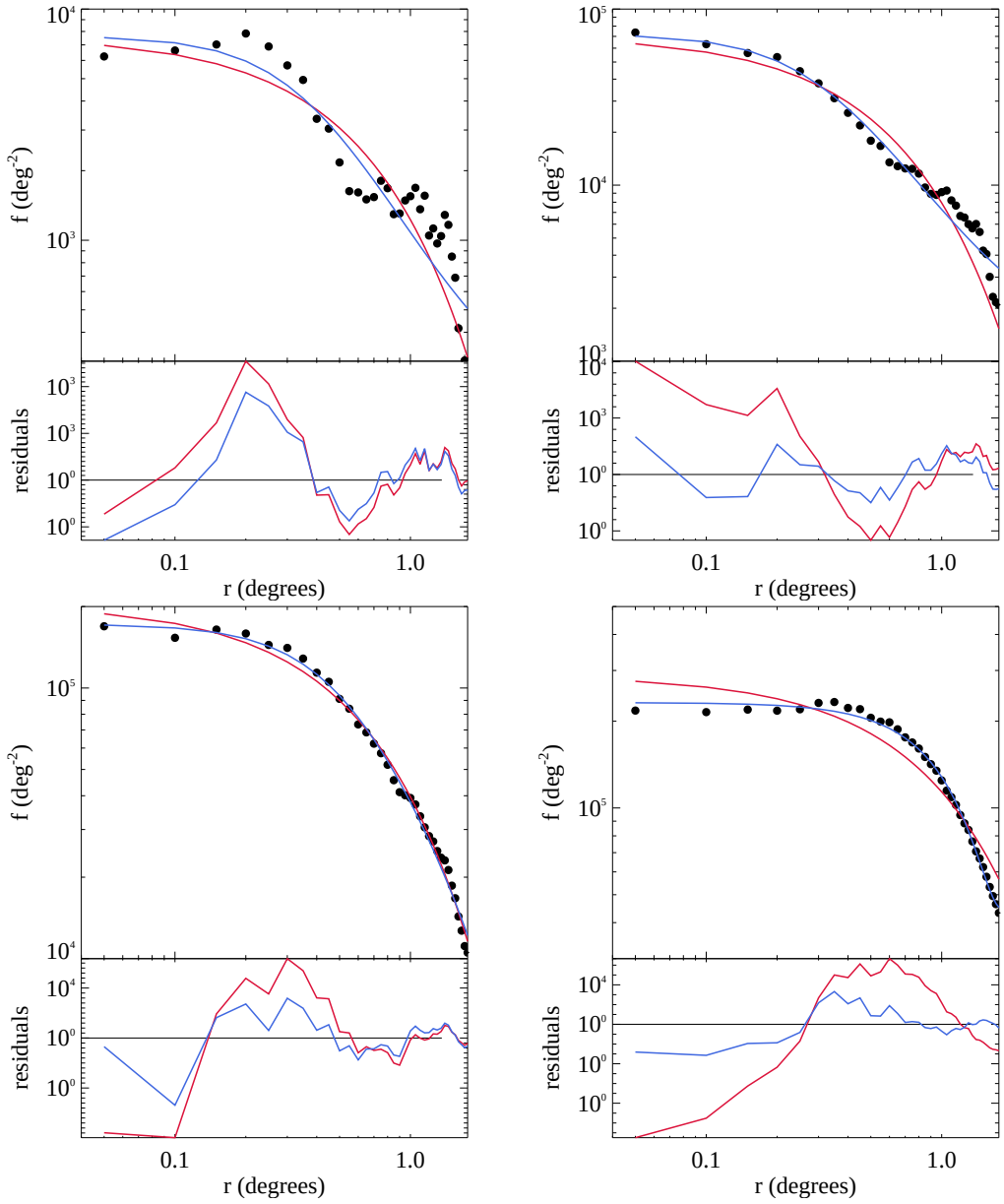

Figure 6.8: RDPs for the subsets of SMC stars from the MCPS, fitted with exponential-disk (red line) and King profiles (blue line). Top row - age groups A and B; bottom row - age groups C and D. Error bars are not shown, because the Poisson errors are comparable in size to or smaller than the symbols. Below each profile are the residuals from the fit.

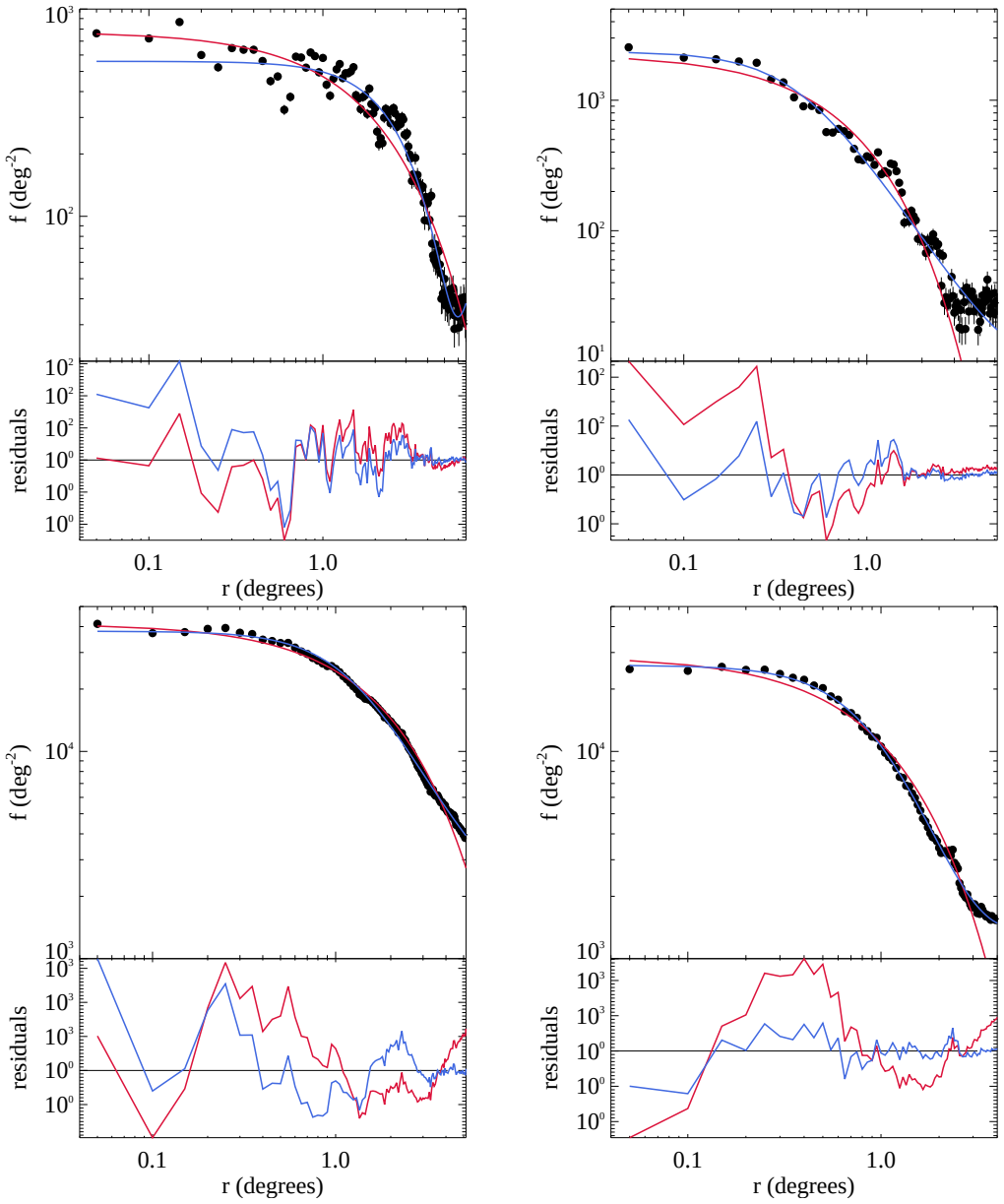

Figure 6.9: RDPs for the subsets of stars from 2MASS, fitted with exponential-disk (red line) and King profiles (blue line). Top row - age group E; bottom row - age group F. Left - LMC; right - SMC. Error bars are not shown, because the poisson errors are comparable in size to or smaller than the symbols. Below each profile are the residuals from the fit.

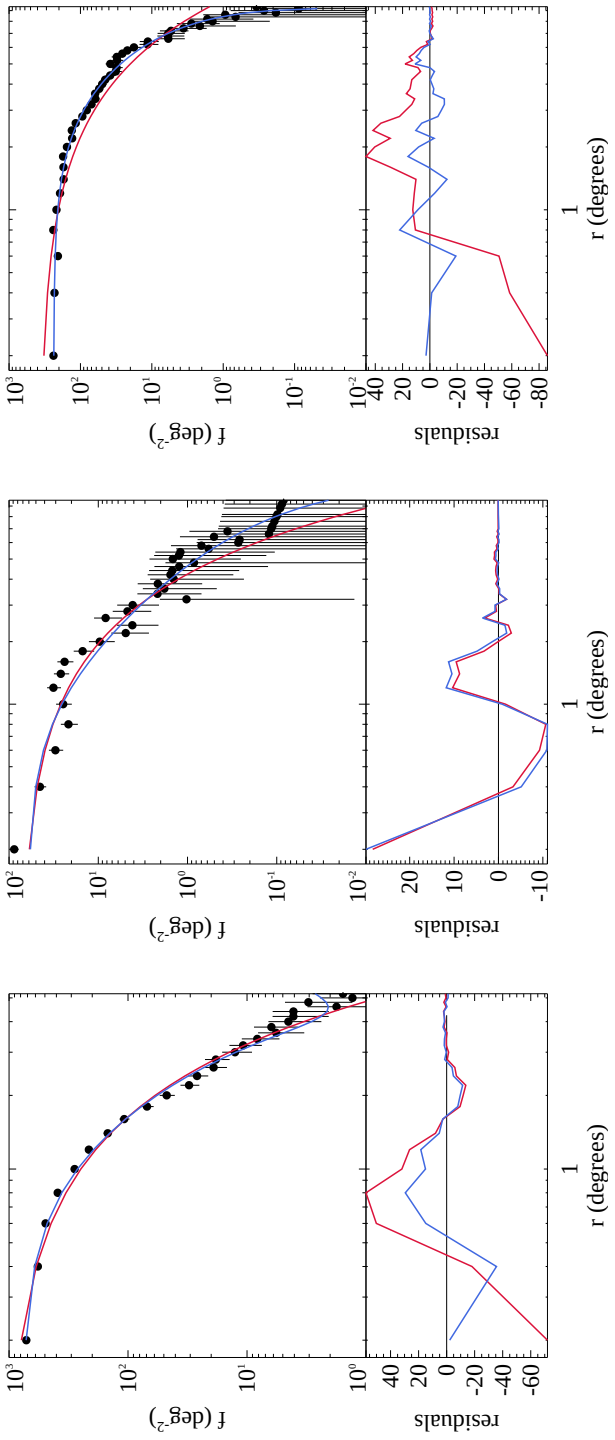

Figure 6.10: RDPs for the carbon stars, fitted with exponential-disk (red line) and King profiles (blue line). Left - LMC; middle - LMC bright; right - SMC. Below each profile are the residuals from the fit.

mostly undisturbed.

Moreover, the spatial distribution of stars from 2MASS and of the carbon stars in the LMC (see Figure 6.5 and 6.6) suggests that there are two subsystems, whose major axes are almost perpendicular to one another. The same behaviour has recently been detected by Bica et al. (2008) for the star clusters in the LMC. This effect has previously been described by Kontizas et al. (1990) and later by Dottori et al. (1996), who found that the young clusters, mainly occupying the bar, are rotated with respect to the older clusters and the major axes of the systems are almost perpendicular.

6.3 Radial Surface Density Profiles

For the RDPs the following centres of the Magellanic Clouds were adopted, given by the SIMBAD Astronomical Database[1] - for LMC: 05^h23^m -69^d45^m and for the SMC: 00^h52^m -72^d48^m.

The RDPs obtained from MCPS are presented in Figures 6.7 and 6.8 for the LMC and SMC, respectively. The RDPs from 2MASS data and the carbon stars catalogues are presented in Figures 6.9 and 6.10. The theoretical models used to fit the RDPs are the exponential-disk (Eq. 2.5) and the King law (Eq. 2.6). The best fit of both models is displayed in each figure. In all figures, except Figure 6.10, error bars are not shown, because the Poisson errors are comparable in size to or smaller than the symbols. Additionally, the residuals below each profile reveal the preferred model and show the dominant model for each part of the galaxy.

Figures 6.7a and 6.8a display a very clumpy distribution for the brightest stellar population. Considering that the stars in this age group are in concentrations, i.e. stellar complexes (Maragoudaki et al. 1998, 2001), then the very wide spread is expected and explained.

The RDPs for the SMC from MCPS show that both the exponential-disk and the King models can be used to describe the stellar distribution. However, as can be seen from Figure 6.8, if the distribution of the youngest stars is almost equally well fitted by both, the oldest stars definitely follow the King law. Such a difference is not observed in the LMC, where the exponential-disk model seems slightly better. This is possibly due to the relatively smaller area available for the LMC, which is dominated by the younger stars. A similar behaviour is observed in the RDPs from 2MASS. Both the younger and the older stars in the LMC are distributed on an exponential disk, while the radial density distribution of the SMC is better described by the King profile.

[1] `http://simbad.u-strasbg.fr/simbad`

Table 6.2: Structural parameters derived from the observed RDPs with the adopted theoretical models (exponential-disk and King profiles)

RDP	f_{0D} [Obj. deg^{-2}]	h_D [deg]	f_{0K} [Obj. deg^{-2}]	r_c [deg]	r_t [deg]	c_p
MCPS						
LMC A	$(1.4 \pm 0.9) \times 10^3$	2.6 ± 0.3	$(1.2 \pm 0.6) \times 10^3$	2.1 ± 0.2	–	–
LMC B	$(18 \pm 1) \times 10^3$	1.33 ± 0.07	$(16 \pm 1) \times 10^3$	1.1 ± 0.06	–	–
LMC C	$(96 \pm 4) \times 10^3$	1.44 ± 0.06	$(83 \pm 4) \times 10^3$	1.2 ± 0.07	–	–
LMC D	$(260 \pm 3) \times 10^3$	1.52 ± 0.02	$(225 \pm 4) \times 10^3$	1.3 ± 0.03	–	–
SMC A	$(7 \pm 0.6) \times 10^3$	0.57 ± 0.04	$(6.7 \pm 0.5) \times 10^3$	0.4 ± 0.03	–	–
SMC B	$(64 \pm 3) \times 10^3$	0.48 ± 0.02	$(62 \pm 2) \times 10^3$	0.4 ± 0.01	–	–
SMC C	$(183 \pm 4) \times 10^3$	0.64 ± 0.01	$(177 \pm 6) \times 10^3$	0.6 ± 0.02	–	–
SMC D	$(259 \pm 11) \times 10^3$	1.13 ± 0.06	$(918 \pm 247) \times 10^3$	1.9 ± 0.2	–	–
2MASS						
LMC E	$(7.7 \pm 0.2) \times 10^2$	2.01 ± 0.05	$(11.1 \pm 1.0) \times 10^2$	2.89 ± 0.2	–	–
LMC F	$(41.3 \pm 0.5) \times 10^3$	1.89 ± 0.02	$(36.3 \pm 0.4) \times 10^3$	1.58 ± 0.02	–	–
SMC E	$(22.6 \pm 1.0) \times 10^2$	0.60 ± 0.01	$(23.8 \pm 0.7) \times 10^2$	0.40 ± 0.01	–	–
SMC F	$(28.7 \pm 0.7) \times 10^3$	1.03 ± 0.02	$(26.3 \pm 0.3) \times 10^3$	0.82 ± 0.01	–	–
Carbon stars						
LMC	368 ± 22	1.69 ± 0.07	514 ± 17	3.3 ± 0.1	9.7 ± 0.2	0.46
LMC bright	72 ± 6	0.98 ± 0.05	71 ± 7	0.9 ± 0.1	12 ± 3	1.12
SMC	1050 ± 40	0.69 ± 0.02	1100 ± 39	0.85 ± 0.04	5.2 ± 0.3	0.78

The structural parameters of the LMC and SMC obtained by fitting RDPs from the adopted data sets in the various catalogues are listed in Table 6.2. Columns (2) and (3) contain the central density of objects f_{0D} and the scale length h_D respectively. Columns (4)-(7) contain the central density of objects f_{0K}, the core radius r_c, the tidal radius r_t where available, and the concentration parameter c_p.

The parametric value of the tidal radius r_t obtained for stars from 2MASS and the MCPS was not reliable enough, because of the relative incompleteness of 2MASS and the small area that is available from the MCPS. The carbon stars, on the other hand, represent a sufficiently complete sample of this particular group of objects as numbers, spatial distribution, and magnitude range. Therefore we can use these objects as prototypes of the major dynamical system in both Clouds.

Bica et al. (2008) derived the structural parameters of the star cluster system of the Magellanic Clouds. The results suggest that the LMC disk scale length is $\approx 1^\circ$, about twice the SMC value, when fitting the profiles with an exponential-disk model. One of their conclusions is that the large-scale structure of both interacting irregular galaxies does not follow the classical disk and/or spheroidal laws, since the $R^{1/4}$ law fails completely. Additionaly, fitting the surface density profiles with a three-parameter King-like profile gives a similar result: the SMC structural radii correspond to about half of the LMC ones.

We detect a similar behaviour for the carbon stars (see Table 6.2) with $h_D = 1.69 \pm 0.07$ for the LMC and $h_D = 0.69 \pm 0.02$ for the SMC. This ratio of h_D in both Clouds is evident also for both the young and old stellar populations from 2MASS data and all but the youngest groups of stars from MCPS data.

6.4 Discussion

It is common for dIrr galaxies to have patchy distributions of young, blue stars but smoother and more extended distributions of older, redder stars that follow exponential or King surface density profiles (Mateo 1998). Our results for the inner region of the Magellanic Clouds and the fairly azimuthally symmetric elliptical exponential profile of the older SMC stars (Nidever et al. 2011) is consistent with this general trend.

Nidever et al. (2011) determine that the SMC star-count density follows a general radial exponential, but the distribution is not well-fitted by a single exponential for all radii and position angles. They find that the distribution of RGB stars is quite different for the inner ($R \lesssim 3^\circ$) and intermediate ($3^\circ \lesssim R \lesssim 7.5^\circ$) radial regions. The intermediate component is much more azimuthally symmetric than the inner component which is quite elliptical, and the major axes of the two components are nearly perpendicular (difference ~105°). The center of the

intermediate component is offset by 0.59° to the northeast of the center of the inner component - along the inner's major axis - and is closer to the HI dynamical center (separation=0.38°; Stanimirović et al. (2004)). In the curent study we cannot confirm nor argue this finding because our data does not reach more than ~2° from the center of the SMC.

However, the SMC is not as undisturbed as might be suggested from the fairly symmetrical density profile of its intermediate component. Hatzidimitriou et al. (1989) and Gardiner and Hawkins (1991) used red clump stars to show that the line-of-sight depth varies significantly across the face of the SMC. It is much thicker in the northeast and extends to smaller distances there (from the Sun) compared to the southwest. Therefore, the three-dimensional structure of the SMC is somewhat irregular and disturbed, likely due to the recent close interaction of the SMC with the LMC. The fact that the projected density profile is still so symmetric might be a coincidence owing to the particular orientation of the Magellanic system relative to our viewing angle.

Based on the surface density distribution and the radial density profile of the red clump stars and RR Lyrae stars the observed structure of the SMC, in which both the red clump stars and RR Lyrae stars are distributed, is approximated as a triaxial ellipsoid (Subramanian and Subramaniam 2011). The line of sight depth (front to back distance) across the SMC is estimated using the dispersion in the I_0 magnitudes of both the red clump stars and the RR Lyrae stars and found to be large (~14 kpc) for both the populations.

The difference in the line-of-sight depths between the eastern and western sides of the SMC suggests a possible explanation for the lack of centration between the inner and outer distributions. Because the stars on the eastern side of the SMC are on average closer than the stars on the western side, the SMC periphery will exhibit a perspective effect. The near-side of the SMC will appear larger than the far-side and the density contours will be "stretched" on the near-side (east) and "bunched-up" on the far-side (west). The net result is that the center of outer contours of a fit to the on-sky densities will be systematically shifted to the near-side, or the east, as observed. A perspective effect has previously been observed to affect the outer contours of the LMC due to the inclination of its stellar disk (van der Marel 2001). However, it is important to note that the lack of any stellar rotation seen in radial velocities (Harris and Zaritsky 2006; Kunkel et al. 2000) or proper motions (Piatek et al. 2008) indicates that the SMC does not have a stellar disk like the LMC, but is pressure supported and likely has a more spheroidal or ellipsoidal shape. The difference in line-of-sight distances across the SMC might be a result of tidal distortions of the SMC shape due to the recent encounter of the Magellanic Clouds ~200 Myr ago.

The structural parameters of the LMC and SMC from the adopted data sets in the various catalogues (MCPS, 2MASS, and carbon stars) are listed in Table

6.2. Neither the exponential-disk, nor King models are always very explicitly determined as the dominant dynamical model. However, we can adopt a criterion for the acceptance of one or the other model. The χ^2 values given by the RDPs fitting allow us to assume one of the models as more appropriate for describing the distribution of the data. A second criterion could be the age of the stellar population, assuming that the very young population might be distributed on an exponential disk-like structure, even if it does not fit the whole galaxy.

It was shown that there is a system of young objects more concentrated in the central region of the LMC with a position angle almost perpendicular to the other system. Of course the inclination of the LMC is small (almost face-on), allowing the difference to be seen. The two systems in the LMC have been previously mentioned, and are explained as one result of the interaction between the Milky Way galaxy and the Magellanic Clouds.

From the carbon stars in the LMC, it was shown that two different systems exist with a core radius of 3.3 ± 0.1 deg for the faint and 0.9 ± 0.1 deg for the bright carbon stars. An exponential model also shows such a difference in the scale height, 1.69 ± 0.07 deg and 0.98 ± 0.05 deg, respectively, revealing a smaller central system of more massive carbon stars. The young clusters are also found in a smaller central system, than for the old ones (Bica et al. 2008). As can be seen in Figures 6.6 and 6.10, we did not observe such a segregation for the SMC carbon stars.

The spatial distribution of the stellar content at the age of the last star formation event shows that the star formation has shrunk to the central regions in the last 100 Myr in both the galaxies. Indu and Subramaniam (2011) propose that the HI gas in the LMC is pulled to the north of the LMC in the last 200 Myr due to the gravitational attraction of our Galaxy at the time of perigalactic passage. The shifted HI gas is preferentially compressed in the north during the last $200 - 40$ Myr and in the north-east in the last 40 Myr, due to the motion of the LMC in the Galactic halo. The recent star formation in the SMC is due to the combined gravitational effect of the LMC and the perigalactic passage.

Although the Magellanic Clouds are assumed to be irregular galaxies, it also seems that the older populations appear to behave as tidally truncated systems, even if they do not show obvious radial symmetry. From Table 6.2 we can see that the parameters of the fitting for the young stellar populations are inconclusive. However, this is no surprise, because even if the bulk of the stars show some radial symmetry, this is not the case for the young bright stars. Both their contour maps and their radial density profiles do not support such an assumption. This is anticipated since clumping of star-forming regions dominates their distribution.

Part III

The Magellanic Clouds and the Universe Model

Part III is devoted to a very important part of this study. The inspiration behind this project was the implementation of galaxies resolved in stars for the Gaia Universe Model, used for simulations in the framework of the Gaia mission preparation. This basically meant to provide a model of the distribution of key stellar populations in nearby galaxies (e.g. the Magellanic Clouds), which would then become a part of the Gaia Universe Model. This part of the Thesis shows how the initial idea evolved and how results from this study were used during simulations by the DPAC CU2.

The Data Processing and Analysis Consortium (DPAC) is a European collaboration including the ESA Gaia Science Operations Centre (SOC) and a broad, international science community, and including six large Data Processing Centres (DPCs). The Consortium is structured around a set of eight Coordination Units (CUs) each in charge of a specific aspect of the data processing. CU2's main task is to develop a software system capable of covering the simulation needs of the Gaia DPAC. Chapter 7 gives a short description of CU2 which is responsible for the development of the Gaia Universe Model. This Chapter also presents the Universe Model itself.

Chapter 8 presents both stages of the implementation of Magellanic Clouds stars into the Gaia Universe Model. First, catalogues of stellar parameters were prepared using existing B, V and I magnitudes and coordinates data and providing rough estimates for the spectral type, effective temperature and the surface gravity. Other global parameters of the Magellanic Clouds were assumed, based on data from the literature. These parameters were the distance to the Clouds, their depth, proper motions, radial velocities and metallicity distribution. Then the provided catalogues were used to analyze the content of a full sky snapshot (for a given moment in time) of the Universe Model (Robin et al. 2012).

Chapter 7

Gaia Data Simulations

7.1 Structure and Goals of DPAC/CU2

The main task of the Coordination Unit 2 (CU2) is to develop a software system capable of covering the simulation needs of the Gaia Data Processing Consortia (DPAC). However, software engineering competence alone is not sufficient for the task; a strong scientific component is also needed to ensure that the system fulfills the scientific needs of the DPAC. The CU2 structure reflects this dual nature and is organised around four teams: i) a core software engineering team; ii) a scientific team for the development of a Universe Model; iii) a scientific team providing the expertise to develop models of the Gaia spacecraft and its instruments and iv) a Quality Assurance and Validation team

CU2 is subdivided into Development Units (DUs), which take the responsibility of specific parts of the CU2 overall task.

DU1 Coordination & management This DU is a placeholder for the management structure of CU2. It is in charge of the overall coordination and management of CU2, from requirements gathering to project control, schedule definition and priority selection. It is constituted by the CU2 and DU managers.

DU2 Software engineering This DU is in charge of the software engineering aspects of the project, a core software engineering team able to professionally manage the development of a complex software system, the Gaia simulator.

DU3 Universe model This DU is in charge of the definition, development and integration of Universe Model into the Gaia simulator. The team composing this group should be essentially made of scientists, in charge of interacting with the wide European Scientific Community to gather the necessary expertise to build

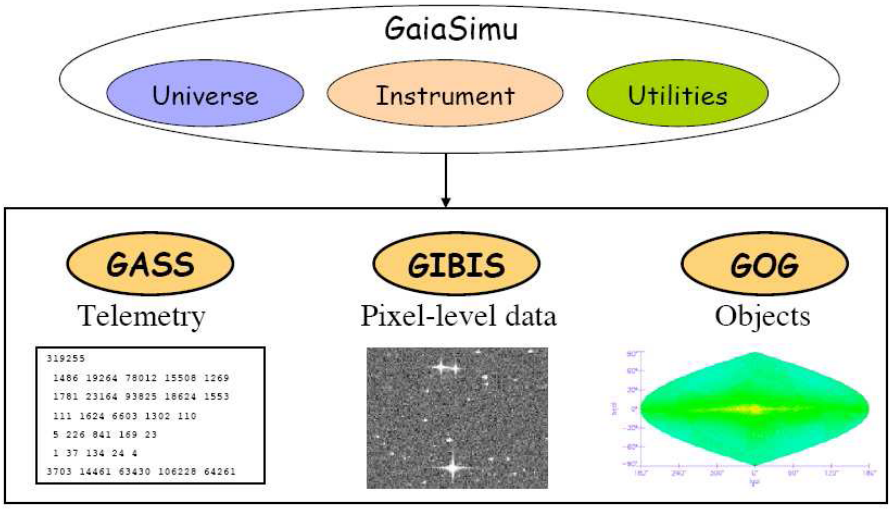

Figure 7.1: Organisation of the simulation development by DPAC (2007). The simulator building blocks are shown - a core library implementing all the tools needed, including models of observable objects (Universe Model) and spacecraft instruments(Instrument Model), a telemetry simulator (GASS), a pixel-level simulator (GIBIS), and a intermediate data simulator (GOG).

the models of the wide variety of objects to be observed by Gaia, but should also be competent in software engineering to enable its integration in the Gaia simulator with the support of the other DUs.

DU4 Instrument models This DU is in charge of the definition, development and integration of the spacecraft and instrument models into the Gaia simulator.

DU5 Gaia System Simulator (GASS) This DU is in charge of the development of the GASS data generator, that will provide simulations of the telemetry stream of the mission. The simulations use some simplifications of the instrument and Universe models allowing a large amount of data to be simulated over a significant period of time.

DU6 Gaia Instrument & Basic Image Simulator (GIBIS) This DU is in charge of the development of the GIBIS data generator, that will provide simulations of the data at the pixel level. The resulting simulations should be as realistic as possible for a limited region of a sky and over a short period of time.

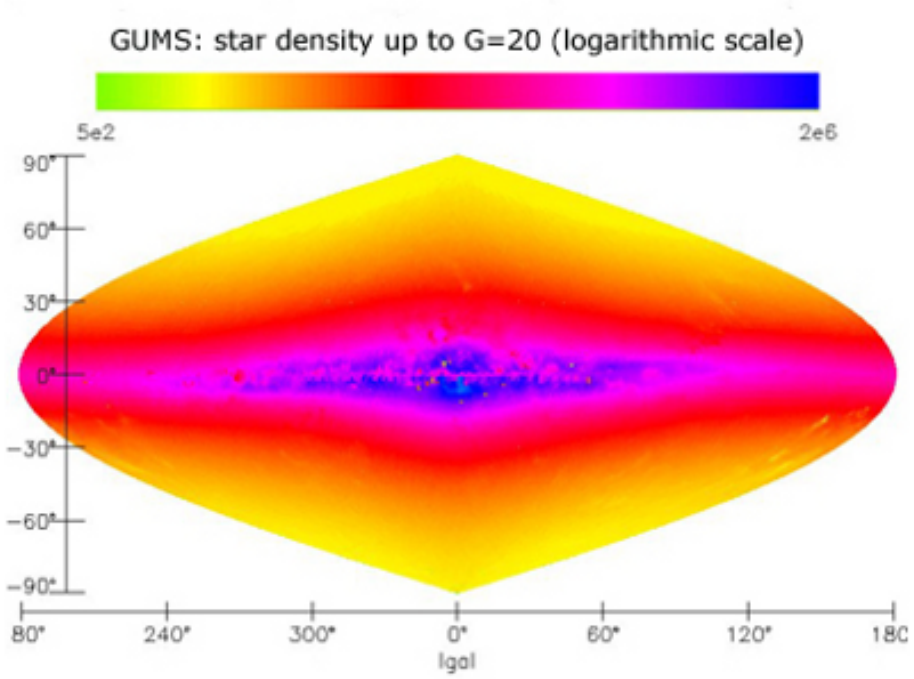

Figure 7.2: Gaia Universe Model Snapshot (`http://www.rssd.esa.int`). The Universe model used in this version includes only galactic stars, generated using the Besançon Galaxy Model (the generation of binaries and variables was deactivated) in combination with the Drimmel extinction model.

DU7 Gaia Object Generator (GOG) This DU is in charge of the development of the GOG data generator, that will provide simulations of number counts and lists of observable objects from the Universe model and, for a given source or a collection of sources, simulations of intermediate and end-of-mission Gaia data.

DU8 Scientific Validation This DU will be in charge of the quality assurance and validation of the Gaia simulator. This will include checking compliance with requirements and design of tests for the validation of simulations, both internal (self-consistency) and external (comparison with real data).

7.2 Gaia Universe Model

The Universe Model developed for the simulation needs of the mission is a set of data bases, theoretical models, and algorithms for computing the positions at any time, and observational properties of any objects expected to be observed by the Gaia instruments. The distributions of these objects and the statistics

of observables should be as realistic as possible for simulations to be usable for estimating telemetry, testing software, simulating images, etc.

Objects which will be simulated are: solar system objects (planets, satellites, asteroids, comets), Galactic objects (stars, nebulae, stellar clusters, diffuse light), extra-galactic objects (galaxies resolved in stars, unresolved galaxies, quasars and active Galactic nuclei, supernovae). For each of these simulated objects one needs to have their three-dimensional spatial distribution together with their spectral characteristics (to be able to compute photometry and spectroscopy, stable or variable in time), and their motions (for astrometric computations and for spectral corrections). Gravitational lensing for stars and galaxies are also to be simulated.

The Gaia Universe Model Snapshot (GUMS) is part of the GOG component of the Gaia simulator. It has been used to generate a synthetic catalogue of objects from the universe model for a given static time t_0 simulating the real environment where Gaia will observe (down to G = 20 mag). Figure 7.2 shows such a Gaia Universe Model Snapshot - this is how the Milky Way galaxy looks through Gaia's "eyes".

The GUMS is a one-billion object catalogue generated using GOG. The purpose of GUMS is to allow validation of the Universe Model used in the full Gaia mission simulation, and to provide useful statistics for the Gaia observations, for example: statistics on G magnitude, parallax, space velocities (proper motion and radial velocity), some astrophysical parameters (T_{eff}, $\log g$, $[Fe/H]$) and stellar masses. The Universe model used in this version (v0. from 2005) includes only galactic stars, generated using the Besançon Galaxy Model (the generation of binaries and variables was deactivated) in combination with the Drimmel extinction model.

It is worth noting that this snapshot is what Gaia will be able to potentially observe but not what it will really detect, since satellite instrument specifications and the available error models are not taken into account in the present statistical analysis.

Chapter 8

Magellanic Clouds: the implementation

8.1 Preparation

One main aspect of the current study was the investigation of the spatial distribution of stellar populations in nearby galaxies, resolved in stars by Gaia. This includes resolved stars only and does not include non-stellar objects, unresolved groups of stars, etc. These are part of the extra-galactic objects to be simulated in the framework of the Gaia mission preparation and are not covered in our investigation. There are no plans to include extended objects like nebulae in the Magellanic Clouds. No other resolved galaxy simulations are planned, unless explicit requests and corresponding manpower exist.

The ultimate goal was to improve the Gaia Universe Model by providing the means to simulate these resolved galaxies in the framework of the Gaia mission preparation. All the work that followed was done in collaboration with CU2 and the people responsible for the development of the Gaia Universe Model (DU3). Initialy there were two options for the implementation of Magellanic Clouds stars in the Gaia Universe Model:

- To include a catalogue in the Universe Model and provide parameters such as R.A., Dec., V, $V-I$, G, distance, radial velocities, proper motions, $\log g$, T_{eff}, $[Fe/H]$, $[\alpha/Fe]$, and the extinction A_V

- To create a model of the distribution of different stellar populations, such as carbon stars, planetary nebulae or star clusters. In this case if the distribution is, for example, exponential it will be necessary to provide the scale length, scale height, inclination, M_V, T_{eff}, $\log g$, A_V

8. MAGELLANIC CLOUDS: THE IMPLEMENTATION

There are still open questions regarding the Magellanic Clouds' spatial structure. So it was decided to use the first option for simulations of the Magellanic Clouds and provide catalogues of Magellanic Clouds stars which include the following parameters: Right Ascension, Declination, V, $V-I$, G, distance, radial velocities, proper motions, $\log g$, T_{eff}, $[Fe/H]$, $[\alpha/Fe]$, and the extinction A_V.

Catalogues of stars known to be part of both Magellanic Clouds (LMC and SMC), containing their B, V, and I magnitudes, have been obtained from the Magellanic Clouds Photometric Survey (Zaritsky et al. 2002, 2004). A detailed description of the MCPS can be found in Chapter 5. It is a good source because its spatial resolution is comparable to that of HST. Gaia's spatial resolution is expected to be comparable to the one of HST, both being located in space, above Earth's atmosphere.

The catalogues are complete down to $V \approx 20$. However, although there is B and V filter data available for all stars, this is not the case for the I magnitude. For the stars with $V \leq 20$ mag, only 5% will be lost due to missing I magnitude. Not taking into account stars with $V = 20$ mag will lower this figure to about 1.6%. The U magnitude, although available for all star in both catalogues, is not used because it is not necessary for the simulations.

Four passbands (and their corresponding magnitudes) are associated with the Gaia instruments: G, G_{BP}, G_{RP} and G_{RVS}. The Gaia G band magnitude for each star can be related to the Johnson-Cousins V and I passband by the following approximation (Perryman et al. 2001):

$$G = V + 0.51 - 0.50\sqrt{0.6 + (V - I - 0.6)^2} - 0.065(V - I - 0.6)^2 \qquad (8.1)$$

for –0.4 < V–I $\lesssim$ 6. The approximation can be simplifed to G–V = 0.0 ± 0.1mag for the range –0.4 < V–I < 1.4. This is the reason we only had to provide the B, V and I magnitudes for the Gaia Universe Model.

The effective temperature T_{eff} was determined for each entry in the catalogue by fitting theoretical evolutionary tracks (isochrones) to the data. The surface gravity has been estimated from the effective temperature and luminosity class but it is very difficult to assert from the available observables. Hence the resulting HR diagrams for the Magellanic Clouds are not as well defined and reliable as they would be if obtained from theoretical isochrones.

Table 8.1 and 8.2 contain sample from the catalogues used to simulate the Magellanic Clouds. Column (1) and (2) contain the coordinates for each entry, columns (3), (4), and (5) contain the B, V, and I magnitudes, respectively. Column (6) contains the $V-I$ colour and column (7) - the spectral type. Columns (8) and (9) contain the effective temperature T_{eff} and the surface gravity $\log g$, respectively.

Table 8.1: Sample of the catalogue of the Large Magellanic Cloud for GaiaSimu

R.A., ° (J2000.0)	Dec, ° (J2000.0)	B	V	I	V-I	Sp.Type	T_{eff}, K	$\log g$
(1)	(2)	(3)	(4)	(5)	(6)	(7)	(8)	(9)
67.2327	-72.4324	13.98	13.46	13.08	-5.12	G5	5010	0.85666
67.3154	-72.1435	14.64	14.04	13.04	-4.54	G5	5010	1.57193
67.3211	-72.3893	14.81	13.78	12.80	-4.80	K0	4720	2.20089
67.3240	-72.3305	14.22	12.93	11.62	-5.65	K3	4210	0.57648
67.3289	-72.2188	15.30	14.42	13.53	-4.16	G5	5010	1.00458
67.3724	-72.2436	14.80	14.24	13.61	-4.34	G5	5010	1.75724
67.3745	-72.3233	15.70	14.52	13.21	-4.06	K3	4210	0.56847
67.3823	-72.3286	15.43	14.37	13.22	-4.21	K1	4580	0.59224
67.4062	-72.2089	12.86	12.08	11.16	-6.50	G5	5010	1.53578
67.4082	-72.1973	13.76	12.84	11.83	-5.74	G8	4870	1.37023
...	...	...	...	...	...	...	...	...

Table 8.2: Sample of the catalogue of the Small Magellanic Cloud for GaiaSimu

R.A., ° (J2000.0)	Dec, ° (J2000.0)	B	V	I	V-I	Sp.Type	T_{eff}, K	$\log g$
(1)	(2)	(3)	(4)	(5)	(6)	(7)	(8)	(9)
5.87561	-74.4108	15.25	14.58	13.82	-4.39	G5	5010	0.55883
5.93255	-74.4240	15.55	14.60	13.57	-4.37	G8	4870	1.02909
5.97008	-74.4639	15.70	14.92	14.01	-4.05	G5	5010	0.89593
5.97683	-74.6296	15.16	14.39	13.67	-4.58	G5	5010	2.18276
6.02841	-74.2178	14.42	13.23	11.38	-5.74	K3	4210	1.55271
6.04169	-74.2504	15.07	14.51	13.64	-4.46	G5	5010	2.30904
6.04746	-74.0216	15.86	14.79	13.51	-4.18	K1	4580	2.46094
6.05019	-74.3814	13.88	13.02	12.12	-5.95	G5	5010	1.07647
6.06167	-73.9335	13.71	12.88	11.85	-6.09	G5	5010	2.20545
6.07420	-74.4921	15.10	14.39	13.55	-4.58	G5	5010	2.01693
...	...	...	...	...	...	...	...	...

Table 8.3: Assumed global parameters of the Magellanic Clouds.

Parameter	Unit	LMC	SMC	Reference
Distance	kpc	48.1	60.6	LMC: Macri et al. (2006) SMC: Hilditch et al. (2005)
Depth	kpc	0.75	1.48	LMC: Sakai et al. (2000) SMC: Subramanian et al. (2009)
$\mu_\alpha \cos\delta$	mas yr^{-1}	1.95	0.95	Costa et al. (2009)
μ_δ	mas yr^{-1}	0.43	-1.14	Costa et al. (2009)
V_{los}	km s^{-1}	283	158	SIMBAD (CDS)*
Fe/H	dex	-0.75±0.5	-1.2±0.2	Kontizas et al. (2011), in prep.
α/Fe	dex	0.00±0.2	0.00±0.5	Kontizas et al. (2011), in prep.

* `http://simbad.u-strasbg.fr/simbad`

8.2 Implementation

In order to simulate the Magellanic clouds, catalogues of stars and their characteristics (B, V, and I magnitudes, T_{eff}, $\log g$, spectral type) have been obtained as described in the previous Section 8.1. The assumed global parameters of the Magellanic Clouds required for the simulations and their references are given in Table 8.3.

For the astrometry, since star by star distance is missing, a single distance, proper motion and radial velocity for all stars of both Magellanic Clouds is assumed. The distances to the stars in the Magellanic Clouds can be expressed using a mean distance to the Magellanic Clouds, which is fairly well known, and the depth of the galaxy, which is more doubtful. In this case the distance from Macri et al. (2006) was used, who studied the relative distance modulus between the LMC and NGC 4258. The distance to the SMC was obtained by Hilditch et al. (2005). They conducted a programme to determine the fundamental parameters of eclipsing binaries of spectral types O and B in the SMC. Each system provided a primary distance indicator and a mean distance modulus was obtained.

For simulating the depth of the clouds a gaussian distribution is assumed along the line of sight with a sigma given in Table 8.3. Sakai et al. (2000) use the MCPS and OGLE to estimate the line of sight depth in the disk and bar regions of the Large and Small Magellanic Clouds. Subramanian and Subramaniam (2009), on the other hand, use the MCPS to study the red giant branch stars in the LMC and obtained the distance modulus and the LMC depth.

The radial velocities, proper motions and metallicity distributions can again

Table 8.4: Spectral types of stars from the LMC and SMC, generated by the Gaia Universe Model Snapshot (Robin et al. 2012).

Spectral type	G < 20 mag	Grvs < 17 mag	Grvs<12 mag
O	0.25%	0.17%	0.39%
B	3.24%	3.40%	1.85%
A	17.20%	5.01%	4.83%
F	0.00%	0.00%	0.00%
G	45.98%	23.16%	55.19%
K	32.62%	64.82%	35.33%
M	0.71%	3.44%	2.41%
Total	8 800 000	1 200 000	6 600

be represented by a mean value and a gradient. The proper motions are provided by Costa et al. (2009). They determined the proper motion of the Magellanic Clouds relative to background quasars. The chemical abundances are also guessed from the mean abundance taken from the literature (Kontizas et al., private communication). Stellar masses are estimated for each star from polynomial fits of the mass as a function of $B - V$ colour, for several ranges of $\log g$, based on Padova isochrones for a metallicity of $z = 0.003$ for the LMC and $z = 0.0013$ for the SMC.

The main goal of Robin et al. (2012) was to analyze the content of a full sky snapshot (for a given moment in time) of the Universe Model. The simulation was performed with MareNostrum, one of the most powerful supercomputers in Europe managed by the Barcelona Supercomputing Centre. The execution took 20 000 hours (equivalent to 28 months) of computation time distributed in 20 jobs, each one using between 16 and 128 CPUs. MareNostrum runs a SUSE Linux Enterprise Server 10SP2 and its 2 560 nodes are powered by 2 dual-core IBM 64-bit PowerPC 970MP processors running at 2.3 GHz.

The generated universe model snapshot has been analyzed by using the Gog Analysis Tool (GAT) statistics framework, which produces all types of diagnostic statistics allowing its scientific validation (e.g. star density distributions, HR diagrams, distributions of the properties of the stars).

Apart from the galactic objects, 38 million unresolved galaxies, 1 million quasars, and supernovae, the model generates 8.8 million additional stars that belong to the Magellanic Clouds. The most abundant spectral type are G stars (46%), followed by K types (33%) and A types (17%). The complete distribution of spectral types generated by the Universe Model in the Magellanic Clouds is presented in Table 8.4. There are no F type stars reachable by Gaia, because

the magnitude cut at the Clouds' distance selects only the upper part of the HR diagram including massive stars on the blue side, and late type giants and supergiants on the red side.

8.3 Summary

The inspiration behind this project was the implementation of galaxies resolved in stars for the Gaia Universe Model, used for simulations in the framework of the Gaia mission preparation. This basically meant to provide a model of the distribution of key stellar populations in nearby galaxies (e.g. the Magellanic Clouds), which would then become a part of the Gaia Universe Model. The ultimate goal was to improve the Gaia Universe Model by providing the means to simulate these resolved galaxies in the framework of the Gaia mission preparation. All the work that followed was done in collaboration with CU2 and the people responsible for the development of the Gaia Universe Model.

It was decided to use the MCPS as a basis for providing catalogues of Magellanic Clouds stars to CU2. The catalogues included the following parameters: Right Ascension, Declination, V, $V-I$, $\log g$, T_{eff}. The other necessary parameters (distance, radial velocities, proper motions, $[Fe/H]$, $[\alpha/Fe]$, and the extinction A_V) were obtained from the literature. Then, Robin et al. (2012) analyzed the content of a full sky snapshot of the Universe Model. The simulation was performed with MareNostrum, one of the most powerful supercomputers in Europe managed by the Barcelona Supercomputing Centre.

The work by Robin et al. (2012) showed that the Gaia Universe Model, and other population synthesis models in general, can be useful tools for survey preparation. In this particular case, it was possible to obtain a general idea of the numbers, percentages and distribution of different objects and characteristics of the environment that Gaia can potentially observe and measure.

Additionally, the analysis of the snapshot has facilitated the detection of several aspects to be improved. Therefore, it has been a quite fruitful quality assurance process from a scientific point of view. Looking forward, the next reasonable step would be to reproduce the same analysis but taking into consideration the instrument specifications and the available error models. By convolving it with the idealized universe model presented in the paper of Robin et al. (2012), it will be possible to evaluate the impact of the instrumental effects on the actual composition of the Gaia catalogue.

Part IV

Other Local Group galaxies

In Part IV we present the results from studying the stellar distribution of six dwarf irregular galaxies in the Local Group. Some are not going to be resolved in stars by Gaia, and others will only have their brightest supergiant stars detected. One of the galaxies might also provide a little bit more than just a few bright stars.

In Chapter 9 we present our sample of dwarf irregular galaxies. The galaxies included in this study are Phoenix, NGC 6822, IC10, WLM, Sextans A, and Sextans B. We present their basic properties, interesting features, and some results from previous studies. They all have diverse properties and are located at various distances throughout the Local Group, some are confirmed members and others lie at the periphery.

The data used for the investigation of these galaxies are presented in Chapter 10. Massey et al. (2007) provide a survey of the resolved stellar content of nearby galaxies currently forming stars. It is a uniform survey ($UBVRI$, $H\alpha$, [SII], and [OIII]) of nearby galaxies selected on the basis of current star formation. This particular catalogue was used because i) the field of view is excellent and it includes the outer regions of the studied dwarf irregular galaxies, and ii) the completeness allows to study the stellar distribution down to the Gaia limit of $V = 20$ mag and fainter.

The spatial distribution of these galaxies is studied using isopleth maps and radial surface density profiles. The isopleth maps of these Local Group galaxies and their radial density profiles are presented in Chapter 11. Moreover, the structural parameters of these galaxies have been derived by fitting the radial density profiles with theoretical models. These models have been presented in detail in Chapter 2.

Chapter 9

Local Group galaxies sample

9.1 Phoenix

The Phoenix galaxy is a member of the Local Group and at 445 kpc it is the most distant of the Milky Ways satellite galaxies (Grebel 1999). Mateo (1998) gives the integrated V band absolute magnitude of the Phoenix dIrr, M_V = -10.1 mag, and the visual luminosity $L_V = 9 \times 10^5 L_\odot$. The total mass is estimated to be $M_{tot} = 33 \times 10^6 M_\odot$.

The Phoenix dIrr was discovered by Schuster and West (1976) who originally suggested it might be a globular cluster. Canterna and Flower (1977) established that it was a galaxy. Though its overall properties are consistent with a classification as a dwarf spheroidal, it also contains a relatively small young component and is thus often referred to as a dIrr/dSph (Mateo 1998). Morras and Bajaja (1986) survey the HI emission from a region including the Phoenix dIrr. They concluded that most of the radiation is due to the neighbouring Magellanic Stream, and it is not related to the galaxy. However, a component possibly related to the galaxy was detected.

Ortolani and Gratton (1988) note that Phoenix dwarf galaxy appears similar to the dwarf galaxy in Pegasus: in both galaxies a recent burst of star formation created a small amount of young population in a dwarf galaxy dominated by an old population. They seem to belong to an intermediate class between typical irregular galaxies (which are presently undergoing star formation) and dwarf spheroidals, where star formation halted a long time ago (some 10^9 yrs ago). The view of Ortolani and Gratton (1988) concerning the classification of the Phoenix dwarf galaxy as a transitional class between the dwarf spheroidal and the dwarf irregular galaxies is shared by van de Rydt et al. (1991). Phoenix like the faint dwarf irregular galaxies has a magnitude well within the range of magnitudes of dwarf spheroidals (Aaronson 1986). The lack of a substantial number of young bright stars explains why some dwarf irregular systems are so faint. In terms of

size, Phoenix is similar to spheroidals such as Leo I or Leo II .

The galaxy is associated with an off-centre HI cloud (Oosterloo et al. 1996; St-Germain et al. 1999; Young and Lo 1997). The origin of this cloud is not clear, although it may be formed from supernovae winds associated with the most recent epoch of star formation in the galaxy (Young et al. 2007).

Table 9.1: Properties of our sample of Local Group galaxies from van den Bergh (2000a). Galaxies are listed in order of increasing distance. Coordinates and information on Sextans A and Sextans B are from Mateo (1998).

Name	α_{2000}	δ_{2000}	Type	M_V	Distance
	hh:mm:ss	dd:mm.m		mag	Mpc
Phoenix	01:51:06	−44 : 26.7	dIrr/dSph	-9.8	0.40
NGC 6822	19:44:56	−14 : 48.1	Irr IV-V	-16.0	0.50
IC10	00:20:25	+59 : 17.5	Irr IV	-16.3	0.66
WLM	00:01:58	−15 : 27.8	Irr IV-V	-14.4	0.95
Sextans B	10:00:00	+05 : 19.7	dIrr	-14.2	1.34
Sextans A	10:11:06	−04 : 42.5	dIrr	-14.6	1.44

9.2 NGC 6822 (Barnard‘s galaxy)

Located at a distance of only 490 ± 40 kpc, NGC 6822 is, apart from the LMC-SMC system, the most nearby dwarf irregular galaxy known. NGC 6822 has no known companions and is not associated with the concentrations of galaxies surrounding M31 and the Milky Way; rather, it belongs to the "Local Group Cloud" an extended cloud of dwarf irregular galaxies. NGC 6822 is a barred dwarf galaxy (type IrrIV-V) with a total luminosity of $M_V = -15.96$ and a mass of $1.9 \times 10^9 M_\odot$ (van den Bergh 2000b). It is brighter, larger (2.9 kpc × 2.9 kpc) and closer than any other dwarf irregular in the LG (Mateo 1998), allowing deeper studies of the properties of individual stars and emission-line objects.

NGC 6822 also possesses an intriguing rotating HI disk of 1.34×10^8 $M_\odot$, that extends far beyond the optical disk (Mateo 1998) and has one of the largest HI holes ever observed in a dwarf galaxy (de Blok and Walter 2000).

The central bar (0.9 kpc × 0.9 kpc) contains much of the young stellar population (de Blok and Walter 2003) and is clearly visible at optical wavelengths. It is oriented almost in a north-south direction (Karampelas et al. 2009). This bar is embedded in a large envelope of neutral hydrogen oriented in a roughly SE-NW direction (Battinelli et al. 2003).

NGC 6822 is gas rich, with a recent star formation whose rate has been more or less continuous but slow during the last Gyr. Gallart et al. (1996) concluded

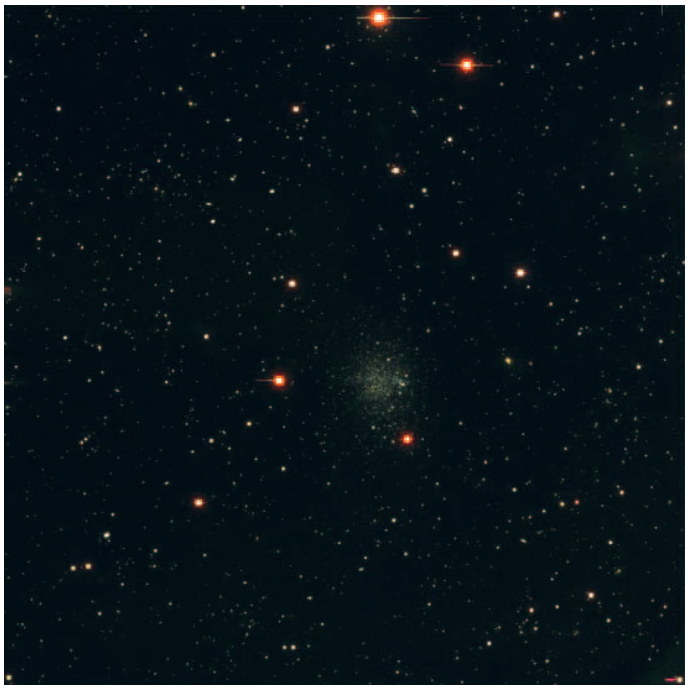

Figure 9.1: Phoenix Mosaic field. The region is the entire $35' \times 35'$ calibrated region by Massey et al. (2007). North is up, east is to the left.

that NGC 6822 started forming stars from the beginning (12 – 15 Gyr), with possible small enhancements 0.4 and 0.1 – 0.2 Gyr ago.

Letarte et al. (2002) identified 904 carbon stars in an area $280' \times 420'$ centered on NGC 6822. The carbon stars reveal that the stellar population of NGC 6822 extends over a much larger volume than its optical image would suggests. Furthermore, carbon stars are not restricted to the HI disk, but are found in a spheroidal halo. Their surface density profile (assuming circular symmetry) is well fitted by a power law with a scale length of $3.0' \pm 0.1'$, corresponding to 436 pc at the distance of NGC 6822. The exponential profile can be followed to 5 scale lengths. The scale length, obtained for the red giants in the same study is $3.3' \pm 0.2'$, a value similar to the one obtained from the carbon stars. The authors conclude that the old- and the intermediate-age halos have the same size and show no pronounced asymmetry like the hydrogen cloud surrounding NGC 6822. Some further extension (6 kpc × 13 kpc, de Blok and Walter (2000)) is revealed by a study of the HI content.

More recently, Karampelas et al. (2009) determine that the spatial distribution of the star complexes of NGC 6822 follows the hierarchical star formation scenario, in terms of the distribution of star forming regions in space and their evolution in time. Star complexes are mainly found inside larger star complexes.

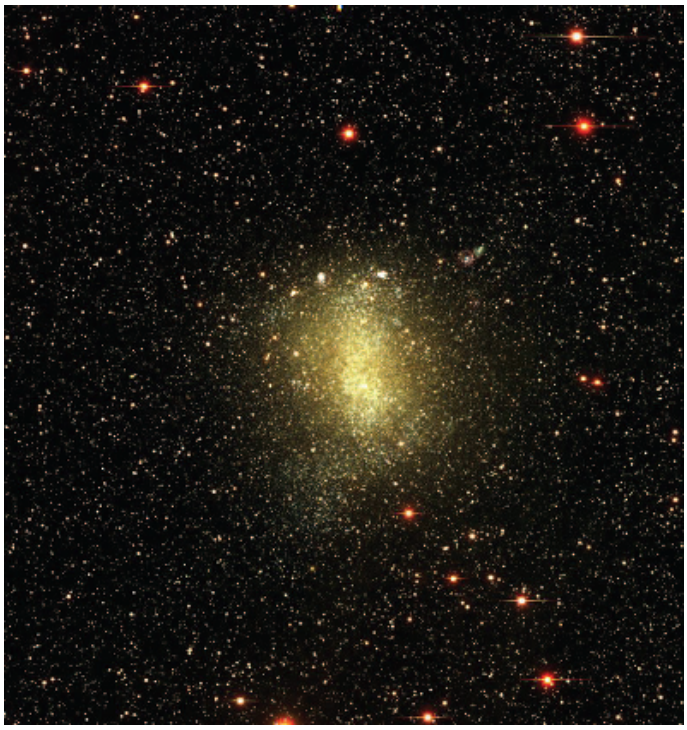

Figure 9.2: NGC 6822 Mosaic field. The region is the entire $35' \times 35'$ calibrated region by Massey et al. (2007). North is up, east is to the left.

Gouliermis et al. (2010) presented a comprehensive study of the star cluster population and the hierarchical structure in the clustering of blue stars with ages ≤ 500 Myr in NGC 6822. They find that some of the larger stellar concentrations, particularly in the northern part of the central star-forming portion of the galaxy, coincide with IR-bright complexes previously identied with Spitzer and associated with high column density neutral gas, indicating structures that currently form stars. The morphological hierarchy in stellar clustering resembles that of the turbulent interstellar matter, suggesting that turbulence on pc and kpc scales has been probably the major agent that regulated clustered star formation in NGC 6822.

Lately, Kacharov et al. (2012) studied the stellar density and the interstellar extinction towards four fields in NGC 6822. They assume that the IR extinction in the field of their entire near-IR catalogue is rather constant. Towards the south-west of NGC 6822 they observe an excess of stars. It seems to be real but a spectroscopic conrmation of their membership to the galaxy is required.

Figure 9.3: IC10 Mosaic field. The region is the entire $20' \times 30'$ calibrated region by Massey et al. (2007). North is up, east is to the left.

9.3 IC10

Among the dwarf irregular galaxies of the Local Group, IC10 is an interesting system, since it underwent strong star formation activity during the last half billion years and it is considered the only LG analog of starburst galaxies. As IC10 is close to the Galactic midplane, estimates of its distance are uncertain due to the unknown level of absorption (Heesen et al. 2011). The likely distance is at best slightly below 1 Mpc. Sanna et al. (2010) provide new estimates of the total luminosity ($L_V \sim 9 \times 10^7 L_\odot$, $M_V \sim -15.1$ mag) that agrees with similar estimates available in the literature. If they only use the regions where rotational velocity measurements are available ($r \sim 13'$), they find a mass-to-light ratio ($\sim 10 M_\odot/L_\odot$) that is at least one order of magnitude larger than previous estimates. The new estimate should be cautiously treated, since it is based on a minimal fraction of the body of the galaxy.

Even though IC10 has been the subject of several investigations ranging from

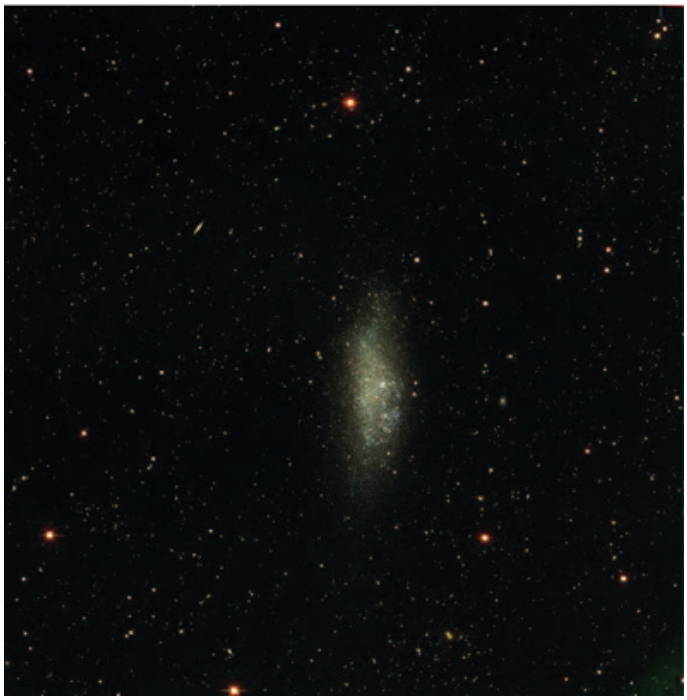

Figure 9.4: WLM Mosaic field. The region is the entire $35' \times 35'$ calibrated region by Massey et al. (2007). North is up, east is to the left.

the radio (Wilcots and Miller 1998) to the near-infrared (NIR, Vacca et al. (2007)), to the UV (Hunter 2001; Richer et al. 2001), and to the X-ray (Wang et al. 2005), its structural parameters and in particular its radial extent are poorly defined. Massey and Armandroff (1995) found that the major axis of IC10 is $\sim 7'$. A similar diameter ($\sim 6'$) was found by Jarrett et al. (2003) using the isophotal radii from 2MASS NIR images. More recently, Tikhonov and Galazutdinova (2009), using both ground-based and space images, suggested that the extent of the thick disk along the minor axis is $\sim 10.5'$. It has also been suggested by Demers et al. (2004), using asymptotic giant branch and red giant branch (RGB) stars, that IC10 should have a halo of $\sim 30'$ diameter. On the other hand, radio measurements by Huchtmeier (1979) indicated that IC10 has a huge envelope of neutral hydrogen extending over more than 1 square degree ($62' \times 80'$) across the sky.

We are also facing a significant uncertainty in the total mass of IC10. By using HI regions Huchtmeier (1979) found $M_{tot} \sim 1.8 \times 10^9 M_\odot$, assuming a distance of 1 Mpc and a Holmberg diameter of $\sim 10'$. Also, Shostak and Skillman (1989), using high resolution maps of HI regions, measured an inclination of 45° and a maximum in the rotation curve of 30 km s^{-1} and the same Holmberg diameter,

from which they found $M_{tot} \sim 1 \times 10^9 M_\odot$. More recently, van den Bergh (2000b), following Huchtmeier (1979), but assuming a smaller distance (660 kpc, Sakai et al. (1999)), found $M_{tot} \sim 6 \times 10^8 M_\odot$.

Sanna et al. (2010) also confirm the significant decrease of the young stellar population when moving from the center toward the outermost regions. They find that the tidal radius of IC10 is significantly larger than previous estimates of $r_t \lesssim 10'$. By using the I versus $V - I$ Color Magnitude Diagram based on the Suprime-Cam data they detected sizable samples of red giant stars up to radial distances of $18 - 23'$ from the galactic center. The ratio between observed star counts (Mega-Cam data) across the tip of the RG branch and star counts predicted by Galactic models indicate a star count excess at least at a 3σ level up to $34 - 42'$ from the center. This finding supports the hypothesis that the huge HI cloud covering more than one degree across the galaxy is associated with IC10 (Cohen 1979; Huchtmeier 1979).

9.4 WLM

Wolf-Lundmark-Melotte galaxy (WLM) is located in an isolated part of the Local Group and is one of the faintest dIrr galaxies with $M_B \simeq -14$ (Urbaneja et al. 2008). It is lying about 1 Mpc away from the dominant massive spirals, the Milky Way and M31. It is considered to be a member of the Local Group (van den Bergh 1994). The closest known galaxy to WLM is the IrrV galaxy IC 1613, at a separation of ~0.37 Mpc. Thus, WLM is a good example of a galaxy at the extreme of galaxy formation. WLM is one of the five least tidally disturbed and most isolated galaxies within a ~ 1 Mpc sphere of the Milky Way.

Skillman et al. (1989b) measured $Z = 0.001$ in the HII regions in the WLM disk. Since the gas reflects the cumulative process of enrichment along the lifetime of a galaxy, it is safe to assume that the stars are not more metal rich than the gas in the WLM disk. The high C/M star ratio (Cook et al. 1986) in the WLM disk confirms that the intermediate-age stellar population is also very metal poor. With this assumption Minniti and Zijlstra (1996) determine the distance to this galaxy to be 0.91 Mpc. They also show the number density of red stars ($20.5 < I < 22.54$, $V - I \gtrsim 0.7$) as function of distance. Most of the stars are concentrated in the disk of the galaxy, within ~ $2'$ of the major axis. However, there is a low-density tail of red stars extending as far as the edge of the field shown in their Figure 1. There is a faint halo around WLM: while the disk extends to about $2.5'$ from the WLM minor axis, the halo can be traced out to about 2 kpc. The surface density profile of this halo follows a de Vaucouleurs law, although the radial extent is not large enough to formally exclude other fits.

Bianchi et al. (2012) present a comprehensive study of young stellar populations in six dwarf galaxies in or near the Local Group, including the WLM dIrr. Their sample includes also Phoenix, Pegasus, Sextans A, Sextans B, and NGC 6822. From this sample WLM is found to show the highest relative abundance of young massive stars.

The stellar velocity dispersion increase with stellar age in WLM coupled with WLM's isolation suggests that the extended vertical structure of its stellar and gaseous components and increase in stellar velocity dispersion with age are due to internal feedback, rather than tidally driven evolution (Leaman et al. 2012).

9.5 Sexstans A

Sextans A is a gas rich dwarf irregular galaxy (Skillman et al. 1988) with active star formation located on the periphery of the Local Group. It is low surface brightness and its metallicity has been measured to be ~4% solar from HII region spectroscopy (Skillman et al. 1989a). The HI is concentrated in two clumps, which correspond to the major star forming regions (Skillman et al. 1988).

Barnes and de Blok (2004) have mapped the neutral gas content of the surroundings of three galaxies on the outskirts of the Local Group - WLM, NGC 1313 and Sextans A - at high velocity resolution and brightness sensitivity. They find no evidence for a substantial population of HI-rich companions with masses $10^5 M_\odot \lesssim M_{HI} \lesssim 10^6 M_\odot$ within ~ 100 kpc radius of the galaxies investigated. Other HI observations also indicate that the gas rotates in solid body rotation, but the axis of rotation is not aligned with the optical axis of symmetry, indicating a barred galaxy.

The optical component has a peculiar square shape. The possible causes of this were considered by van Dyk et al. (1998), including the generation of a bar potential by the interaction with small nearby HI clouds, or the stimulation of star formation by a merger or accretion event occurring in the last ~ 0.2 Gyr.

Dohm-Palmer et al. (2002) have measured stellar photometry from deep HST WFPC2 imaging of the galaxy. The depth of the photometry allowed to compare recent star formation histories recovered from both the main-sequence stars and the BHeB stars for the last 0.3 Gyr. They have also calculated the spatially resolved star formation history. The star-forming regions are found in three major zones of the galaxy. One of these zones is extremely young, consisting of only a single star-forming region that is less than 20 Myr old. Two of these zones are associated with high column density neutral gas, while the third, and oldest, is not. Their interpretation of this pattern of star formation is that it is an orderly stochastic process. Star formation begins on the edge of a gas structure and progressively eats away at the cloud, breaking it up and inducing further star

Figure 9.5: Sextans A Mosaic field. The region is the entire $20' \times 30'$ calibrated region by Massey et al. (2007). North is up, east is to the left.

formation.

Dolphin et al. (2003) have measured star formation history and chemical enrichment history through modeling of the color-magnitude diagram. They find evidence for differential extinction in the youngest populations, caused by the preferential proximity of young stars to dusty star-forming regions. Such an effect has been observed in the LMC by Harris et al. (1997), who find extinction values in excess of $A_V = 1.5$ for OB stars but very few red giants with extinction values in excess of $A_V = 0.6$, based on their $UBVI$ photometric survey. As Sextans A is also actively forming stars, one should expect to see such an effect here as well, albeit with lower overall extinction values due to its lower metallicity.

9.6 Sextans B

Sextans B (UGC 5373, DDO 70) is a rather isolated dwarf irregular galaxy, possibly a member of the Local Group, or it may lie just beyond it (Sharina et al. 2007). Sextans B is 1345 kpc away and thus is one of most distant members of the

Figure 9.6: Sextans B Mosaic field. The region is the entire $20' \times 30'$ calibrated region by Massey et al. (2007). North is up, east is to the left.

Local Group, if it is indeed a member. Although its radial velocity is consistent with membership of the LG, it might form, together with NGC 3109, Antlia, Sextans A and perhaps AM1013-394A, a physical association of galaxies lying just beyond the boundaries of the LG, which would be the nearest association outside the LG (van den Bergh 2000b). Mateo (1998) gives for the integrated V-band absolute magnitude M_V = -14.2 and a total luminosity $L_V = 40.7 \times 10^6 L_\odot$. The quoted mass is $M_{tot} = 885 \times 10^6 M_\odot$.

The resolved stellar population of Sextans B is dominated by red giants (Sakai et al. 1997), with a prominent contribution of intermediate-age asymptotic branch stars. A young population is also present, indicating a complex, low-rate and likely discontinuous star formation throughout the galaxy lifetime (Tosi et al. 1991; van den Bergh 2000b). A dozen HII regions are known (Strobel et al. 1991), but no planetary nebulae (PNe) have been identified prior to the study of Magrini et al. (2002), who discovered five new candidate PNe in the Sextans B dIrr galaxy. This is a notable result considering the limited number of PNe known in the other dwarf galaxies of the LG.

Kniazev et al. (2005) presented the results of high-quality long-slit spectroscopy of PNe and HII regions in the two dIrr galaxies Sextans A and Sextans B. Both show generally similar star formation histories in the sense of continuous star formation with amplitude variations but differ in their detailed enrichment timescales and star formation rates as a function of time. If we combine the photometrically derived estimates for the mean metallicity of the old red giant branch population in both dIrrs with the present-day metallicity of the HII regions, both dIrrs have experienced chemical enrichment by at least 0.8 dex throughout their history.

Bianchi et al. (2012), as mentioned above, derive the physical parameters of massive stars by analyzing the multi-band stellar photometry with model-atmosphere colours. The results were used to infer ages, number of massive stars, extinction, and spatial characteristics of the young stellar populations. Sextans B shows a very young population (a few Myrs), and older ones (a few 10^7 years).

Chapter 10

Data

Massey et al. (2007) took advantage of the NOAO Survey Program to use the new wide-field Mosaic CCD cameras on the Kitt Peak National Observatory (KPNO) and Cerro Tololo Inter-American Observatory (CTIO) 4 m telescopes to image the Local Group galaxies currently actively forming stars. They conducted a uniform survey ($UBVRI$, $H\alpha$, [SII], and [OIII]) of nearby galaxies selected on the basis of current star formation. Their sample includes M31, M33, NGC 6822, IC 1613, IC10, WLM, Pegasus, and Phoenix; they exclude the Milky Way and Magellanic Clouds, which are being surveyed separately by several groups, and include Sextans A and Sextans B, located near the periphery of the Local Group.

The Local Group Galaxies Survey (LGGS) project imaged the nearby spiral galaxies M31 in 10 fields, and M33 in three fields, as well as the dwarf irregular galaxies NGC 6822, WLM, IC10, Phoenix, Pegasus, Sextans A, and Sextans B, each in a single field. The goal was to obtain uniform large-area coverage of the star-forming regions in these galaxies, with broadband photometry good to 1%-2% for massive stars ($\geqq 20M_{\odot}$). The data would be taken under good, but not always excellent, seeing conditions ($< 1.0 - 1.2$ arcsec). The produced catalogues contain $UBVRI$ photometry of roughly a million stars. For distinguishing stellar members from compact HII regions $H\alpha$, [SII], and [OIII] are used.

Three southern galaxies (WLM, NGC 6822, and Phoenix) were observed with the CTIO Blanco 4m telescope; the other four (IC10, Sextans B, Sextans A, and Pegasus) were observed at Kitt Peak with the Mayall 4 m. The two Mosaic cameras are nearly identical instruments and consist of a 2×4 array of 2048×4096 SITe CCDs, yielding images containing 8192×8192 pixels. The scale of the final rectified images is 0.27 arcsec pixel^{-1}. The field of view (FOV) of the Mosaic camera is $35' \times 35'$, but for three of the smaller galaxies (IC10, Sextans B, and Sextans A) observed at Kitt Peak the galaxy was centered on just one of the eight chips in order to avoid the effects of the ghost image caused by the Mayalls prime focus corrector. A fourth galaxy observed at Kitt Peak, Pegasus, was centered

on the array, but the calibration data extend only over the central four chips.

The $UBVRI$ survey of M31 and M33 by Massey et al. (2006) produced catalogues containing 371 781 and 146 622 stars, respectively. This survey covered large areas (2.2 and 0.8 deg^2), including all of the regions currently known to be actively forming massive stars. Comparison of their data with an ACS image of OB48, a crowded M31 OB association rich in massive stars, suggests that the catalogues did a respectable job of detecting blends.

Massey et al. (2007) have obtained broadband photometry of 88 144 stars (identified in B, V, and R) in IC10 (20 663 stars), NGC 6822 (51 877 stars), WLM (7656 stars), Sextans B (800 stars), Sextans A (1516 stars), Pegasus (1390 stars), and Phoenix (4242 stars). All of the CMDs reveal a strong or modest number of blue supergiants. All but Pegasus and Phoenix also show the clear presence of red supergiants in the CMD, although IC10 appears to be decient in these objects given its large Wolf-Rayet star population. The bright stars of intermediate colour in the CMD are badly contaminated by foreground stars (30%-100%), and considerable spectroscopy is needed before statistics on the yellow supergiants in these systems will be known.

Colour-magnitude diagrams of these systems and of the Magellanic Clouds were intercompared. This led to improved estimates of the typical reddening of an OB star in these systems, based on the colours of the plume of blue supergiants, and adopting the reddening values for the LMC and SMC based on spectroscopy of hundreds of stars.

Due to the small angular sizes of the galaxies the coverage is excellent. For IC10 and NGC 6822 this provides for both complete coverage and a good sampling of the Milky Way foreground; in the case of the smaller systems (such as Sextans B) the galaxies are almost lost in the field. The whole data set is complete down to Gaia's limiting magnitude, which makes it very suitable for this project.

The premise of the NOAO Survey Program was that data should be useful to others for their own research. Toward that end the full catalogs and images have been made available; in addition, the reduction techniques were carefully documented and the software was also made available.

The complete M31 and M33 catalogues are available in machine-readable format via the electronic edition of the Astronomical Journal. The catalogues for all galaxies, as well as the complete set of images, are also available via the NOAO Science Archive [1] and Lowell Web sites [2].

In the Thesis we use the catalogues of IC10, WLM, Phoenix, Sextans B, Sextans A, and NGC 6822. Although small, this sample contains a variety of

[1] See `http://archive.noao.edu/nsa`

[2] See `http://www.lowell.edu/users/massey/lgsurvey`

galaxies at various distances and with very different properties. A sample excerpt from the Sextant B dwarf irregular galaxy catalogue is given in Table 10.1. Apart from the catalogues, a header is provided in each table containing information about the authors, the galaxy, and a description of the columns in the table. The various columns contain the name of the object (LGGS designation), the coordinates, the V magnitude, as well as several colours, such as $B - V$, $U - B$, $V - R$, $R - I$, and the respective errors. An entry of "99.999" denotes no measurement.

```
Title: A Survey of Local Group Galaxies Currently Forming Stars: II. UBVRI Photometry of Stars in the Seven Dwarfs
Authors: Massey, Olsen, Hodge, Jacoby, McNeill, Smith, & Strong
Table: Sextans B Catalog
================================================================================
Byte-by-byte Description of file: tab8.txt
--------------------------------------------------------------------------------
   Bytes Format Units    Label      Explanations
--------------------------------------------------------------------------------
   1- 20 A20    --       Name       LGGS Designation
  22- 23 I2     h        RAh        Right ascension 2000 (hours)
  25- 26 I2     min      RAm        Right ascension 2000 (minutes)
  28- 32 F5.2   s        RAs        Right accension 2000 (seconds)
  34- 34 A1     --       DE-        Declination 2000 (sign)
  35- 36 I2     deg      DEd        Declination 2000 (degrees)
  38- 39 I2     arcmin   DEm        Declination 2000 (minutes)
  41- 44 F4.1   arcsec   DEs        Declination 2000 (seconds)
  46- 51 F6.3   mag      Vmag       V magnitude
  53- 58 F6.3   mag    u_Vmag       V error
  60- 65 F6.3   mag      Bmag-Vmag  B-V magnitude
  67- 72 F6.3   mag    u_Bmag-Vmag  B-V error
  74- 79 F6.3   mag      Umag-Bmag  U-B magnitude (1)
  81- 86 F6.3   mag    u_Umag-Bmag  U-B error (1)
  88- 93 F6.3   mag      Vmag-Rmag  V-R magnitude
  95-100 F6.3   mag    u_Vmag-Rmag  V-R error
 102-107 F6.3   mag      Rmag-Imag  R-I magnitude (1)
 109-114 F6.3   mag    u_Rmag-Imag  R-I error (1)
--------------------------------------------------------------------------------
Note (1):   99.999 = No value
--------------------------------------------------------------------------------
J095922.35+051211.7  09 59 22.35 +05 12 11.7 18.184  0.008  0.571  0.013 -0.111  0.014  0.370  0.009  0.352  0.005
J095922.44+051221.6  09 59 22.44 +05 12 21.6 19.964  0.023  1.526  0.053  1.223  0.156  0.979  0.025  0.942  0.010
J095922.83+052943.4  09 59 22.83 +05 29 43.4 18.091  0.008  0.668  0.011 -0.041  0.010  0.402  0.011  0.388  0.007
```

Table 10.1: Example catalogue for the Sextant B dIrr galaxy. Note that an entry of "99.999" denotes no measurement.

Chapter 11

Results

There is a structural difference between the early-type dwarf galaxies (dSph) and the irregular dwarfs (dIrr). In the optical, the structure of LG dIrr galaxies is dominated by star-forming complexes and OB associations with typical diameters of 200-300 pc (Fisher and Tully 1979; Hodge et al. 1991). The early-type dwarfs of the Local Group, on the other hand, are dominated by a symmetric spheroidal component (Hodge 1971; Irwin and Hatzidimitriou 1995), with occasional instances of superimposed concentrations of relatively young stars; nearly the inverse of the dIrr galaxies.

We are studying the spatial distribution of the six dwarf irregular galaxies in our sample (IC10, WLM, Phoenix, Sextans A, Sextans B, and NGC 6822) using isodensity contour maps. The contours in these maps trace areas with equal stellar density. We also fit radial surface density profiles to theoretical models in order to obtain the structural parameters of these galaxies.

Historically, the surface brightness profiles for the dIrr galaxies are fit with exponential profiles, while for dSph systems King profiles are preferred. Many authors have noted that both profiles produce acceptable fits to the red populations of dIrr and dSph systems (Hodge et al. 1991; Irwin and Hatzidimitriou 1995). Although we are using star counts (surface density) instead of surface brightness, we decided to use the exponential and King profiles to fit the radial density profiles of the galaxies.

11.1 Colour-Magnitude Diagrams

The clearest and most useful way to understand these galaxies is to use the most classical approach possible: comparing the colour-magnitude diagrams (CMDs) of these systems. We obtained the CMDs for six dwarf galaxies in the Local Group (Phoenix, NGC 6822, IC10, WLM, Sextans A, and Sextans B) using the

catalogues of $UBVRI$ photometry by Massey et al. (2007). In Figures 11.1, 11.2, 11.3, 11.4, 11.5, and 11.6 we present V versus $B-V$ plots for our sample of dIrr galaxies.

The contamination by Galactic foreground stars was assessed using the Besançon galaxy model[1]. Simulated catalogues were obtained for the same magnitude range and area on the sky as the data available for the six dwarf galaxies. The left panel in each of the figures shows the total CMD of each of the galaxies. In the right panel of Figures 11.1, 11.4, 11.5, and 11.6 the red points indicate the position and number of Galactic stars on the colour-magnitude diagram predicted by the Besançon galaxy model in the direction towards each galaxy in the same solid angle as the data available. In the case of NGC 6822 and IC10 (Figures 11.2 and 11.3) the number of the Galactic stars was very high, so instead of points we used contours to show the stellar density. The contour levels for each galaxy are given in the figure caption.

As Massey et al. (2007) determined, four general regions can be distinguished on these diagrams: the blue supergiants (BSG) on the left, the red supergiants (RSG) on the right, and two sequences of (mainly) foreground stars near $B-V \sim$ 0.6 and 1.6 for the galaxies at modest galactic latitudes. Their estimation of the galactic foreground contamination at intermediate colours ranges from ~ 80% for WLM to almost 100% for IC10. Phoenix is the exception with 30%.

The lowest luminosity galaxy in the sample, Phoenix, contains a blue supergiant population (Figure 11.1). It also contains a very strong population of intermediate age stars. As such, Phoenix appears to be intermediate between an irregular galaxy and a dwarf spheroidal (Massey et al. 2007). The galaxy does not appears to have a significant number of RSGs.

Figure 11.2 shows the CMD of NGC 6822. The blue supergiants are well distinguished from the foreground dwarfs, despite the large number of the latter, due to NGC 6822's relatively low Galactic latitude ($b = -18.4°$). Karampelas et al. (2009) suggest an age of ~0.4 Gyr for the main sequence stars with $18 \leq V \leq 23$ and $-0.4 < B-V < 0.3$. In the CMD we also see a strong RSG component starting at $B-V = 1.6$ and $V = 19.5$ and extending to $B-V > 2$ and possibly $V = 17.5$. The position of the two supergiant components is shown in the left panel of Figure 11.2 with the two blue boxes.

In Figure 11.3 we show the CMD for IC10. The CMD of the galaxy reveals a strong population of blue supergiants, as well as some red ones, but high extinction, $E(B-V) = 0.81$, has shifted the sequences to considerably redder colors and fainter magnitudes. Quite noticeable is the large amount of reddening. The foreground sequence is very tilted, as expected very close to the plane of the Milky Way, as more distant stars will be more heavily reddened, and the line of sight

[1] `http://model.obs-besancon.fr/`

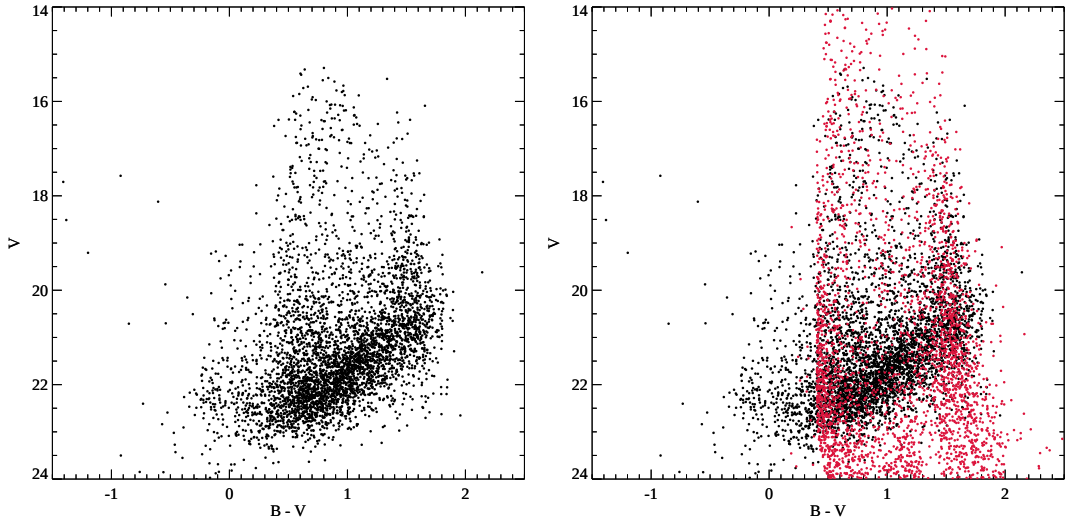

Figure 11.1: CMD for Phoenix. The red points in the right panel indicate the position and number of Galactic stars on the colour-magnitude diagram as predicted by the Besançon model. The CMD of the galaxy reveals a wealth of faint stars of intermediate and red colour and a few blue supergiants.

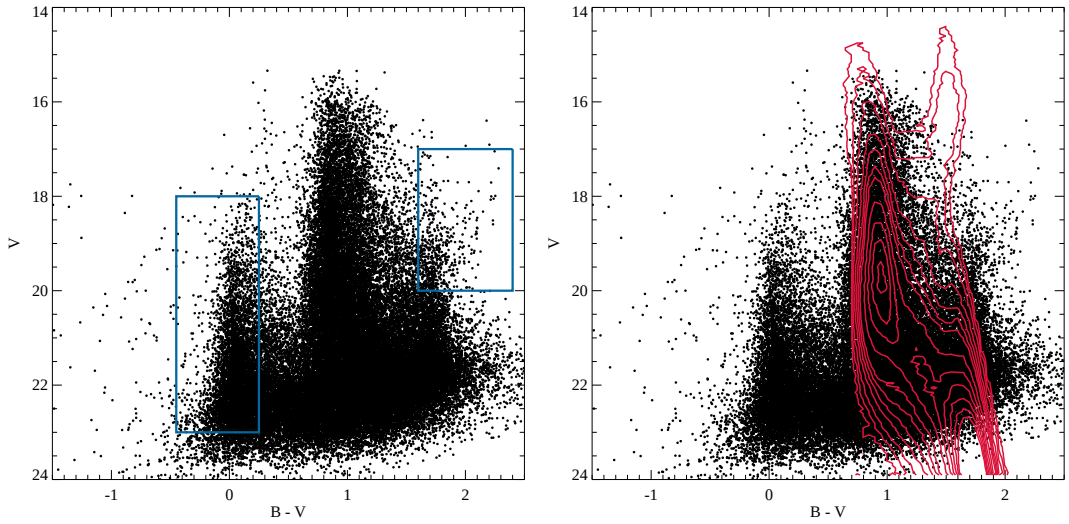

Figure 11.2: CMD for NGC 6822. The CMD of the galaxy in the left panel reveals a strong population of blue supergiants and RSGs, plus bright stars of intermediate colour which are dominated by foreground stars. The position on the CMD of the BSG and RSG is indicated with the blue boxes. The red contours in the right panel indicate the position and number of Galactic stars on the colour-magnitude diagram as predicted by the Besançon model. Levels are 5, 10, 20, 40, 60, 80, 100, 150, 200, 250, 300, 350, and 400 deg^{-2}.

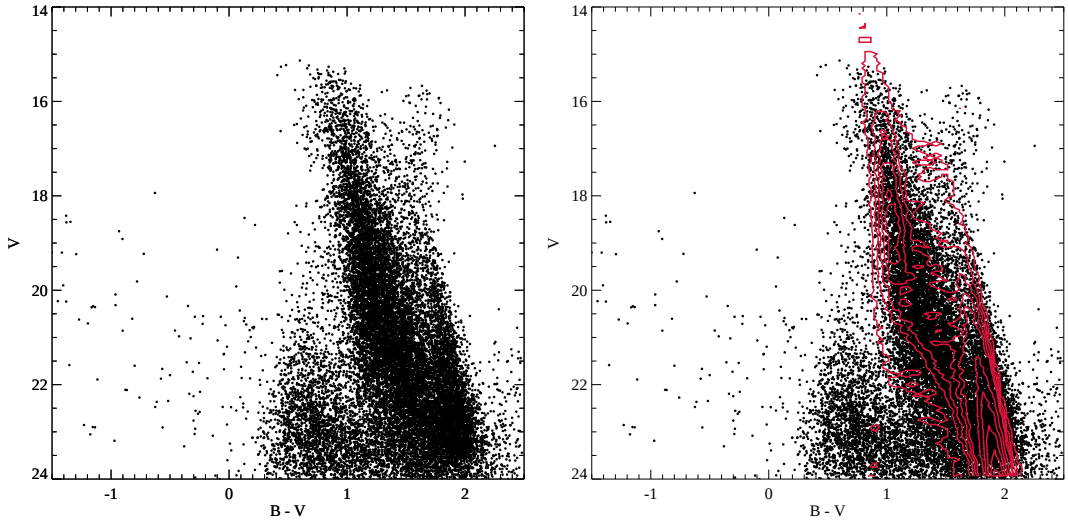

Figure 11.3: CMD for IC10. The CMD of the galaxy in the left panel reveals a strong population of blue supergiants, as well as some red ones, but high extinction has shifted the sequences to considerably redder colours and fainter magnitudes. The red contours in the right panel indicate the position and number of Galactic stars on the colour-magnitude diagram as predicted by the Besançon model. Levels are 2, 6, 10, 15, 20, 40, 60, 80, 100, 120, 140, and 160 deg^{-2}.

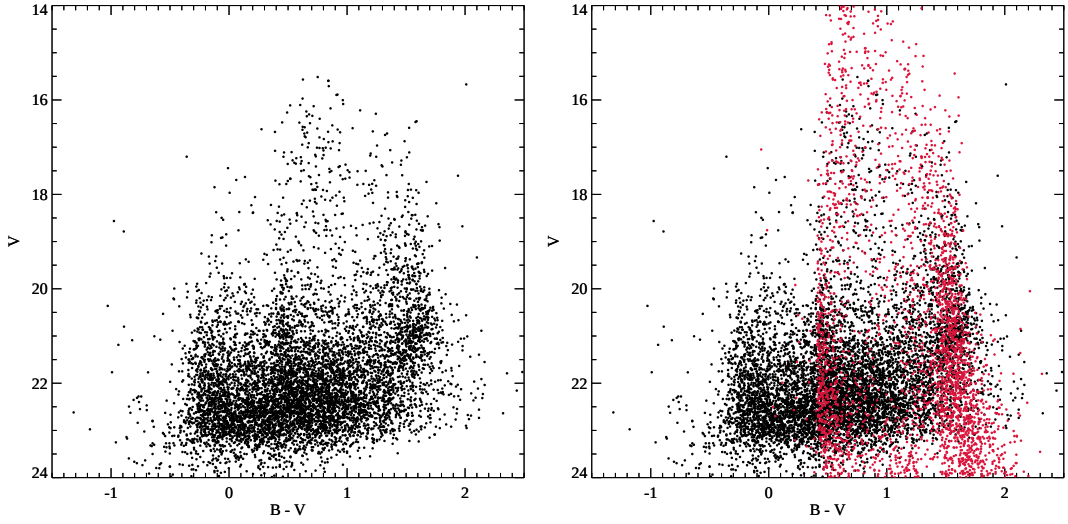

Figure 11.4: CMD for WLM. The red points in the right panel indicate the position and number of Galactic stars on the colour-magnitude diagram as predicted by the Besançon model. The CMD of the galaxy reveals blue supergiants and RSGs, plus a handful of bright stars of intermediate colour which are dominated by foreground stars.

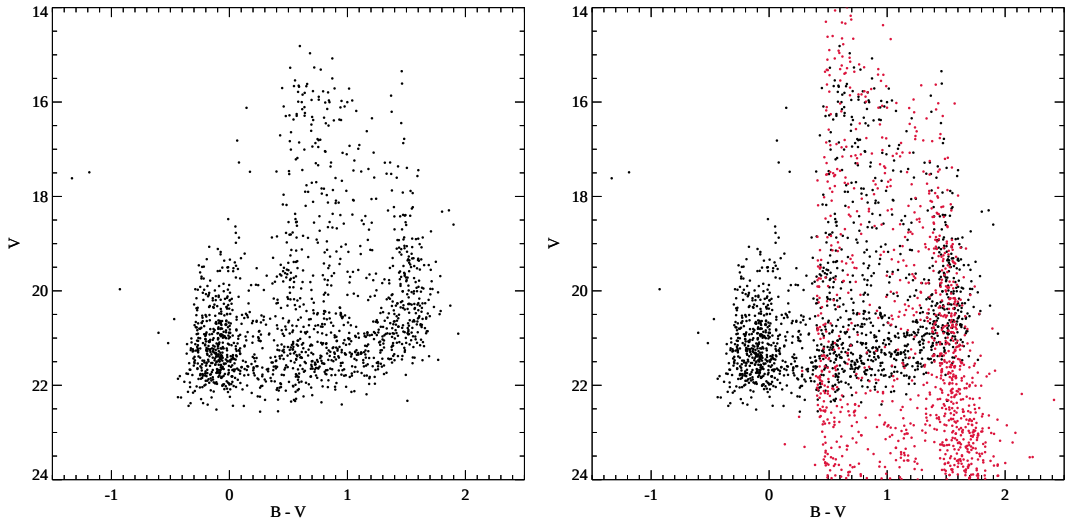

Figure 11.5: CMD for Sextans A. The red points in the right panel indicate the position and number of Galactic stars on the colour-magnitude diagram as predicted by the Besançon model. The CMD of the galaxy reveals blue supergiants, plus a few stars of intermediate colour dominated by foreground stars, as well as some red stars, some of which are native to Sextans A

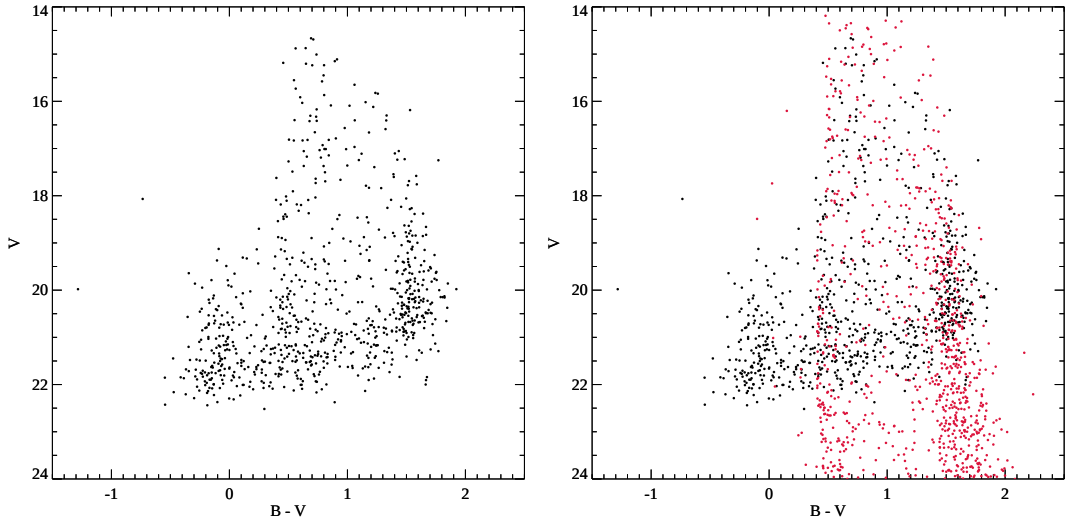

Figure 11.6: CMD for Sextans B. The red points in the right panel indicate the position and number of Galactic stars on the colour-magnitude diagram as predicted by the Besançon model. The CMD of the galaxy reveals blue supergiants, plus a few stars of intermediate colour dominated by foreground stars, as well as some red stars, some of which are native to Sextans B.

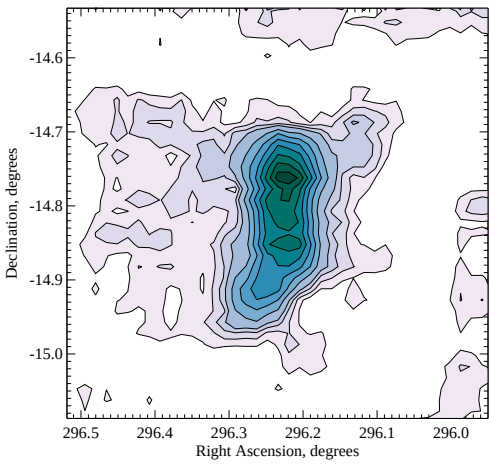

Figure 11.7: Isodensity contour maps of NGC 6822 for all the stars in the galaxy as faint as 20 mag showing what is available down to Gaia's limit. Levels are (2.25, 2.5, 2.75, 3, 3.5, 4, 4.5, 5, 5.5, 6, 6.5)×10^4 deg^{-2}.

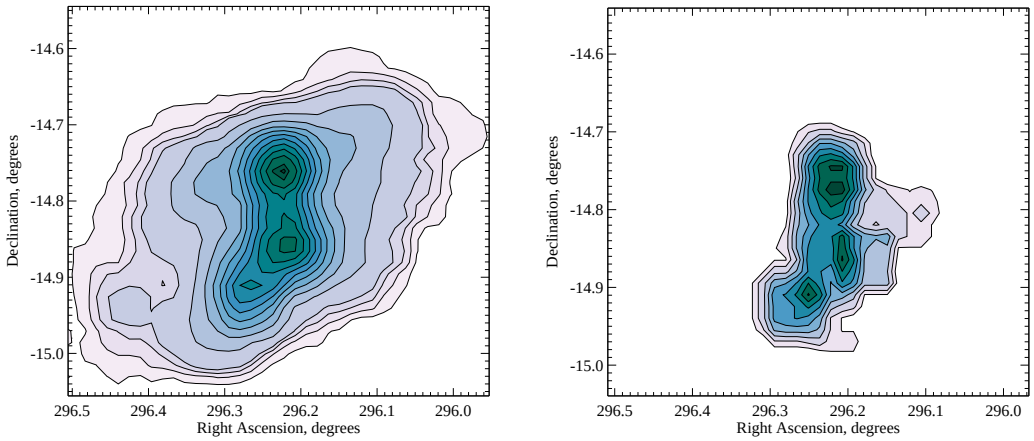

Figure 11.8: Isodensity contour maps of supergiant stars in NGC 6822. The left panel contains the contour map for blue supergiants with $18 \leq V \leq 23$ and $-0.4 \leq B - V \leq 0.3$. Levels are (0.25, 0.5, 0.75, 1, 2.5, 5, 7.5, 10, 12.5, 15, 17.5, 20, 22.5, 25, 26)×10^4 deg^{-2}. The right panel shows the distribution of the red supergiant stars with $16 \leq V \leq 20$ and $B - V \geq 1.6$. Levels are (0.6, 1, 1.5, 2, 2.5, 3, 3.5, 4, 4.5)×10^3 deg^{-2}.

goes through a substantial part of the Galaxy. In other galaxies, the foreground CMDs are nearly vertical, as one quickly runs past the edge of the dust plane.

The CMD of the galaxy reveals blue and red supergiants, plus a handful of bright stars of intermediate colour which are dominated by foreground stars. As can be seen from Figure 11.4 WLM is still relatively rich in massive stars, as shown by the strength of the "plume" of blue stars with $B - V \leq 0.2$.

Although Sextans B is more luminous than Sextans A (Table 9.1), it is clear from comparing the CMDs (Figures 11.5 and 11.6) that there are considerably more massive stars present in Sextans A. Both show some enhancement of bright red stars over the adjacent foreground fields, so it is likely that these galaxies contain some RSGs (Massey et al. 2007).

From our sample of six dwarf galaxies in the Local Group we consider only NGC 6822 as probable for detection by Gaia. The rest of the galaxies might offer a limited sample of blue supergiant stars and individual red supergiant stars.

11.2 Isopleth Maps

Figures 11.7, 11.9, 11.10, 11.11, and 11.12 show the isodensity contour maps of the studied dIrr galaxies. Each figure contains two surface density maps - one for all the stars in the galaxy as faint as V = 20 mag showing what is available down to Gaia's limit and the other shows the distribution of the bright massive stars (BSGs) in these galaxies.

The contour levels were chosen manually for better clarity because neither equidistant nor logarithmic levels gave the necessary detail. The levels are given in each figure and the lowest levels in the left panels were selected in such a way as to have a value higher than the stellar density predicted by the Besançon Galaxy model in the direction towards each galaxy in the same solid angle as the data available and for the same magnitude limit. The right panels contain only the blue supergiant stars of each galaxy where there is almost no foreground contamination.

From the CMD of the Phoenix dIrr galaxy (Figure 11.1 *left*) it is evident that in Figure 11.9 *left* the bulk of stars resolved by Gaia comprises more red than blue supergiants. Figure 11.9 *right* shows the distribution of main sequence stars in the galaxy with $B - V \leq 0.3$. The smoother appearance in comparison with the magnitude limited left panel is due to the larger number of stars available for the contour maps.

In NGC 6822 the stars accessible to Gaia are main sequence stars occupying the central bar-like structure (Figure 11.7 *left*). The rest of the stellar content seems beyond Gaia's reach. Figure 11.8 *right* shows the density distribution of main sequence stars (BSG) younger than ~0.4 Gyr (Karampelas et al. 2009) with

$18 \leq V \leq 23$ and $-0.4 < B-V < 0.3$. shows the distribution of the red supergiant stars with $16 \leq V \leq 20$ and $B-V \geq 1.6$. The distribution of the BSG is very similar to the distribution of the stars brighter than 20 mag. This is no surprise, however, since only the brighter stars are accessible in these galaxies. The RSG are far less numerous than the BSG but still their distribution is comparable to the first two.

In IC10 again only the brightest and most massive stars in the central parts of the galaxy will be detected by Gaia (Figure 11.10 *left*). In Figure 11.10 *right* the young stars ($0.0 < B-V < 0.8$) cover the whole extent of the galaxy. We find a slight contamination of foreground stars for this galaxy, as can be expected from the CMD (Figure 11.3 *right*). Apart from that, it is interesting to note that the centres of the density distributions in both panels do not coincide and the centre of the brightest stars distribution is shifted towards the north.

Figure 11.11 *left* shows the distribution of the brightest stars in WLM. The blue and red supergiants are smoothly distributed in the central parts of the galaxy. The CMD (Figure 11.4 *right*) suggests that there might also be some bright stars at intermediate colours, but they are probably dominated by the foreground stars. Figure 11.11 *right* contains main sequence stars ($B-V \leq 0.2$) which extend over the whole body of the galaxy. For WLM there is again a difference in the stellar distribution in the two panels. Here, however, there is no displacement of the centres of the two distributions as in IC10. Instead, the blue supergiants are distributed along the elongated shape of the body of the galaxy and the brightest stars occupy only the central area.

Sextans A and Sextans B are the most distant galaxies in our sample at ~ 1.4 Mpc and a distance modulus of $(m-M)_0 \approx 25.7$. This is the reason very few blue supergiants can be confidently identified, especially in Sextans B. Figure 11.12 shows the distribution of all stars in the galaxies down to 20 mag. The number of main sequence stars (mostly blue supergiants), however, was too small to produce reliable density maps of these galaxies.

11.3 Surface Density Profiles

In comparison with the Magellanic Clouds, in these galaxies there are not enough brighter stars to confidently differentiate between stellar populations. This is why it was decided to produce the RDPs for the whole galaxies only using stars brighter than V ≈ 20 mag in order to investigate the stellar density distribution as it will be observed by Gaia. In this way the RDPs can be directly connected to the isodensity maps in the left panels of Figures 11.7, 11.9, 11.10, 11.11, and Figure 11.12. The only exception is NGC 6822, where it was possible to produce the RDPs for the main sequence stars younger than ~0.4 Gyr using stars with

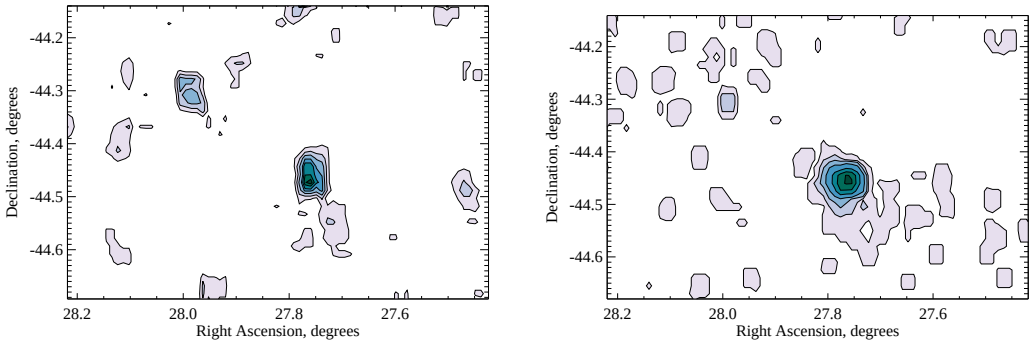

Figure 11.9: Isodensity contour maps of Phoenix. The left panel contains the contour map for all the stars in the galaxy as faint as 20 mag showing what is available down to Gaia's limit. Levels are (3, 4, 5, 6, 6.5, 7, 7.4)×10^3 deg^{-2}. The right panel shows the distribution of the bright massive stars in the galaxy with $B - V \leq 0.3$. Levels are (1.5, 5, 10, 20, 40, 60, 80)×10^3 deg^{-2}.

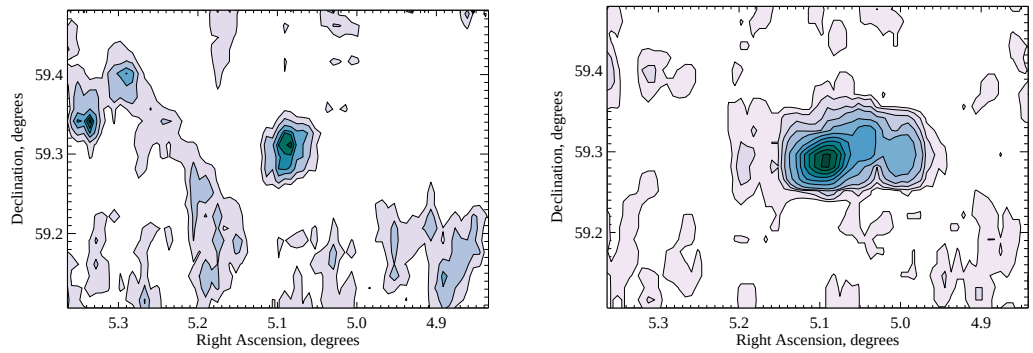

Figure 11.10: Isodensity contour maps of IC10. The left panel contains the contour map for all the stars in the galaxy as faint as 20 mag showing what is available down to Gaia's limit. Levels are (3.5, 4, 4.5, 4.9, 5.1, 5.3)×10^4 deg^{-2}. The right panel shows the distribution of the bright massive stars in the galaxy with $B - V \leq 0.8$. Levels are (0.7, 1.5, 3, 5, 10, 20, 30, 40, 50, 60, 70)×10^4 deg^{-2}.

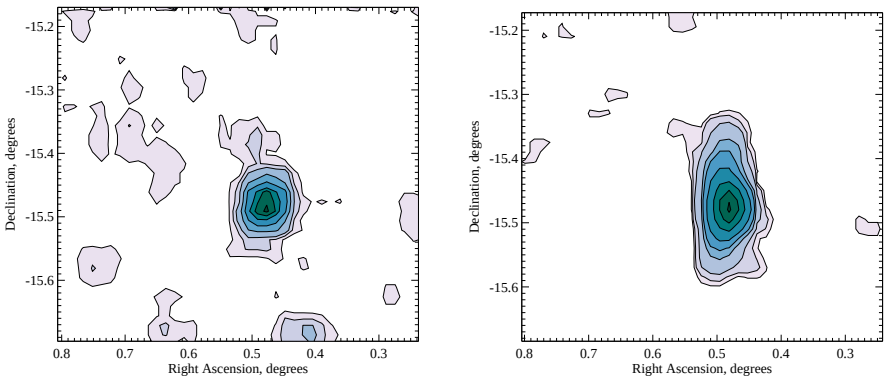

Figure 11.11: Isodensity contour maps of WLM. The left panel contains the contour map for all the stars in the galaxy as faint as 20 mag showing what is available down to Gaia's limit. Levels are (2, 3, 4, 6, 8, 10, 11, 12)×10^3 deg^{-2}. The right panel shows the distribution of the bright massive stars in the galaxy with $B - V \leq 0.2$. Levels are (0.3, 0.5, 1, 3, 5, 10, 20, 30, 40)×10^4 deg^{-2}.

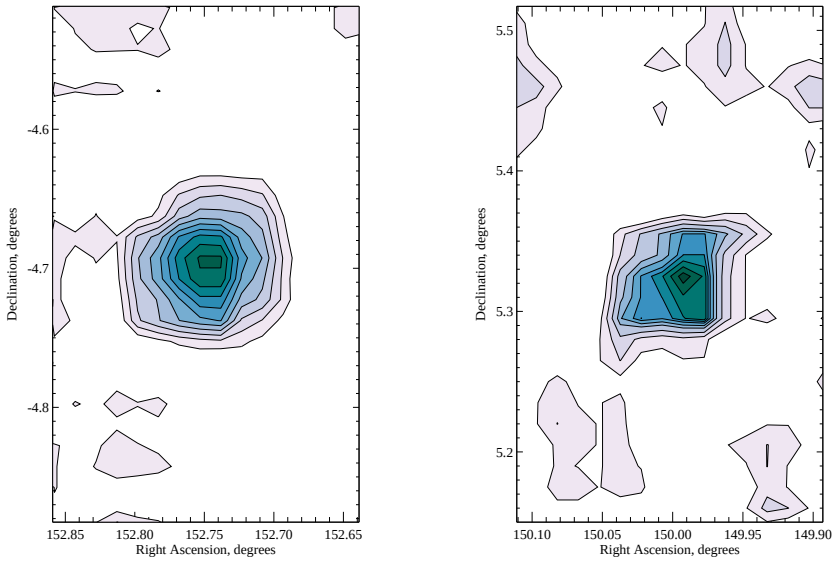

Figure 11.12: Isodensity contour maps of Sextans A and Sextans B for all the stars in the galaxy as faint as 20 mag showing what is available down to Gaia's limit. Levels for Sextans A are (3, 4, 5, 6, 7, 8, 9, 10, 11, 12, 12.2)×10^3 deg^{-2} and for Sextans B are (2, 2.5, 3, 3.5, 3.8, 4.1, 4.3, 4.5, 4.7, 4.9)×10^3 deg^{-2}.

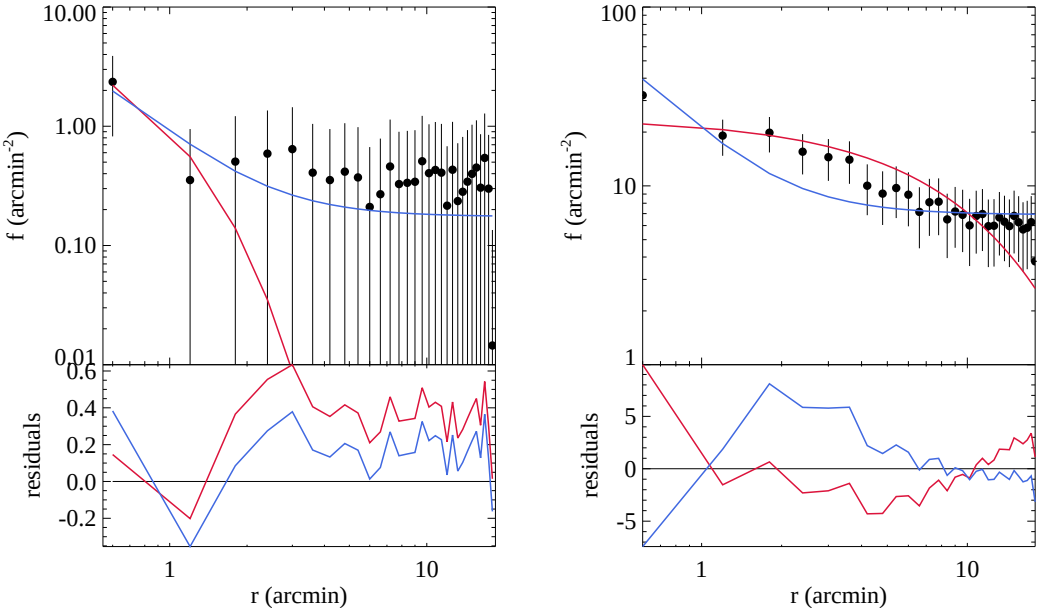

Figure 11.13: RDPs for Phoenix (left) and NGC 6822 (right) fitted with exponential-disk (red line) and King profiles (blue line). Below each profile are the residuals from the fit.

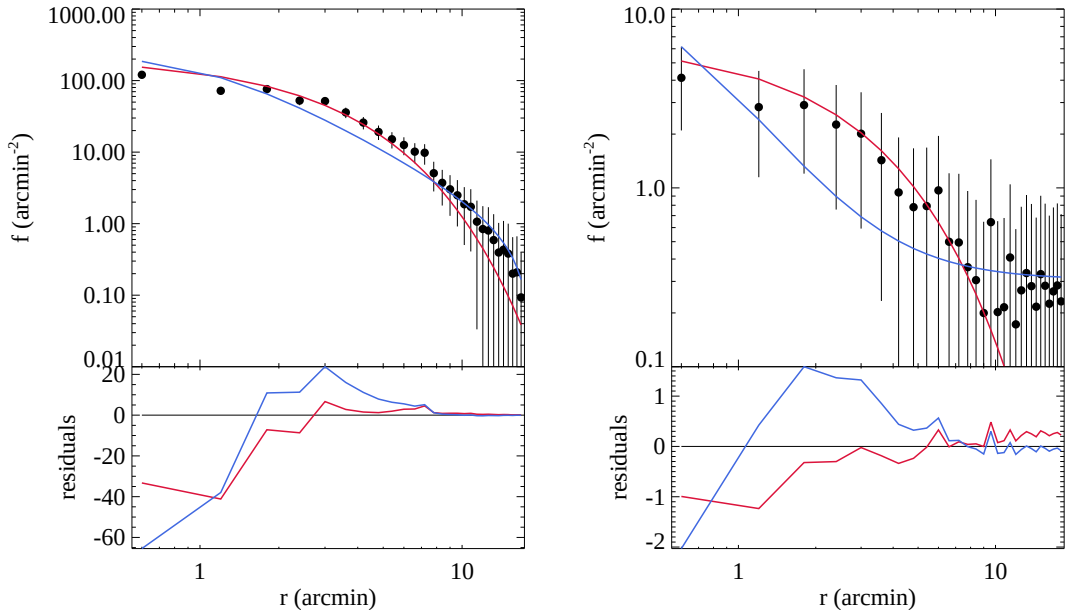

Figure 11.14: RDPs for NGC 6822 blue supergiants (left) with $18 \leq V \leq 23$ and $-0.4 \leq B-V \leq 0.3$ and red supergiants (right) with $16 \leq 20$ and $B-V \geq 1.6$ fitted with exponential-disk (red line) and King profiles (blue line). Below each profile are the residuals from the fit.

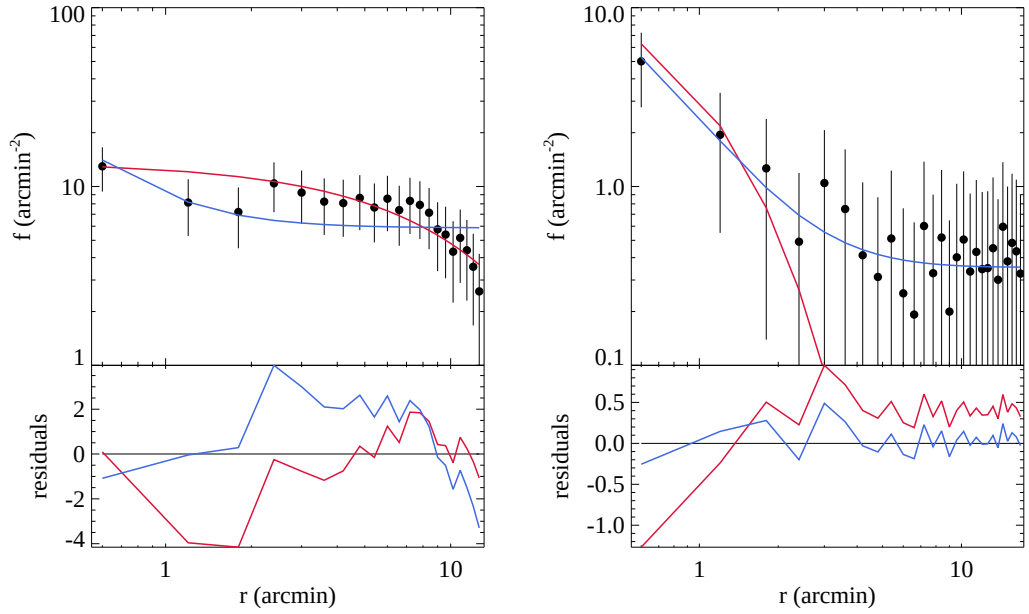

Figure 11.15: RDPs for IC10 (left) and WLM (right) fitted with exponential-disk (red line) and King profiles (blue line). Below each profile are the residuals from the fit.

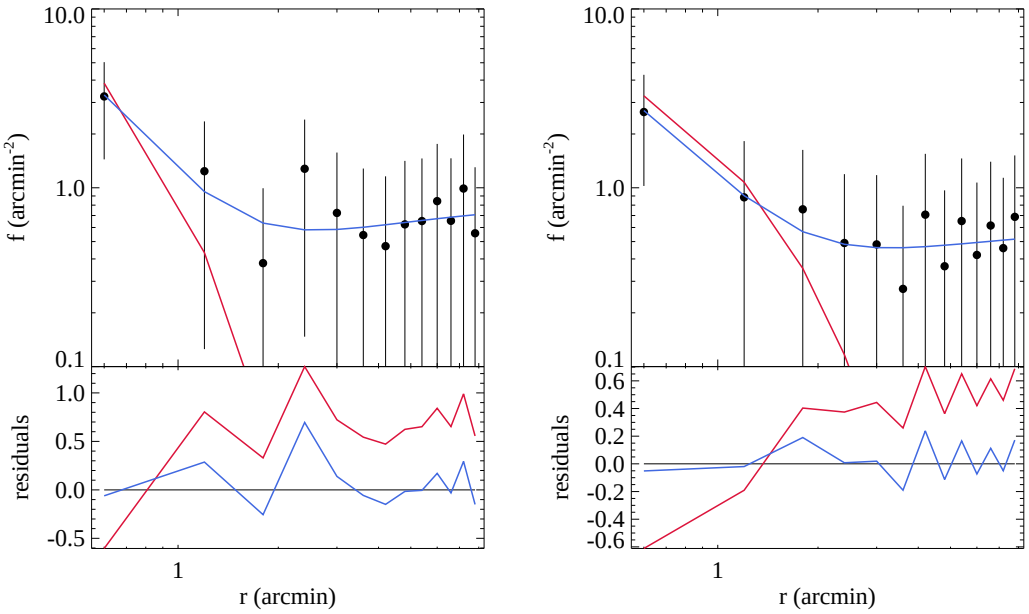

Figure 11.16: RDPs for Sextans A (left) and Sextans B (right) fitted with exponential-disk (red line) and King profiles (blue line). Below each profile are the residuals from the fit.

$18 < V < 20$ and $-0.4 < B - V < 0.3$ and the red supergiants with $16 \leq V \leq 20$ and $B - V \geq 1.6$.

The radial density profiles are presented in Figures 11.13, 11.14, 11.15, and 11.16. The best fit of both models is displayed in each figure - the exponential-disk with a red line and the King profiles with a blue line. The exponential disk and King models used are presented both in detail in Chapter 2. In all figures error bars show the Poisson errors. Additionaly, the residuals below each profile reveal the preferred model and show the dominant model for each part of the galaxy.

The structural parameters obtained from the model fitting are presented in Table 11.1. Column (1) contains the designations of the galaxies. Columns (2) and (3) contain the central density of objects f_{0D} and the scale length h_D respectively for the exponential disk model (Eq. 2.5). Columns (4)-(7) contain the central density of objects f_{0K}, the core radius r_c, the tidal radius r_t where available, and the concentration parameter c_p for the King model (Eq. 2.6).

Figure 11.13 *left* shows the RDP of the Phoenix dwarf. Phoenix is located in an area with lower density of Galactic stars. However, this is not enough to obtain a quality profile of this galaxy because the stellar density is not sufficient. Therefore, even with the use of the residuals we cannot safely distinguish between the exponential disk and the King model for this galaxy.

NGC 6822 is the galaxy with the geatest chance to provide resolved stars for Gaia. In contrast to the other galaxies from our sample NGC 6822 stars seem to be distributed on an exponential disk and the attempt to fit a King profile is not

Table 11.1: Structural parameters derived from the observed RDPs with the adopted theoretical models (exponential-disk and King profiles). The central density of objects f_{0D} and the scale length h_D for the exponential disk model (Eq. 2.5) are in columns (2) and (3). Columns (4)-(7) contain the central density of objects f_{0K}, the core radius r_c, the tidal radius r_t where available, and the concentration parameter c_p for the King model (Eq. 2.6).

Name	f_{0D} [arcmin^{-2}]	h_D [arcmin]	f_{0K} [arcmin^{-2}]	r_c [arcmin]	r_t [arcmin]	c_p
(1)	(2)	(3)	(4)	(5)	(6)	(7)
Phoenix	8.8 ± 1.7	0.43 ± 0.09	8.7 ± 1.3	0.31 ± 0.06	–	–
NGC 6822	23.9 ± 4.5	8.2 ± 1.8	116.6 ± 9.2	0.37 ± 0.04	–	–
NGC 6822 BSG	209 ± 23	1.9 ± 0.2	242 ± 36	1.10 ± 0.17	–	–
NGC 6822 RSG	6.3 ± 0.9	2.6 ± 0.4	14.6 ± 1.8	0.48 ± 0.07	–	–
IC10	13.7 ± 2.6	9.5 ± 2.8	53.3 ± 6.8	0.26 ± 0.06	–	–
WLM	18.0 ± 2.7	0.57 ± 0.08	19.8 ± 1.7	0.36 ± 0.04	19 ± 33	1.72
Sextans A	34.1 ± 4.9	0.27 ± 0.05	40.4 ± 3.4	0.22 ± 0.03	2.6 ± 0.7	1.07
Sextans B	9.9 ± 2.1	0.5 ± 0.1	12.9 ± 1.5	0.38 ± 0.05	3.3 ± 1.1	0.94

as successful (Figure 11.13 *right*). This is even clearer from Figure 11.14 which shows the RDPs for the blue and red supergiants in the left and right panel, respectively. Both density distributions are fitted quite well with an exponential disk model (Eq. 2.5). The King law also manages to fit the distribution, only around ~3 arcmin from the centre the King model slightly underestimates the stellar density of the blue supergiants. In the case of the RSGs, however, the King law fails.

IC10 is in a region of the sky heavily contaminated with Milky Way stars. This is also obvious from Figure 11.10 *left*. This combined with the elongated shape of IC10 makes the fitting of the RDP less successful. The central parts of the galaxy containing the brightest stars up to a distance of ~ 2 arcmin from the centre of the galaxy is fitted well by the King profile at first glance. On closer inspection, however, it seems that both models have difficulties fitting the density distributions of this star-burst galaxy.

For the WLM dwarf irregular galaxy it is evident from Figure 11.11 that the King law provides a good fit to the available data not only in the central parts but also in the outer parts. Due to the less regular shape of WLM and especially IC10, which is also reflected in the profiles, the fit is not perfect. However, it is still better than the fit with the exponential disk model.

The galaxies which are at the largest distances are Sextans A and Sextans B, which means that there are very few stars which Gaia will be able to resolve and detect. As can be seen in Figure 11.16 the small angular size of the galaxies combined with the low number of resolved stars makes it very difficult to obtain any valuable information about their structural parameters from the radial density profiles. Test model fitting was performed with the models described in Chapter 2. From the data available and up to a distance of ~2 arcmin from the centre of the galaxy it seems that the King law offers a reasonable fit. However, considering the fact that the number of resolved stars is so limited it is not unexpected that the obtained parameters are extremely unreliable.

11.4 Discussion

It is common for dIrr galaxies to have patchy distributions of young, blue stars but smoother and more extended distributions of older, redder stars that follow exponential or King surface density profiles (Mateo 1998). All of the galaxies, with the exception of NGC 6822, are too faint to actually see this irregularity in the distribution of the younger stellar component and too far away to provide a reasonable density profile.

Data form the Local Group Galaxies Survey project was used to study the spatial distribution of six dwarf irregular galaxies - Phoenix, NGC 6822, WLM,

IC10, Sextans A, and Sextans B. Isodensity maps were obtained for two subsets of the data - first, for the stars brighter than V = 20 mag in order to show what is available down to Gaia's limit, and second, for the bright massive stars (blue supergiants) in these galaxies. Radial density profiles were used to obtain the structural parameters of these galaxies by fitting theoretical models (exponential and King profiles) to their density distributions. The structural parameters are listed in Table 11.1.

The isodensity contour maps with the V = 20 mag limit give an initial idea how much of the galaxies Gaia will actually see. Both the Gaia BP and RP spectra have similar lengths in order to provide similar angular resolution, which is able to deal with stellar densities of up to $\sim 7.5 \times 10^5$ deg^{-2} (Jordi and Carrasco 2007). This means that none of the galaxies will be crowded (although NGC 6822 and IC10 seem close judging by the maximum stellar density from Figures 11.7 and 11.10) and stars will be more or less resolved. On the other hand there will be very few supergiant stars that are probably going to be detected anyway.

The RDPs indicate in all cases the King law as marginally the dominant model. The only exception is NGC 6822, where the exponential law is more appropriate. Although NGC 6822 and Phoenix are at the same distance, NGC 6822 is more massive and luminous than Phoenix. Thus, the density profiles are based on more stars and this can be the reason for this difference. The rest of the galaxies are located at larger distances and there are not enough stars which are bright enough to produce reliable surface density profiles.

On the other hand, comparing the values of the structural parameters for NGC 6822 when using the whole data set with stars as faint as 24 mag with the ones compiled by Mateo (1998) we find that the values for the core radius are in fact the same. The difference in the values for the tidal radius is due to the smaller area available in the survey we are using data from - the quoted tidal radius in Table 3 of Mateo (1998) is 40±10 arcmin, whereas our data goes out to ~15 arcmin from the centre of the galaxy. We believe that the difference in the exponential scale lengths is due to the fact that we are using star counts for the density distribution and not surface brightness. G. Nikolov (private communication) has shown that the structural parameters obtained from surface brightness usually underestimate the stellar density in crowded regions where the most massive stars dominate.

IC10 is considered the only LG analog of starburst galaxies and a fundamental laboratory for the analysis of massive young stars and evolved intermediate-mass stars. Even though it has been the cross-road of several investigations, its structural parameters and in particular its radial extent are poorly defined (Bono et al. 2010). Sadly, Gaia will not be able to contribute much for IC10 since almost all of the massive blue stars will not be accessible given the V = 20 mag limit. This is obvious from Figures 11.3 and 11.10.

Conclusions

Concluding Remarks

The current study had two main goals. We have presented the results concerning:

1. the investigation of the spatial distribution of stellar populations in nearby galaxies, expected to be resolved in stars by Gaia. These are part of the extra-galactic objects to be simulated in the framework of the Gaia mission preparation. The main targets were the Large and Small Magellanic Clouds, along with six dwarf irregular galaxies in the Local Group - NGC 6822, WLM, IC10, Phoenix, Sextans A and Sextans B;

2. the implementation of results from this investigation in the Gaia Universe Model. Catalogues of stars known to be part of both the Large and Small Magellanic Clouds and their characteristics (BVI magnitudes) were provided to be used for simulations, including parameters such as Right Ascension, Declination, V magnitude, $V-I$ colour, G magnitude, distance, radial velocities, proper motions, surface gravity $\log g$, effective tempearture T_{eff}, metallicity $[Fe/H]$, α enhancement $[\alpha/Fe]$, and extinction A_V.

Initially a list of requirements (coverage, completeness, depth) for the data sources was created in order to account for the specific needs of the Gaia Universe Model. Various catalogues were considered but many of them did not satisfy most of our requirements, like SuperCOSMOS, MC2, and the UBVR CCD survey. In fact, some of them actually did not satisfy any of the requirements, like the MACS. On the other hand, there were also catalogues, which presented an acceptable compromise and in the end they were approved to be used for this study. The three data sources finally selected were the Magellanic Clouds Photometric Survey (Zaritsky et al. 2002, 2004), the 2MASS (Skrutskie et al. 2006), and catalogues of carbon stars, produced by Rebeirot et al. (1993), Morgan and Hatzidimitriou (1995), and Kontizas et al. (2001).

The survey by Massey et al. (2007) has allowed us to study a few more galaxies other than the Magellanic Clouds - NGC 6822, WLM, IC10, Phoenix, Sextans A, and Sextans B. It provided a good sample of interesting galaxies in the Local Group with various properties and at various distances. They have all been observed and reduced in a consistent way and because of the small angular sizes of the galaxies the coverage is excellent. Some of these galaxies might be resolved in stars by Gaia (NGC 6822), and others might not due to the larger distance (Sextans A, Sextans B).

The results we obtained from the isopleth maps for the inner region of the Magellanic Clouds and the fairly azimuthally symmetric elliptical exponential profile of the older SMC stars is consistent with the general trend of more fragmented young stellar components and smoother and more regular intermediate

age and older populations (Gonidakis et al. 2009; Nidever et al. 2011). The stellar distribution in all dwarf galaxies appears smooth and without the patchiness, seen in the distribution of the distribution of the young population in the Magellanic Clouds. In these galaxies there are not enough young bright stars to produce their isodensity maps and the isodensity maps are dominated by the much more numerous older populations.

Then, radial density profiles (RDPs) were used to obtain the stellar distribution in the galaxies. The RDPs for the SMC from the MCPS show that both the exponential-disk and the King models can be used to describe the stellar distribution. The distribution of the youngest stars is almost equally well fitted by both models but the oldest stars definitely follow the King law. Such a difference is not observed in the LMC, where the exponential-disk model seems slightly better. This is possibly due to the relatively smaller area available for the LMC, which is dominated by the younger stars. A similar behaviour is observed in the RDPs from 2MASS. Both the younger and the older stars in the LMC are distributed on an exponential disk, while the radial density distribution of the SMC is better described by the King profile.

The RDPs of the other six dwarf irregular galaxies indicate in all cases the King law as marginally the dominant model. The only exception is NGC 6822, where the exponential law is more appropriate. Although NGC 6822 and Phoenix are at the same distance, NGC 6822 is more massive and luminous than Phoenix. Thus, the density profiles are based on more stars and this can be the reason for this difference. The rest of the galaxies are located at larger distances and there are not enough stars which are bright enough to produce reliable surface density profiles.

The structural parameters of the LMC and SMC from fitting a King or an exponential model to the RDPs obtained from the adopted data sets in the various catalogues (MCPS, 2MASS, and carbon stars) are listed in Table 6.2. The structural parameters of the other six dwarf galaxies (NGC 6822, WLM, IC 10, Phoenix, Sextans A, and Sextans B) from the adopted data set are listed in Table 11.1.

Comparing the values of the structural parameters for NGC 6822 when using the whole data set with stars as faint as 24 mag with the ones compiled by Mateo (1998) we find that the values for the core radius are in fact the same. We believe that the difference in the exponential scale lengths is due to the fact that we are using star counts for the density distribution and not surface brightness. G. Nikolov (private communication) has shown that the structural parameters obtained from surface brightness usually underestimate the stellar density in crowded regions where the most massive stars dominate.

It was shown that there is a system of young objects more concentrated in the central region of the Large Magellanic Cloud with a position angle almost

perpendicular to the other system. Of course the inclination of the LMC is small (almost face-on), allowing the difference to be seen. The two systems in the LMC have been previously mentioned, and are explained as one result of the interaction between the Milky Way galaxy and the Magellanic Clouds.

From the carbon stars isopleth maps in the LMC, it was also shown that two different systems exist with a core radius of 3.3 ± 0.1 deg for the faint and 0.9 ± 0.1 deg for the bright carbon stars. An exponential model also shows such a difference in the scale height, 1.69 ± 0.07 deg and 0.98 ± 0.05 deg, respectively, revealing a smaller central system of more massive carbon stars. A similar result has been observed for the young clusters in the LMC by Kontizas et al. (1990), Dottori et al. (1996), and Bica et al. (2008).

Additionaly, fitting the surface density profiles with both the exponential and the King-like profile suggests that the LMC disk scale length is about twice the SMC value. A similar behaviour is detected also for the carbon stars (see Table 6.2). This ratio of h_D in both Clouds is evident also for both the young and old stellar populations from 2MASS data and all but the youngest groups of stars from MCPS data.

Although the Magellanic Clouds are assumed to be irregular galaxies, it also seems that the older populations appear to behave as tidally truncated systems, even if they do not show obvious radial symmetry. From Table 6.2 we can see that the parameters of the fitting for the young stellar populations are inconclusive. However, this is no surprise, because even if the bulk of the stars show some radial symmetry, this is not the case for the young bright stars. Both their contour maps and their radial density profiles do not support such an assumption. This is anticipated since clumping of star-forming regions dominates their distribution.

One of the goals of the current study was the investigation of the spatial distribution of stellar populations in nearby galaxies, expected to be resolved in stars by Gaia. These are part of the extra-galactic objects to be simulated in the framework of ESA's Gaia mission preparation by the Data Processing and Analysis Consortium.

Simulations of the Magellanic Clouds have been implemented Robin et al. (2012) by including a catalogue in the Universe Model and providing parameters such as Right Ascension, Declination, V, $V-I$, G, distance, radial velocities, proper motions, $\log g$, T_{eff}, $[Fe/H]$, $[\alpha/Fe]$, and the extinction A_V. Catalogues of stars known to be part of both Clouds (LMC and SMC) and their characteristics (BVI magnitudes) have been obtained from the literature. Magellanic Clouds Photometric Survey was a good source because its spatial resolution is comparable to that of Hubble Space Telescope and it is complete down to $V \approx 20$.

Future Opportunities

Although with the current study we have achieved our goals of investigating the stellar distribution in the Magellanic Clouds and several dwarf irregular galaxies in the Local Group and consequently providing the means to implement the Magellanic Clouds for simulations in the framework of the Gaia mission preparation by DPAC, there are some interesting aspects of this work which were not within the primary subject of the current study but which are maybe worth pursuing independently.

Of course, the first thing that comes to mind when considering how the analysis can be improved is to use more ground-based surveys to complement the already used data. These would have to be deeper and to provide a better coverage of the galaxies. It would also be desirable that they include the inter-Cloud region, where the SMC tail is located and the Magellanic Stream begins.

The VISTA near-infrared $YJKs$ survey of the Magellanic System might provide such an opportunity (Cioni et al. 2011). This survey aims to obtain $YJKs$ band photometry across the system down to Ks = 20.3 at S/N=10. This sensitivity corresponds to the bottom of the red giant branch field stellar population and allows the determination of the global spatially resolved star formation history with unprecedented quality and the construction of a three-dimensional map of the system.

Another possible improvement in the analysis of the stellar spatial distribution is not to stop with the radial density profiles but to study the galaxies in parts. The difference in the line-of-sight depths between the south-east and north-west sides of the SMC suggests a possible explanation for the lack of centration between the inner and outer distributions. This asymmetry can be studied further by dividing the galaxy in sections and obtaining the star counts in these separate parts.

The prospect of Gaia astrometry motivated An et al. (2012) to perform a detailed study of the use of proper motions in mass estimators. Particularly in the case of the Milky Way, the proper motions are crucial as the line-of-sight velocity closely coincides with the radial velocity as measured from the Galactic Centre. Hence, proper motions from Gaia will provide new information on the velocity anisotropy that is not available in the line-of-sight velocities alone.

The photometric aspect of the Gaia mission is also eagerly anticipated. Even if the distances to the Magellanic Clouds are not known precisely, they can be considered at a fixed distance with only moderate depth and therefore the difference in apparent magnitude can be interpreted as a difference in luminosity. This is why the Magellanic Clouds have offered such a high scientific potential. Gaia, as a wholesky survey, will observe the Magellanic clouds, as well as the halo and the plane of the Galaxy (with parallaxes). The inter-comparison of differ-

ent populations of standard candle classes with a single instrument will have an enourmous impact, since, for the first time, they can be calibrated to a homogeneous reference (Eyer et al. 2012).

With the current instrumentation (wide-area multi-object spectrographs on 8 – 10m class telescopes) the use of the near-infrared CaII triplet lines from intermediate resolution spectroscopy has proven to be a valuable tool for providing accurate line-of-sight velocities and $[Fe/H]$ measurements over a wide $[Fe/H]$ range within the Local Group. These samples have allowed us to greatly improve our knowledge of the large scale metallicity and kinematics properties of the Milky Way satellites, uncovering in several of these systems the presence of metallicity and velocity gradients, multiple stellar components and allowing more accurate mass determinations. At its outskirts, however, there are challenges limiting the variety of galaxy types and environments that we can explore at a similar degree of detail. Future ground-based facilities such as the European Extremely Large Telescope (E-ELT) will be needed to carry out resolved stellar population studies at larger distances (Battaglia 2011).

The Gaia simulator is now in a mature state. As of the end of 2011 it is stable. The simulator (which includes the Gass, Gibis and Gog) relies on the Universe Model to obtain the astronomical sources to be observed by Gaia. The Universe Model includes information on the Milky Way, resolved galaxies (Large and Small Magellanic Clouds), extragalactic objects (QSOs, unresolved galaxies), Solar System objects, exoplanets. Our contribution was therefore quite important - the ultimate goal of our studies was to provide the means to simulate the Magellanic Clouds in the framework of the Gaia mission preparation.

This was done by providing catalogues of Magellanic Clouds stars to DPAC/ CU2 which included the following parameters: Right Ascension, Declination, V, $V - I$, $\log g$, T_{eff}. The other necessary parameters (distance, radial velocities, proper motions, $[Fe/H]$, $[\alpha/Fe]$, and the extinction A_V) were obtained from the literature. For now more detailed data on various stella populations is not required. However, providing an actual model of the Magellanic Clouds as it has been done over the years for the Milky Way seems the logical next step.

List of Figures

LIST OF FIGURES

LIST OF FIGURES

List of Tables

LIST OF TABLES

References

M. Aaronson. Local group dwarf galaxies - The red stellar population. In C. A. Norman, A. Renzini, & M. Tosi, editor, *Stellar Populations*, pages 45–70, 1986.

J. An, N. W. Evans, and A. J. Deason. Mass estimators in the Gaia era. *MNRAS*, 420:2562–2568, March 2012. doi: 10.1111/j.1365-2966.2011.20226.x.

J. Anderson and I. R. King. Erratum: "The Rotation of the Globular Cluster 47 Tucanae in the Plane of the Sky". *AJ*, 128:950–950, August 2004. doi: 10.1086/423222.

A. Aparicio. Synthetic Color-Magnitude Diagram and the Star Formation History in the Local Group. In T. Lejeune & J. Fernandes, editor, *Observed HR Diagrams and Stellar Evolution*, volume 274 of *Astronomical Society of the Pacific Conference Series*, pages 429–+, 2002.

D. G. Barnes and W. J. G. de Blok. The neutral hydrogen environments of the nearby galaxies WLM, NGC 1313 and Sextans A. *MNRAS*, 351:333–338, June 2004. doi: 10.1111/j.1365-2966.2004.07790.x.

G. Battaglia. Spectroscopy of Resolved Stellar Populations in Dwarf Galaxies with the European Extremely Large Telescope. In M. Koleva, P. Prugniel, & I. Vauglin, editor, *EAS Publications Series*, volume 48 of *EAS Publications Series*, pages 467–472, July 2011. doi: 10.1051/eas/1148102.

P. Battinelli, S. Demers, and B. Letarte. Young stars in the periphery of NGC 6822. *A&A*, 405:563–569, July 2003. doi: 10.1051/0004-6361:20030640.

M. K. Belcheva, E. Livanou, M. Kontizas, G. B. Nikolov, and E. Kontizas. Spatial distribution of stellar populations in the Magellanic Clouds: implementation to Gaia. *A&A*, 527:A31, March 2011. doi: 10.1051/0004-6361/201015835.

G. Bertelli, A. Bressan, C. Chiosi, F. Fagotto, and E. Nasi. Theoretical isochrones from models with new radiative opacities. *A&AS*, 106:275–302, August 1994.

G. Besla, N. Kallivayalil, L. Hernquist, B. Robertson, T. J. Cox, R. P. van der Marel, and C. Alcock. Are the Magellanic Clouds on Their First Passage about the Milky Way? *ApJ*, 668:949–967, October 2007. doi: 10.1086/521385.

L. Bianchi, B. Efremova, P. Hodge, P. Massey, and K. A. G. Olsen. A Treasury Study of Star-forming Regions in the Local Group. I. HST Photometry of Young Populations in Six Dwarf Galaxies. *AJ*, 143:74, March 2012. doi: 10.1088/0004-6256/143/3/74.

E. Bica, C. Bonatto, C. M. Dutra, and J. F. C. Santos. A general catalogue of extended objects in the Magellanic System. *MNRAS*, 389:678–690, September 2008. doi: 10.1111/j.1365-2966.2008.13612.x.

B. Binggeli, G. A. Tammann, and A. Sandage. Studies of the Virgo cluster. VI - Morphological and kinematical structure of the Virgo cluster. *AJ*, 94:251–277, August 1987. doi: 10.1086/114467.

B. J. Bok. The Magellanic Clouds. *JRASC*, 63:105, June 1969.

G. Bono, P. B. Stetson, M. Monelli, M. Fabrizio, N. Sanna, M. Nonino, A. R. Walker, F. Bresolin, R. Buonanno, F. Caputo, M. Castellani, C. E. Corsi, M. Dall'Ora, I. Ferraro, P. François, G. Iannicola, M. Matsunaga, L. Pulone, M. Romaniello, J. Storm, and F. Thévenin. Dwarf galaxies in the Local Group: cornerstones for stellar astrophysics and cosmology. In S. Boissier, M. Heydari-Malayeri, R. Samadi, & D. Valls-Gabaud , editor, *SF2A-2010: Proceedings of the Annual meeting of the French Society of Astronomy and Astrophysics*, pages 327–+, December 2010.

M. L. Boyer, S. Srinivasan, J. T. van Loon, I. McDonald, M. Meixner, D. Zaritsky, K. D. Gordon, F. Kemper, B. Babler, M. Block, S. Bracker, C. W. Engelbracht, J. Hora, R. Indebetouw, M. Meade, K. Misselt, T. Robitaille, M. Sewiło, B. Shiao, and B. Whitney. Surveying the Agents of Galaxy Evolution in the Tidally Stripped, Low Metallicity Small Magellanic Cloud (SAGE-SMC). II. Cool Evolved Stars. *AJ*, 142:103, October 2011. doi: 10.1088/0004-6256/142/4/103.

R. Braun and D. A. Thilker. The WSRT wide-field H I survey. II. Local Group features. *A&A*, 417:421–435, April 2004. doi: 10.1051/0004-6361:20034423.

J. A. R. Caldwell and I. M. Coulson. The geometry and distance of the Magellanic Clouds from Cepheid variables. *MNRAS*, 218:223–246, January 1986.

R. Canterna and P. J. Flower. A new dwarf irregular galaxy in the constellation Phoenix. *ApJ*, 212:L57–L58, March 1977. doi: 10.1086/182374.

M. Capaccioli, E. V. Held, H. Lorenz, and M. Vietri. Photographic and CCD surface photometry of the standard elliptical galaxy NGC 3379. *AJ*, 99:1813–1822, June 1990. doi: 10.1086/115459.

M.-R. L. Cioni, H. J. Habing, and F. P. Israel. The morphology of the Magellanic Clouds revealed by stars of different age: results from the DENIS survey. *A&A*, 358:L9–L12, June 2000.

M.-R. L. Cioni, G. Clementini, L. Girardi, R. Guandalini, M. Gullieuszik, B. Miszalski, M.-I. Moretti, V. Ripepi, S. Rubele, G. Bagheri, K. Bekki, N. Cross, W. J. G. de Blok, R. de Grijs, J. P. Emerson, C. J. Evans, B. Gibson, E. Gonzales-Solares, M. A. T. Groenewegen, M. Irwin, V. D. Ivanov, J. Lewis, M. Marconi, J.-B. Marquette, C. Mastropietro, B. Moore, R. Napiwotzki, T. Naylor, J. M. Oliveira, M. Read, E. Sutorius, J. T. van Loon, M. I. Wilkinson, and P. R. Wood. The VMC survey. I. Strategy and first data. *A&A*, 527: A116, March 2011. doi: 10.1051/0004-6361/201016137.

L. Ciotti. Stellar systems following the R exp 1/m luminosity law. *A&A*, 249: 99–106, September 1991.

R. J. Cohen. The unusual kinematics of the galaxy IC 10. *MNRAS*, 187:839–845, June 1979.

T. W. Connors, D. Kawata, and B. K. Gibson. N-body simulations of the Magellanic stream. *MNRAS*, 371:108–120, September 2006. doi: 10.1111/j.1365-2966.2006.10659.x.

K. H. Cook, M. Aaronson, and J. Norris. Carbon and M stars in nearby galaxies - A preliminary survey using a photometric technique. *ApJ*, 305:634–644, June 1986. doi: 10.1086/164277.

E. Costa, R. A. Méndez, M. H. Pedreros, M. Moyano, C. Gallart, N. Noël, G. Baume, and G. Carraro. The Proper Motion of the Magellanic Clouds. I. First Results and Description of the Program. *AJ*, 137:4339–4360, May 2009. doi: 10.1088/0004-6256/137/5/4339.

W. J. G. de Blok and F. Walter. Evidence for Tidal Interaction and a Supergiant H I Shell in the Local Group Dwarf Galaxy NGC 6822. *ApJ*, 537:L95–L98, July 2000. doi: 10.1086/312777.

W. J. G. de Blok and F. Walter. Young stars in the outer HI disc of NGC 6822. *MNRAS*, 341:L39–L43, June 2003. doi: 10.1046/j.1365-8711.2003.06669.x.

G. de Vaucouleurs. Recherches sur les Nebuleuses Extragalactiques. *Annales d'Astrophysique*, 11:247–+, January 1948.

G. de Vaucouleurs. The Magellanic Clouds and the Galaxy. *The Observatory*, 74:23–31, February 1954.

G. de Vaucouleurs and M. Capaccioli. Luminosity distribution in galaxies. I - The elliptical galaxy NGC 3379 as a luminosity distribution standard. *ApJS*, 40:699–731, August 1979. doi: 10.1086/190602.

N. Delmotte, C. Loup, D. Egret, M.-R. Cioni, and F. Pierfederici. The Master Catalogue of stars towards the Magellanic Clouds. I. Multispectral surveys of the Large Magellanic Cloud. *A&A*, 396:143–155, December 2002. doi: 10.1051/0004-6361:20021307.

S. Demers, P. Battinelli, and B. Letarte. A Carbon star approach to IC 10: Distance and correct size. *A&A*, 424:125–132, September 2004. doi: 10.1051/0004-6361:20040552.

R. C. Dohm-Palmer, E. D. Skillman, M. Mateo, A. Saha, A. Dolphin, E. Tolstoy, J. S. Gallagher, and A. A. Cole. Deep Hubble Space Telescope Imaging of Sextans A. I. The Spatially Resolved Recent Star Formation History. *AJ*, 123:813–831, February 2002. doi: 10.1086/324635.

A. E. Dolphin, A. Saha, E. D. Skillman, R. C. Dohm-Palmer, E. Tolstoy, A. A. Cole, J. S. Gallagher, J. G. Hoessel, and M. Mateo. Deep Hubble Space Telescope Imaging of Sextans A. III. The Star Formation History. *AJ*, 126:187–196, July 2003. doi: 10.1086/375761.

H. Dottori, E. Bica, J. J. Claria, and I. Puerari. Spatial Distributions of Young Large Magellanic Cloud Clusters as Tracers of a Bar Perturbation. *ApJ*, 461:742–+, April 1996. doi: 10.1086/177098.

DPAC. Gaia Data Processing and Analysis Consortium. Response to ESA's Announcement of Opportunity. Proposal for the Gaia Data Processing. *GAIA-CD-DPAC-FM-030-2*, 2007.

L. Eyer, L. Palaversa, N. Mowlavi, P. Dubath, R. I. Anderson, D. W. Evans, T. Lebzelter, V. Ripepi, L. Szabados, S. Leccia, and G. Clementini. Standard candles from the Gaia perspective. *Ap&SS*, page 49, February 2012. doi: 10.1007/s10509-012-0998-5.

G. Fabbiano. X-Ray Emission and Extranuclear Activity in Galaxies. In E. J. A. Meurs & R. A. E. Fosbury, editor, *European Southern Observatory Conference and Workshop Proceedings*, volume 32 of *European Southern Observatory Conference and Workshop Proceedings*, pages 325–+, July 1989.

J. R. Fisher and R. B. Tully. Photographs of dwarf irregular galaxies in the vicinity of the Local Group and the M81 group. *AJ*, 84:62–70, January 1979. doi: 10.1086/112388.

P. C. Freire, F. Camilo, M. Kramer, D. R. Lorimer, A. G. Lyne, R. N. Manchester, and N. D'Amico. Further results from the timing of the millisecond pulsars in 47 Tucanae. *MNRAS*, 340:1359–1374, April 2003. doi: 10.1046/j.1365-8711.2003.06392.x.

C. Gallart, A. Aparicio, and J. M. Vilchez. The Local Group Dwarf Irregular Galaxy NGC 6822.I.The Stellar Content. *AJ*, 112:1928–+, November 1996. doi: 10.1086/118153.

L. T. Gardiner and D. Hatzidimitriou. Stellar populations and the large-scale structure of the Small Magellanic Cloud. IV - Age distribution studies of the outer regions. *MNRAS*, 257:195–224, July 1992.

L. T. Gardiner and M. R. S. Hawkins. Stellar populations and large-scale structure of the SMC. III - The geometry of the northern and north-western outlying regions. *MNRAS*, 251:174–191, July 1991.

L. T. Gardiner, T. Sawa, and M. Fujimoto. Numerical Simulations of the Magellanic System - Part One - Orbits of the Magellanic Clouds and the Global Gas Distribution. *MNRAS*, 266:567–+, February 1994.

J. E. Gizis, J. R. Mould, and S. Djorgovski. An X-ray image of the Fornax dwarf spheroidal galaxy. *PASP*, 105:871–874, August 1993. doi: 10.1086/133248.

I. Gonidakis, E. Livanou, E. Kontizas, U. Klein, M. Kontizas, M. Belcheva, P. Tsalmantza, and A. Karampelas. Structure of the SMC. Stellar component distribution from 2MASS data. *A&A*, 496:375–380, March 2009. doi: 10.1051/0004-6361/200809828.

K. D. Gordon, C. Bot, E. Muller, K. A. Misselt, A. Bolatto, J.-P. Bernard, W. Reach, C. W. Engelbracht, B. Babler, S. Bracker, M. Block, G. C. Clayton, J. Hora, R. Indebetouw, F. P. Israel, A. Li, S. Madden, M. Meade, M. Meixner, M. Sewilo, B. Shiao, L. J. Smith, J. T. van Loon, and B. A. Whitney. The Dust-to-Gas Ratio in the Small Magellanic Cloud Tail. *ApJ*, 690:L76–L80, January 2009. doi: 10.1088/0004-637X/690/1/L76.

REFERENCES

D. A. Gouliermis, S. Schmeja, R. S. Klessen, W. J. G. de Blok, and F. Walter. Hierarchical Stellar Structures in the Local Group Dwarf Galaxy NGC 6822. *ApJ*, 725:1717–1734, December 2010. doi: 10.1088/0004-637X/725/2/1717.

E. K. Grebel. Evolutionary Histories of Dwarf Galaxies in the Local Group. In P. Whitelock & R. Cannon, editor, *The Stellar Content of Local Group Galaxies*, volume 192 of *IAU Symposium*, pages 17–+, January 1999.

E. K. Grebel. The Local Group. In J. W. Menzies & P. D. Sackett, editor, *Microlensing 2000: A New Era of Microlensing Astrophysics*, volume 239 of *Astronomical Society of the Pacific Conference Series*, page 280, 2001a.

E. K. Grebel. Star Formation Histories of Nearby Dwarf Galaxies. *Astrophysics and Space Science Supplement*, 277:231–239, 2001b. doi: 10.1023/A:1012742903265.

J. Harris and D. Zaritsky. Spectroscopic Survey of Red Giants in the Small Magellanic Cloud. I. Kinematics. *AJ*, 131:2514–2524, May 2006. doi: 10.1086/500974.

J. Harris, D. Zaritsky, and I. Thompson. On the Distribution of Dust in the Large Magellanic Cloud. *AJ*, 114:1933–+, November 1997. doi: 10.1086/118615.

D. Hatzidimitriou and M. R. S. Hawkins. Stellar populations and large-scale structure of the SMC. II - Geometry of the north-eastern and south-western outlying regions. *MNRAS*, 241:667–690, December 1989.

D. Hatzidimitriou, M. R. S. Hawkins, and K. Gyldenkerne. Stellar populations and large-scale structure of the SMC. I - Photometry. *MNRAS*, 241:645–666, December 1989.

V. Heesen, U. Rau, M. P. Rupen, E. Brinks, and D. A. Hunter. Deep Radio Continuum Imaging of the Dwarf Irregular Galaxy IC 10: Tracing Star Formation and Magnetic Fields. *ApJ*, 739:L23, September 2011. doi: 10.1088/2041-8205/739/1/L23.

P. Heller and K. Rohlfs. The dynamical evolution of the Magellanic system. *A&A*, 291:743–753, November 1994.

R. W. Hilditch, I. D. Howarth, and T. J. Harries. Forty eclipsing binaries in the Small Magellanic Cloud: fundamental parameters and Cloud distance. *MNRAS*, 357:304–324, February 2005. doi: 10.1111/j.1365-2966.2005.08653.x.

J. V. Hindman, F. J. Kerr, and R. X. McGee. A Low Resolution Hydrogen-line Survey of the Magellanic System. II. Interpretation of Results. *Australian Journal of Physics*, 16:570–+, 1963a.

J. V. Hindman, R. X. McGee, A. W. L. Carter, E. C. J. Holmes, and M. Beard. A Low Resolution Hydrogen-line Survey of the Magellanic System. I. Observations and Digital Reduction Procedures. *Australian Journal of Physics*, 16:552–+, 1963b.

P. Hodge, T. Smith, P. Eskridge, H. MacGillivray, and S. Beard. A COSMOS study of the structure and content of NGC 6822. *ApJ*, 379:621–630, October 1991. doi: 10.1086/170534.

P. W. Hodge. The Fornax dwarf galaxy. II. The distribution of stars. *AJ*, 66: 249–+, August 1961a. doi: 10.1086/108404.

P. W. Hodge. The distribution of stars in the Sculptor dwarf galaxy. *AJ*, 66: 384–+, October 1961b. doi: 10.1086/108443.

P. W. Hodge. Distribution of stars in the Leo II Dwarf Galaxy. *AJ*, 67:125–+, March 1962. doi: 10.1086/108680.

P. W. Hodge. Dwarf Galaxies. *ARA&A*, 9:35–+, 1971. doi: 10.1146/annurev.aa.09.090171.000343.

W. K. Huchtmeier. The giant H I-envelope of the irregular galaxy IC 10. *A&A*, 75:170–175, May 1979.

D. A. Hunter. The Stellar Population and Star Clusters in the Unusual Local Group Galaxy IC 10. *ApJ*, 559:225–242, September 2001. doi: 10.1086/322399.

G Indu and A. Subramaniam. Recent star formation history of the Large and Small Magellanic Clouds. *ArXiv e-prints*, September 2011.

M. Irwin and D. Hatzidimitriou. Structural parameters for the Galactic dwarf spheroidals. *MNRAS*, 277:1354–1378, December 1995.

M. J. Irwin, W. E. Kunkel, and S. Demers. A blue stellar population in the H I bridge between the two Magellanic Clouds. *Nature*, 318:160–+, November 1985. doi: 10.1038/318160a0.

M. J. Irwin, S. Demers, and W. E. Kunkel. The proper motion of the SMC. In *Bulletin of the American Astronomical Society*, volume 28 of *Bulletin of the American Astronomical Society*, pages 932–+, May 1996.

T. H. Jarrett, T. Chester, R. Cutri, S. E. Schneider, and J. P. Huchra. The 2MASS Large Galaxy Atlas. *AJ*, 125:525–554, February 2003. doi: 10.1086/345794.

T. E. Jeltema and S. Profumo. Searching for Dark Matter with X-Ray Observations of Local Dwarf Galaxies. *ApJ*, 686:1045–1055, October 2008. doi: 10.1086/591495.

C. Jordi and J. M. Carrasco. Photometry with GAIA. In C. Sterken, editor, *The Future of Photometric, Spectrophotometric and Polarimetric Standardization*, volume 364 of *Astronomical Society of the Pacific Conference Series*, page 215, April 2007.

N. Kacharov, M. Rejkuba, and M.-R. L. Cioni. Spectra probing the number ratio of C- to M-type AGB stars in the NGC 6822 galaxy . *A&A*, 537:A108, January 2012. doi: 10.1051/0004-6361/201117383.

N. Kallivayalil, R. P. van der Marel, and C. Alcock. Is the SMC Bound to the LMC? The Hubble Space Telescope Proper Motion of the SMC. *ApJ*, 652: 1213–1229, December 2006a. doi: 10.1086/508014.

N. Kallivayalil, R. P. van der Marel, C. Alcock, T. Axelrod, K. H. Cook, A. J. Drake, and M. Geha. The Proper Motion of the Large Magellanic Cloud Using HST. *ApJ*, 638:772–785, February 2006b. doi: 10.1086/498972.

A. Karampelas, A. Dapergolas, E. Kontizas, E. Livanou, M. Kontizas, I. Bellas-Velidis, and J. M. Vílchez. Star complexes and stellar populations in NGC 6822. Comparison with the Magellanic Clouds. *A&A*, 497:703–711, April 2009. doi: 10.1051/0004-6361/200811081.

F. J. Kerr, J. F. Hindman, and B. J. Robinson. Observations of the 21 cm Line from the Magellanic Clouds. *Australian Journal of Physics*, 7:297–+, 1954.

I. King. The structure of star clusters. I. an empirical density law. *AJ*, 67:471–+, October 1962. doi: 10.1086/108756.

S. A. Klioner. A Practical Relativistic Model for Microarcsecond Astrometry in Space. *AJ*, 125:1580–1597, March 2003.

A. Y. Kniazev, E. K. Grebel, S. A. Pustilnik, A. G. Pramskij, and D. B. Zucker. Spectrophotometry of Sextans A and B: Chemical Abundances of H II Regions and Planetary Nebulae. *AJ*, 130:1558–1573, October 2005. doi: 10.1086/432931.

E. Kontizas, A. Dapergolas, D. H. Morgan, and M. Kontizas. A Catalogue of carbon stars in the LMC. *aap*, 369:932–938, April 2001. doi: 10.1051/0004-6361:20010152.

M. Kontizas, D. H. Morgan, D. Hatzidimitriou, and E. Kontizas. The cluster system of the Large Magellanic Cloud. *A&AS*, 84:527–547, September 1990.

M. Kontizas, E. Kontizas, and A. G. Michalitsianos. Radial distribution of metallicity in the LMC cluster systems. *A&A*, 269:107–110, March 1993.

P. Kroupa and U. Bastian. The HIPPARCOS proper motion of the Magellanic Clouds. *New A*, 2:77–90, May 1997. doi: 10.1016/S1384-1076(97)00006-7.

A. Kucinskas, L. Lindegren, and V. Vansevicius. Beyond the Galaxy with Gaia: Evolutionary Histories of Galaxies in the Local Group. In C. Turon, K. S. O'Flaherty, & M. A. C. Perryman, editor, *The Three-Dimensional Universe with Gaia*, volume 576 of *ESA Special Publication*, pages 695–+, January 2005.

W. E. Kunkel, S. Demers, and M. J. Irwin. Magellanic Cloud Periphery Carbon Stars. IV. The SMC. *AJ*, 119:2789–2800, June 2000. doi: 10.1086/301401.

A. Kučinskas, L. Lindegren, T. Tanabé, and V. Vansevičius. Star Formation Histories with Gaia: the Galaxy and Beyond. *Baltic Astronomy*, 12:526–531, 2003.

M. G. Lattanzi, A. Spagna, A. Sozzetti, and S. Casertano. Space-borne global astrometric surveys: the hunt for extrasolar planets. *MNRAS*, 317:211–224, September 2000. doi: 10.1046/j.1365-8711.2000.03637.x.

R. Leaman, K. A. Venn, A. M. Brooks, G. Battaglia, A. A. Cole, R. A. Ibata, M. J. Irwin, A. W. McConnachie, J. T. Mendel, and E. Tolstoy. The Resolved Structure and Dynamics of an Isolated Dwarf Galaxy: A VLT and Keck Spectroscopic Survey of WLM. *ArXiv e-prints*, February 2012.

B. Letarte, S. Demers, P. Battinelli, and W. E. Kunkel. The Extent of NGC 6822 Revealed by Its C Star Population. *AJ*, 123:832–839, February 2002. doi: 10.1086/338319.

L. M. Macri, K. Stanek, D. Bersier, L. Greenhill, and M. Reid. Improving the Distance Scale: NICMOS and ACS/HRC observations of Cepheids in the Maser Galaxy NGC 4258. In *American Astronomical Society Meeting Abstracts*, volume 38 of *Bulletin of the American Astronomical Society*, pages 102–107, December 2006.

L. Magrini, R. L. M. Corradi, N. A. Walton, A. A. Zijlstra, D. L. Pollacco, J. R. Walsh, M. Perinotto, D. J. Lennon, and R. Greimel. The Local Group Census: Planetary nebulae in Sextans B. *A&A*, 386:869–873, May 2002. doi: 10.1051/0004-6361:20020296.

J. Makino, K. Akiyama, and D. Sugimoto. On the apparent universality of the R exp 1/4 law for brightness distribution in galaxies. *PASJ*, 42:205–215, April 1990.

F. Maragoudaki, M. Kontizas, E. Kontizas, A. Dapergolas, and D. H. Morgan. The LMC stellar complexes in luminosity slices. Star formation indicators. *A&A*, 338:L29–L32, October 1998.

F. Maragoudaki, M. Kontizas, D. H. Morgan, E. Kontizas, A. Dapergolas, and E. Livanou. The recent structural evolution of the SMC. *A&A*, 379:864–869, December 2001. doi: 10.1051/0004-6361:20011454.

P. Marigo, L. Girardi, A. Bressan, M. A. T. Groenewegen, L. Silva, and G. L. Granato. Evolution of asymptotic giant branch stars. II. Optical to far-infrared isochrones with improved TP-AGB models. *A&A*, 482:883–905, May 2008. doi: 10.1051/0004-6361:20078467.

T. H. Markert and M. E. Donahue. Observations of four nearby galaxies with the Einstein Observatory. *ApJ*, 297:564–571, October 1985. doi: 10.1086/163552.

C. B. Markwardt. Non-linear Least-squares Fitting in IDL with MPFIT. In D. A. Bohlender, D. Durand, & P. Dowler, editor, *Astronomical Society of the Pacific Conference Series*, volume 411 of *Astronomical Society of the Pacific Conference Series*, pages 251–+, September 2009.

I. Márquez, G. B. Lima Neto, H. Capelato, F. Durret, and D. Gerbal. Gravothermal properties and formation of elliptical galaxies. *A&A*, 353:873–886, January 2000.

I. Márquez, G. B. Lima Neto, H. Capelato, F. Durret, B. Lanzoni, and D. Gerbal. Energy, entropy and mass scaling relations for elliptical galaxies. Towards a physical understanding of their photometric properties. *A&A*, 379:767–780, December 2001. doi: 10.1051/0004-6361:20011370.

N. Martin, E. Maurice, and J. Lequeux. The structure of the Small Magellanic Cloud. *A&A*, 215:219–242, May 1989.

R. O. Marzke and L. N. da Costa. The Galaxy Luminosity Function at z≤0.05: Dependence on Color. *AJ*, 113:185–+, January 1997. doi: 10.1086/118243.

P. Massey. A UBVR CCD Survey of the Magellanic Clouds. *ApJS*, 141:81–122, July 2002a. doi: 10.1086/338286.

P. Massey. UBVR CCD survey of the Magellanic clouds (Massey+, 2002). *VizieR Online Data Catalog*, 2236:0–+, July 2002b.

P. Massey and T. E. Armandroff. The Massive Star Content, Reddening, and Distance of the Nearby Irregular Galaxy IC 10. *AJ*, 109:2470–+, June 1995. doi: 10.1086/117465.

P. Massey, K. A. G. Olsen, P. W. Hodge, S. B. Strong, G. H. Jacoby, W. Schlingman, and R. C. Smith. A Survey of Local Group Galaxies Currently Forming Stars. I. UBVRI Photometry of Stars in M31 and M33. *AJ*, 131:2478–2496, May 2006. doi: 10.1086/503256.

P. Massey, K. A. G. Olsen, P. W. Hodge, G. H. Jacoby, R. T. McNeill, R. C. Smith, and S. B. Strong. A Survey of Local Group Galaxies Currently Forming Stars. II. UBVRI Photometry of Stars in Seven Dwarfs and a Comparison of the Entire Sample. *AJ*, 133:2393–2417, May 2007. doi: 10.1086/513319.

C. Mastropietro, B. Moore, L. Mayer, J. Wadsley, and J. Stadel. The gravitational and hydrodynamical interaction between the Large Magellanic Cloud and the Galaxy. *MNRAS*, 363:509–520, October 2005. doi: 10.1111/j.1365-2966.2005.09435.x.

M. L. Mateo. Dwarf Galaxies of the Local Group. *ARA&A*, 36:435–506, 1998. doi: 10.1146/annurev.astro.36.1.435.

D. S. Mathewson and V. L. Ford. H I surveys of the Magellanic System. In S. van den Bergh & K. S. D. de Boer, editor, *Structure and Evolution of the Magellanic Clouds*, volume 108 of *IAU Symposium*, pages 125–136, September 1984.

D. S. Mathewson, M. P. Schwarz, and J. D. Murray. The Magellanic stream - The turbulent wake of the Magellanic clouds in the halo of the Galaxy. *ApJ*, 217:L5–L8, October 1977. doi: 10.1086/182527.

D. S. Mathewson, S. R. Wayte, V. L. Ford, and K. Ruan. The 'high velocity cloud' origin of the Magellanic system. *Proceedings of the Astronomical Society of Australia*, 7:19–25, 1987.

N. M. McClure-Griffiths, D. J. Pisano, M. R. Calabretta, H. A. Ford, F. J. Lockman, L. Staveley-Smith, P. M. W. Kalberla, J. Bailin, L. Dedes, S. Janowiecki, B. K. Gibson, T. Murphy, H. Nakanishi, and K. Newton-McGee. Gass: The

Parkes Galactic All-Sky Survey. I. Survey Description, Goals, and Initial Data Release. *ApJS*, 181:398–412, April 2009. doi: 10.1088/0067-0049/181/2/398.

A. W. McConnachie, A. Huxor, N. F. Martin, M. J. Irwin, S. C. Chapman, G. Fahlman, A. M. N. Ferguson, R. A. Ibata, G. F. Lewis, H. Richer, and N. R. Tanvir. A Trio of New Local Group Galaxies with Extreme Properties. *ApJ*, 688:1009–1020, December 2008. doi: 10.1086/591313.

R. X. McGee and L. M. Newton. H I profiles in the bridge region of the Megallanic Clouds. *Proceedings of the Astronomical Society of Australia*, 6:471–500, 1986.

J. Meaburn. Young Star Formation in the Magellanic HI Bridge. *MNRAS*, 223: 317–+, November 1986.

D. Minniti and A. A. Zijlstra. Dwarf Galaxies Also Have Stellar Halos. *ApJ*, 467: L13+, August 1996. doi: 10.1086/310189.

D. H. Morgan and D. Hatzidimitriou. A survey of carbon stars in the Small Magellanic Cloud. *aaps*, 113:539–+, November 1995.

R. Morras and E. Bajaja. H I around the dwarf galaxy in Phoenix. *Rev. Mexicana Astron. Astrofis.*, 13:69–71, June 1986.

D. L. Nidever, S. R. Majewski, and W. B. Burton. The Origin of the Magellanic Stream and Its Leading Arm. *ApJ*, 679:432–459, May 2008. doi: 10.1086/587042.

D. L. Nidever, S. R. Majewski, R. R. Muñoz, R. L. Beaton, R. J. Patterson, and W. E. Kunkel. Discovery of a Large Stellar Periphery Around the Small Magellanic Cloud. *ApJ*, 733:L10+, May 2011. doi: 10.1088/2041-8205/733/1/L10.

E. W. Olszewski. Intermediate-age Magellanic cloud globular clusters. In J. E. Grindlay & A. G. D. Philip, editor, *The Harlow-Shapley Symposium on Globular Cluster Systems in Galaxies*, volume 126 of *IAU Symposium*, pages 159–170, 1988.

T. Oosterloo, G. S. Da Costa, and L. Staveley-Smith. HI Observations of the Tucana Dwarf Elliptical Galaxy. *AJ*, 112:1969–+, November 1996. doi: 10.1086/118155.

S. Ortolani and R. G. Gratton. Stellar photometry in the PHOENIX dwarf galaxy. *PASP*, 100:1405–1422, November 1988. doi: 10.1086/132341.

M. A. C. Perryman, L. Lindegren, and C. Turon. The Scientific Goals of the GAIA Mission. In R. M. Bonnet, E. Høg, P. L. Bernacca, L. Emiliani, A. Blaauw, C. Turon, J. Kovalevsky, L. Lindegren, H. Hassan, M. Bouffard, B. Strim, D. Heger, M. A. C. Perryman, & L. Woltjer, editor, *Hipparcos - Venice '97*, volume 402 of *ESA Special Publication*, pages 743–748, August 1997.

M. A. C. Perryman, K. S. de Boer, G. Gilmore, E. Høg, M. G. Lattanzi, L. Lindegren, X. Luri, F. Mignard, O. Pace, and P. T. de Zeeuw. GAIA: Composition, formation and evolution of the Galaxy. *A&A*, 369:339–363, April 2001. doi: 10.1051/0004-6361:20010085.

S. Piatek, C. Pryor, and E. W. Olszewski. Proper Motions of the Large Magellanic Cloud and Small Magellanic Cloud: Re-Analysis of Hubble Space Telescope Data. *AJ*, 135:1024–1038, March 2008. doi: 10.1088/0004-6256/135/3/1024.

M. E. Putman, L. Staveley-Smith, K. C. Freeman, B. K. Gibson, and D. G. Barnes. The Magellanic Stream, High-Velocity Clouds, and the Sculptor Group. *ApJ*, 586:170–194, March 2003. doi: 10.1086/344477.

E. Rebeirot, M. Azzopardi, and B. E. Westerlund. Carbon stars in the Small Magellanic Cloud. II - Catalogue of 1707 objects with identifications and spectrophotometry. *aaps*, 97:603–728, February 1993.

M. G. Richer, A. Bullejos, J. Borissova, M. L. McCall, H. Lee, R. Kurtev, L. Georgiev, R. L. Kingsburgh, R. Ross, and M. Rosado. IC 10: More evidence that it is a blue compact dwarf. *A&A*, 370:34–42, April 2001. doi: 10.1051/0004-6361:20010206.

A. C. Robin, C. Reylé, S. Derrière, and S. Picaud. A synthetic view on structure and evolution of the Milky Way. *A&A*, 409:523–540, October 2003. doi: 10.1051/0004-6361:20031117.

A. C. Robin, X. Luri, C. Reylé, Y. Isasi, E. Grux, S. Blanco-Cuaresma, F. Arenou, C. Babusiaux, M. Belcheva, R. Drimmel, C. Jordi, A. Krone-Martins, E. Masana, J. C. Mauduit, F. Mignard, N. Mowlavi, B. Rocca-Volmerange, P. Sartoretti, E. Slezak, and A. Sozzetti. Gaia Universe Model Snapshot : A statistical analysis of the expected contents of the Gaia catalogue. *ArXiv e-prints*, February 2012.

H. C. Russell. Notes on Celestial Photographs taken at the Sydney Observatory. *MNRAS*, 51:96–+, December 1890.

A. Ružička, C. Theis, and J. Palouš. Spatial Motion of The Magellanic Clouds: Tidal Models Ruled Out? *ApJ*, 691:1807–1815, February 2009. doi: 10.1088/0004-637X/691/2/1807.

S. Sakai, B. F. Madore, and W. L. Freedman. Tip of the Red Giant Branch Distances to Galaxies. IV. Sextans B. *ApJ*, 480:589, May 1997. doi: 10.1086/304000.

S. Sakai, B. F. Madore, and W. L. Freedman. Cepheid and Tip of the Red Giant Branch Distances to the Dwarf Irregular Galaxy IC 10. *ApJ*, 511:671–679, February 1999. doi: 10.1086/306716.

S. Sakai, D. Zaritsky, and R. C. Kennicutt, Jr. The Tip of the Red Giant Branch Distance to the Large Magellanic Cloud. *AJ*, 119:1197–1204, March 2000. doi: 10.1086/301266.

N. Sanna, G. Bono, P. B. Stetson, A. Pietrinferni, M. Monelli, S. Cassisi, R. Buonanno, E. Sabbi, F. Caputo, M. Castellani, C. E. Corsi, S. Degl'Innocenti, I. Drozdovsky, I. Ferraro, G. Iannicola, M. Nonino, P. G. Prada Moroni, L. Pulone, M. Romaniello, and A. R. Walker. On the Stellar Content of the Starburst Galaxy IC10. *ApJ*, 699:L84–L87, July 2009. doi: 10.1088/0004-637X/699/2/L84.

N. Sanna, G. Bono, P. B. Stetson, I. Ferraro, M. Monelli, M. Nonino, P. G. Prada Moroni, R. Bresolin, R. Buonanno, F. Caputo, M. Cignoni, S. Degl'Innocenti, G. Iannicola, N. Matsunaga, A. Pietrinferni, M. Romaniello, J. Storm, and A. R. Walker. On the Radial Extent of the Dwarf Irregular Galaxy IC10. *ApJ*, 722:L244–L249, October 2010. doi: 10.1088/2041-8205/722/2/L244.

H.-E. Schuster and R. M. West. A very distant globular cluster? *A&A*, 49:129–131, May 1976.

J. L. Sérsic. Influence of the atmospheric and instrumental dispersion on the brightness distribution in a galaxy. *Boletin de la Asociacion Argentina de Astronomia La Plata Argentina*, 6:41, 1963.

M. E. Sharina, T. H. Puzia, and A. S. Krylatyh. A globular cluster in the dwarf galaxy Sextans B. *Astrophysical Bulletin*, 62:209–216, September 2007. doi: 10.1134/S1990341307030029.

G. S. Shostak and E. D. Skillman. Neutral hydrogen observations of the irregular galaxy IC 10. *A&A*, 214:33–42, April 1989.

E. D. Skillman, R. Terlevich, P. J. Teuben, and H. van Woerden. H I synthesis observations of the dwarf irregular galaxy Sextans A. *A&A*, 198:33–42, June 1988.

E. D. Skillman, R. C. Kennicutt, and P. W. Hodge. Oxygen abundances in nearby dwarf irregular galaxies. *ApJ*, 347:875–882, December 1989a. doi: 10.1086/168178.

E. D. Skillman, R. Terlevich, and J. Melnick. Abundances in southern Local Group dwarf irregular galaxies. *MNRAS*, 240:563–572, October 1989b.

E. D. Skillman, E. Tolstoy, A. A. Cole, A. E. Dolphin, A. Saha, J. S. Gallagher, R. C. Dohm-Palmer, and M. Mateo. Deep Hubble Space Telescope Imaging of IC 1613. II. The Star Formation History. *ApJ*, 596:253–272, October 2003. doi: 10.1086/377635.

M. F. Skrutskie, R. M. Cutri, R. Stiening, M. D. Weinberg, S. Schneider, J. M. Carpenter, C. Beichman, R. Capps, T. Chester, J. Elias, J. Huchra, J. Liebert, C. Lonsdale, D. G. Monet, S. Price, P. Seitzer, T. Jarrett, J. D. Kirkpatrick, J. E. Gizis, E. Howard, T. Evans, J. Fowler, L. Fullmer, R. Hurt, R. Light, E. L. Kopan, K. A. Marsh, H. L. McCallon, R. Tam, S. Van Dyk, and S. Wheelock. The Two Micron All Sky Survey (2MASS). *AJ*, 131:1163–1183, February 2006. doi: 10.1086/498708.

S. Söderhjelm. Census of Binaries the Big Picture. In C. Turon, K. S. O'Flaherty, & M. A. C. Perryman, editor, *The Three-Dimensional Universe with Gaia*, volume 576 of *ESA Special Publication*, pages 97–+, January 2005.

J. St-Germain, C. Carignan, S. Côte, and T. Oosterloo. H I in the Field of the Dwarf Spheroidal/Irregular Galaxy PHOENIX. *AJ*, 118:1235–1244, September 1999. doi: 10.1086/301021.

S. Stanimirović, L. Staveley-Smith, and P. A. Jones. A New Look at the Kinematics of Neutral Hydrogen in the Small Magellanic Cloud. *ApJ*, 604:176–186, March 2004. doi: 10.1086/381869.

L. Staveley-Smith, S. Kim, M. Putman, and S. Stanimirović. Neutral Hydrogen in the Magellanic System. In R. E. Schielicke, editor, *Reviews in Modern Astronomy*, volume 11 of *Reviews in Modern Astronomy*, page 117, 1998.

N. V. Strobel, P. Hodge, and R. C. Kennicutt, Jr. H II regions in seven dwarf irregular galaxies. *ApJ*, 383:148–163, December 1991. doi: 10.1086/170771.

S. Subramanian and A. Subramaniam. Depth estimation of the Large and Small Magellanic Clouds. *A&A*, 496:399–412, March 2009. doi: 10.1051/0004-6361/200811029.

S. Subramanian and A. Subramaniam. The 3D structure of the Small Magellanic Cloud. *ArXiv e-prints*, September 2011.

O. Szewczyk, G. Pietrzyński, W. Gieren, J. Storm, A. Walker, L. Rizzi, K. Kinemuchi, F. Bresolin, R.-P. Kudritzki, and M. Dall'Ora. The Araucaria Project. The Distance of the Large Magellanic Cloud from Near-Infrared Photometry of RR Lyrae Variables. *AJ*, 136:272–279, July 2008. doi: 10.1088/0004-6256/136/1/272.

O. Szewczyk, G. Pietrzyński, W. Gieren, A. Ciechanowska, F. Bresolin, and R.-P. Kudritzki. The Araucaria Project: The Distance to the Small Magellanic Cloud from Near-Infrared Photometry of RR Lyrae Variables. *AJ*, 138:1661–1666, December 2009. doi: 10.1088/0004-6256/138/6/1661.

N. A. Tikhonov and O. A. Galazutdinova. Stellar population of the irregular galaxy IC 10. *Astronomy Letters*, 35:748–763, November 2009. doi: 10.1134/S1063773709110036.

M. Tosi. Chemical Evolution models of Local Group galaxies. *ArXiv Astrophysics e-prints*, August 2003.

M. Tosi, L. Greggio, G. Marconi, and P. Focardi. Star formation in dwarf irregular galaxies - Sextans B. *AJ*, 102:951–974, September 1991. doi: 10.1086/115925.

H.-J. Tucholke, K. S. de Boer, and W. C. Seitter. The Magellanic Catalogue of Stars - MACS (Tucholke+ 1996). *VizieR Online Data Catalog*, 1221:0–+, November 1995.

H.-J. Tucholke, K. S. de Boer, and W. C. Seitter. The Magellanic Catalogue of Stars (MACS). *A&AS*, 119:91–98, October 1996.

M. A. Urbaneja, R.-P. Kudritzki, F. Bresolin, N. Przybilla, W. Gieren, and G. Pietrzyński. The Araucaria Project: The Local Group Galaxy WLM-Distance and Metallicity from Quantitative Spectroscopy of Blue Supergiants. *ApJ*, 684:118–135, September 2008. doi: 10.1086/590334.

W. D. Vacca, C. D. Sheehy, and J. R. Graham. Imaging of the Stellar Population of IC 10 with Laser Guide Star Adaptive Optics and the Hubble Space Telescope. *ApJ*, 662:272–283, June 2007. doi: 10.1086/516725.

F. van de Rydt, S. Demers, and W. E. Kunkel. PHOENIX - an intermediate dwarf galaxy in the Local Group. *AJ*, 102:130–136, July 1991. doi: 10.1086/115861.

S. van den Bergh. The outer fringes of the local group. *AJ*, 107:1328–1332, April 1994. doi: 10.1086/116946.

S. van den Bergh. Updated Information on the Local Group. *PASP*, 112:529–536, April 2000a. doi: 10.1086/316548.

S. van den Bergh. *The Galaxies of the Local Group*. Cambridge, May 2000b.

S. van den Bergh. History of the Local Group. In M. Livio & T. M. Brown, editor, *The Local Group as an Astrophysical Laboratory*, pages 1–15, 2006.

R. P. van der Marel. Magellanic Cloud Structure from Near-Infrared Surveys. II. Star Count Maps and the Intrinsic Elongation of the Large Magellanic Cloud. *AJ*, 122:1827–1843, October 2001. doi: 10.1086/323100.

R. P. van der Marel and M.-R. L. Cioni. Magellanic Cloud Structure from Near-Infrared Surveys. I. The Viewing Angles of the Large Magellanic Cloud. *AJ*, 122:1807–1826, October 2001. doi: 10.1086/323099.

S. D. van Dyk, D. Puche, and T. Wong. The Recent Star Formation in Sextans A. *AJ*, 116:2341–2362, November 1998. doi: 10.1086/300584.

F. van Leeuwen and D. W. Evans. On the use of the HIPPARCOS intermediate astrometric data. *A&AS*, 130:157–172, May 1998. doi: 10.1051/aas:1998218.

A. Vecchiato, M. G. Lattanzi, B. Bucciarelli, M. Crosta, F. de Felice, and M. Gai. Testing general relativity by micro-arcsecond global astrometry. *A&A*, 399:337–342, February 2003. doi: 10.1051/0004-6361:20021785.

Q. D. Wang, K. E. Whitaker, and R. Williams. An XMM-Newton and Chandra study of the starburst galaxy IC 10. *MNRAS*, 362:1065–1077, September 2005. doi: 10.1111/j.1365-2966.2005.09379.x.

P. Wannier, G. T. Wrixon, and R. W. Wilson. A Survey of Positive Velocity Neutral Hydrogen above the Galactic Plane between 1 2520 and 1 = 3220. *A&A*, 18:224–+, May 1972.

D. R. Weisz, J. J. Dalcanton, B. F. Williams, K. M. Gilbert, E. D. Skillman, A. C. Seth, A. E. Dolphin, K. B. W. McQuinn, S. M. Gogarten, J. Holtzman, K. Rosema, A. Cole, I. D. Karachentsev, and D. Zaritsky. The ACS Nearby Galaxy Survey Treasury. VIII. The Global Star Formation Histories of 60 Dwarf Galaxies in the Local Volume. *ApJ*, 739:5–+, September 2011. doi: 10.1088/0004-637X/739/1/5.

D. L. Welch, R. A. McLaren, B. F. Madore, and C. W. McAlary. Distance moduli and structure of the Magellanic Clouds from near-infrared photometry of classical Cepheids. *ApJ*, 321:162–185, October 1987. doi: 10.1086/165622.

REFERENCES

B. E. Westerlund. Review: an Overview of the Structure and Kinematics of the Magellanic Clouds. In R. Haynes & D. Milne, editor, *The Magellanic Clouds*, volume 148 of *IAU Symposium*, pages 15–+, 1991.

E. M. Wilcots and B. W. Miller. The Kinematics and Distribution of H I in IC 10. *AJ*, 116:2363–2394, November 1998. doi: 10.1086/300595.

M. I. Wilkinson, J. Kleyna, N. W. Evans, and G. Gilmore. Dark matter in dwarf spheroidals - I. Models. *MNRAS*, 330:778–791, March 2002. doi: 10.1046/j.1365-8711.2002.05154.x.

L. M. Young and K. Y. Lo. The Neutral Interstellar Medium in Nearby Dwarf Galaxies. III. Sagittarius DIG, LGS 3, and PHOENIX. *ApJ*, 490:710–+, December 1997. doi: 10.1086/304909.

L. M. Young, E. D. Skillman, D. R. Weisz, and A. E. Dolphin. The Aptly Named Phoenix Dwarf Galaxy. *ApJ*, 659:331–338, April 2007. doi: 10.1086/512153.

D. Zaritsky and J. Harris. Quantifying the Drivers of Star Formation on Galactic Scales. I. The Small Magellanic Cloud. *ApJ*, 604:167–175, March 2004. doi: 10.1086/381795.

D. Zaritsky, J. Harris, E. K. Grebel, and I. B. Thompson. The Morphologies of the Small Magellanic Cloud. *ApJ*, 534:L53–L56, May 2000. doi: 10.1086/312649.

D. Zaritsky, J. Harris, I. B. Thompson, E. K. Grebel, and P. Massey. The Magellanic Clouds Photometric Survey: The Small Magellanic Cloud Stellar Catalog and Extinction Map. *Astronomical Journal*, 123:855–872, February 2002. doi: 10.1086/338437.

D. Zaritsky, J. Harris, I. B. Thompson, and E. K. Grebel. The Magellanic Clouds Photometric Survey: The Large Magellanic Cloud Stellar Catalog and Extinction Map. *AJ*, 128:1606–1614, October 2004. doi: 10.1086/423910.